Quarterly Reviews of Biophysics **35**, 1 (2002), pp. 1–62. © 2002 Cambridge University Press
DOI: 10.1017/S0033583501003754 Printed in the United Kingdom

Photosynthetic apparatus of purple bacteria

Xiche Hu[1], Thorsten Ritz[2], Ana Damjanović[2], Felix Autenrieth[2] and Klaus Schulten[2,*]

[1] Department of Chemistry, University of Toledo, Toledo, OH 43606, USA
[2] Beckman Institute and Department of Physics, University of Illinois at Urbana-Champaign, Urbana, IL 61801, USA

* Author to whom correspondence should be addressed. E-mail: kschulte@ks.uiuc.edu

1. Introduction

Life as we know it today exists largely because of photosynthesis, the process through which light energy is converted into chemical energy by plants, algae, and photosynthetic bacteria (Priestley, 1772; Barnes, 1893; Wurmser, 1925; Van Niel, 1941; Clayton & Sistrom, 1978; Blankenship *et al*. 1995; Ort & Yocum, 1996). Historically, photosynthetic organisms are grouped into two classes. When photosynthesis is carried out in the presence of air it is called oxygenic photosynthesis (Ort & Yocum, 1996). Otherwise, it is anoxygenic (Blankenship *et al*. 1995). Higher plants, algae and cyanobacteria perform oxygenic photosynthesis, which involves reduction of carbon dioxide to carbohydrate and oxidation of water to produce molecular oxygen. Some photosynthetic bacteria, such as purple bacteria, carry out anoxygenic photosynthesis that involves oxidation of molecules other than water. In spite of these differences, the general principles of energy transduction are the same in anoxygenic and oxygenic photosynthesis (Van Niel, 1931, 1941; Stanier, 1961; Wraight, 1982; Gest, 1993). The primary processes of photosynthesis involve absorption of photons by light-harvesting complexes (LHs), transfer of excitation energy from LHs to the photosynthetic reaction centers (RCs), and the primary charge separation across the photosynthetic membrane (Sauer, 1975; Knox, 1977; Fleming & van Grondelle, 1994; van Grondelle *et al*. 1994). In this article, we will focus on the anoxygenic photosynthetic process in purple bacteria, since its photosynthetic system is the most studied and best characterized during the past 50 years.

The photosynthetic apparatus of purple bacteria is a nanometric assembly in the intracytoplasmic membranes and consists of two types of pigment–protein complexes, the photosynthetic RC and LHs (Kaplan & Arntzen, 1982; Zuber & Brunisholz, 1991). The function of LHs is to capture sunlight and to transfer the excitation energy to the RC where it serves to initiate a charge separation process (Fleming & van Grondelle, 1994; Lancaster *et al*. 1995; Parson & Warshel, 1995; Woodbury & Allen, 1995; Hu *et al*. 1998). Depicted in Fig. 1 schematically is the intracytoplasmic membrane of purple bacteria with its primary photosynthetic apparatus. This apparatus, one of the simplest of its kind, feeds through excitation by sunlight a cyclic flow of electrons and protons that leads to synthesis of ATP.

Over the past few decades, extensive biochemical and spectroscopic studies of bacterial photosynthetic systems have revealed the following structural and dynamical principles for bacterial light harvesting:

(1) Bacterial photosynthetic membranes contain thousands of pigment molecules (bacteriochlorophylls and carotenoids) that are non-covalently bound to proteins to form well organized pigment–protein complexes (Stoll, 1936; Smith, 1938; Rees & Clayton, 1968; Thornber *et al*. 1983; Zuber, 1986; Scheer, 1988; Zuber & Brunisholz, 1991; Zuber & Cogdell, 1995). Out of all these pigments, only very few bacteriochlorophylls (BChls) in the primary reaction site, termed the photosynthetic RC, directly take part in photochemical reactions; most BChls serve as light-harvesting antennae capturing the

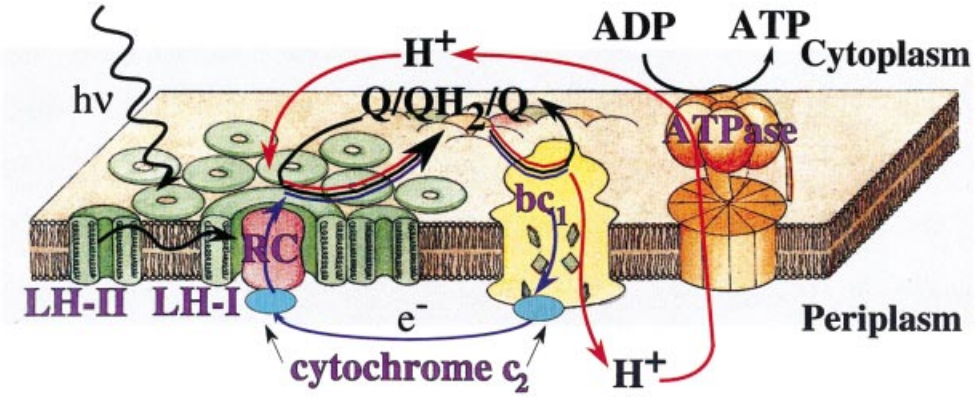

Fig. 1. Schematic representation of the photosynthetic apparatus in the intracytoplasmic membrane of purple bacteria. The reaction center (RC, red) is surrounded by the light-harvesting complex I (LH-I, green) to form the LH-I–RC complex, which is surrounded by multiple light-harvesting complexes (LH-IIs) (green), forming altogether the photosynthetic unit (PSU). Photons are absorbed by LHs and excitation is transferred to the RC initiating a charge (electron-hole) separation. Electrons are shuttled back by the cytochrome c_2 complex (blue) from the ubiquinone-cytochrome bc_1 complex (yellow) to the RC. The electron transfer across the membrane produces a large proton gradient that drives the synthesis of ATP from ADP by the ATPase (orange). Electron flow is represented in blue, proton flow in red, quinone flow, likely confined to the intramembrane space, in black.

sunlight and funneling electronic excitation towards the RC (Emerson & Arnold, 1932; Arnold & Kohn, 1934; Duysens, 1952, 1964). By convention, the photosynthetic RC and the associated LHs are collectively named the photosynthetic unit (PSU) (Mauzerall & Greenbaum, 1989; Francke & Amesz, 1995; Freiberg, 1995; Cogdell *et al*. 1996). As a matter of fact, the organization of pigments into PSUs in which multiple light-harvesting antennae serve the RC has been adopted by all photosynthetic organisms (Duysens, 1988; Mauzerall & Greenbaum, 1989; Grossman *et al*. 1995; Fromme, 1996; Gantt, 1996; Green & Durnford, 1996; Hankamer *et al*. 1997). With it they can collect light from a broader spectral range and use energy much more efficiently. Light-harvesting antennae enlarge the cross-section for capturing sunlight by the RC. The latter possesses light-absorbing chlorophylls itself, but photons absorbed by the RC chlorophylls are not sufficient to saturate its maximum turnover rate. When exposed to direct sunlight, chlorophylls absorb at a rate of at most 10 Hz and, in dim light, at a rate of 0·1 Hz (Borisov & Godik, 1973). However, the chemical reaction of the RC can 'turn over' at 1000 Hz. LHs fuel excitation energy to the RC, which keeps the RC running at an optimal rate.

(2) The light-harvesting antenna is composed of multiple LHs with varying spectral characteristics and a particular structural organization in the whole antenna. In most purple bacteria, the PSUs contain two types of LHs, commonly referred to as B875 (LH-I) and B800–850 (LH-II) complexes according to their *in vivo* absorption maxima in the near-infrared (Thornber *et al*. 1983; Zuber & Brunisholz, 1991; Hawthornthwaite & Cogdell, 1991). LH-I is found surrounding directly the RCs (Miller, 1982; Walz & Ghosh, 1997), while LH-II is not in direct contact with the RC, but transfers energy to it via LH-I (Monger & Parson, 1977; Sundström & van Grondelle, 1991, 1995; van Grondelle *et al*. 1994). For some bacteria, such as *Rhodopseudomonas* (*Rps*.) *acidophila* and

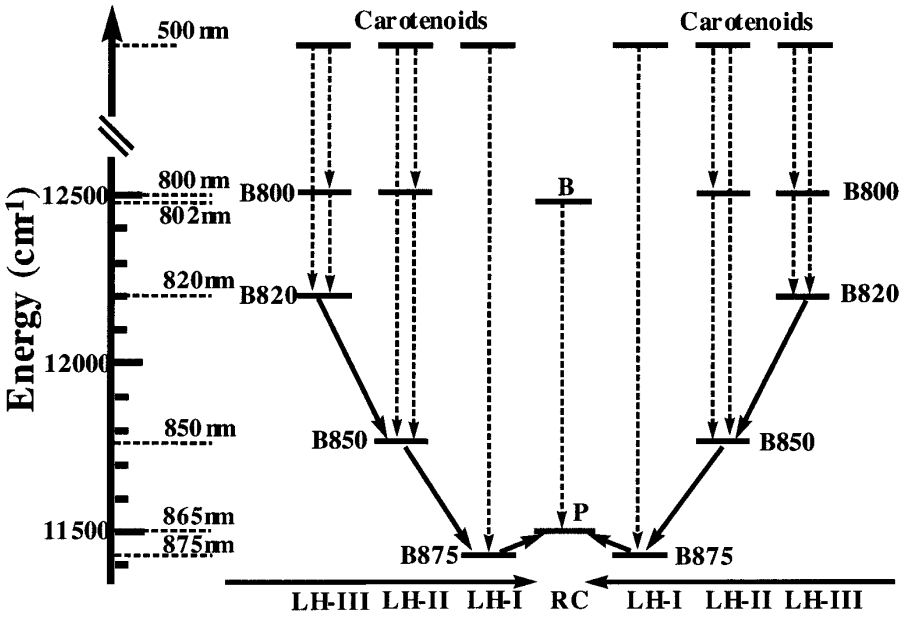

Fig. 2. Energy levels of the electronic excitations in the PSU of BChl *a* containing purple bacteria. The diagram illustrates a funneling of excitation energy towards the photosynthetic RC. The vertical dashed lines indicate intra-complex excitation transfer; the diagonal solid lines inter-complex excitation transfer. LH-I exists in all purple bacteria; LH-II exists in most species; LH-III arises in certain species only and it is usually regulated by ambience light.

Rhodospirillum (*Rs.*) *molischianum* strain DSM 120 (Germeroth *et al.* 1993), there exists a third type of light-harvesting complex, LH-III. The number of LH-IIs and LH-IIIs in the PSU varies according to growth conditions such as light intensity and temperature (Aagaard & Sistrom, 1972).

(3) Photosynthetic bacteria evolved a pronounced energetic hierarchy in the light-harvesting system. Purple bacteria absorb light in a spectral region complementary to that of plants and algae, mainly at wavelengths of approximately 500 nm through carotenoids and above 800 nm through BChls. Shown in Fig. 2 are the energy levels for the key electronic excitations in the PSU. Pigments of outer LHs absorb at a higher energy than do the inner ones. For example, the LH-II, which surrounds LH-I, absorbs maximally at 800 and 850 nm; LH-I, which in turn surrounds the RC, absorbs at a lower energy (875 nm) (Thornber *et al.* 1983; Zuber & Brunisholz, 1991; van Grondelle *et al.* 1994; Sundström & van Grondelle, 1995). The energy cascade serves to funnel electronic excitations from the LH-IIs through LH-I to the RC.

(4) Time-resolved picosecond and femtosecond spectroscopy revealed that excitation energy transfer within the PSU occurs on an ultrafast timescale and at near unit (95 %) efficiency (Pullerits & Sundström, 1996; Fleming & van Grondelle, 1997). It takes less than 100 ps for the energy of the excited LHs to reach the RC. Timescales for elementary energy transfer steps range from femtoseconds to picoseconds.

Tremendous progress in our understanding of bacterial photosynthesis has been achieved during the last 15 years with the determination of the atomic structures of the bacterial photosynthetic RC, followed by two high-resolution crystal structures of LH-II. Structures

of the RC for *Rps. viridis* (Deisenhofer *et al*. 1985) as well as for *Rhodobacter* (*Rb*.) *sphaeroides* (Allen *et al*. 1987; Ermler *et al*. 1994) were determined by X-ray crystallography. Recently, high-resolution crystal structures of LH-IIs from two species (*Rps. acidophila* and *Rs. molischianum*) have been determined (McDermott *et al*. 1995; Koepke *et al*. 1996). The structure of LH-I is not yet known to atomic resolution, although an 8.5 Å resolution projection map observed by electron microscopy was reported for LH-I of *Rs. rubrum* (Karrasch *et al*. 1995).

The structures mentioned provide detailed knowledge of the organization of chromophores in the photosynthetic membrane and stimulated a new wave of more focused theoretical and experimental investigations of bacterial photosynthesis in an already active field of research (Clayton, 1973; Clayton & Sistrom, 1978; Govindjee, 1982; Scheer, 1991; Deisenhofer & Norris, 1993; Fleming & van Grondelle, 1994; Blankenship *et al*. 1995; Fyfe & Cogdell, 1996; Hu & Schulten, 1997; Hu *et al*. 1998; Sundström *et al*. 1999; Krueger *et al*. 1999a; Cogdell *et al*. 1999). In this review, we will look at our current understanding of structure and dynamics of bacterial light harvesting and highlight some pressing issues that merit further investigation. The scope of this review will be limited to the molecular model of the bacterial PSU and structure-based theoretical studies of excitation energy transfer mechanisms. Spectroscopic probe of the excitation transfer dynamics in the PSU, when relevant, will be discussed, but will not be emphasized. Readers interested in the subject are referred to other reviews (Sauer, 1975; Borisov, 1978; Hunter *et al*. 1989; Sundström & van Grondelle, 1991; van Grondelle *et al*. 1994; Pullerits & Sundström, 1996; Fleming & van Grondelle, 1997; Sundström *et al*. 1999; Krueger *et al*. 1999a: van Amerongen *et al*. 2000).

2. Structure of the bacterial PSU

The PSU combines in the intracytoplasmic membrane of purple bacteria a nanometric assembly of the photosynthetic RC and an array of LHs. During the last 15 years, structural details of many of these individual pigment–protein complexes have emerged, albeit not from the same species. All the known crystal structures of RCs and LH-IIs are from BChl *a*-containing purple bacteria except that of RC from *Rps. viridis* (Deisenhofer *et al*. 1985) which contains BChl *b* as the major pigment. Consequently, we will describe the structural organization of PSU based on BChl *a*-containing purple bacteria. At first, we will introduce the overall organization of the bacterial PSU. We will then describe structural features of individual pigment–protein complexes. In particular, we will present the crystal structure of the RC from *Rb. sphaeroides* (Allen *et al*. 1987; Ermler *et al*. 1994), the modeled structure of LH-I from *Rb. sphaeroides*, and the crystal structure of LH-II from *Rs. molischianum* with a comparison to the crystal structure of LH-II from *Rps. acidophila*.

2.1 Organization of the bacterial PSU

It has been firmly established that the bacterial PSU consists of multiple pigment–protein complexes, including the RCs, LH-Is and LH-IIs. However, the inter-complex organization of RCs, LH-Is and LH-IIs inside the PSU is currently a matter of hot debate (Papiz *et al*. 1996; Nagarajan & Parson, 1997; Westerhuis *et al*. 1998). Figure 3 depicts two proposed models for the bacterial PSU, denoted model A and model B, that are based on low-resolution

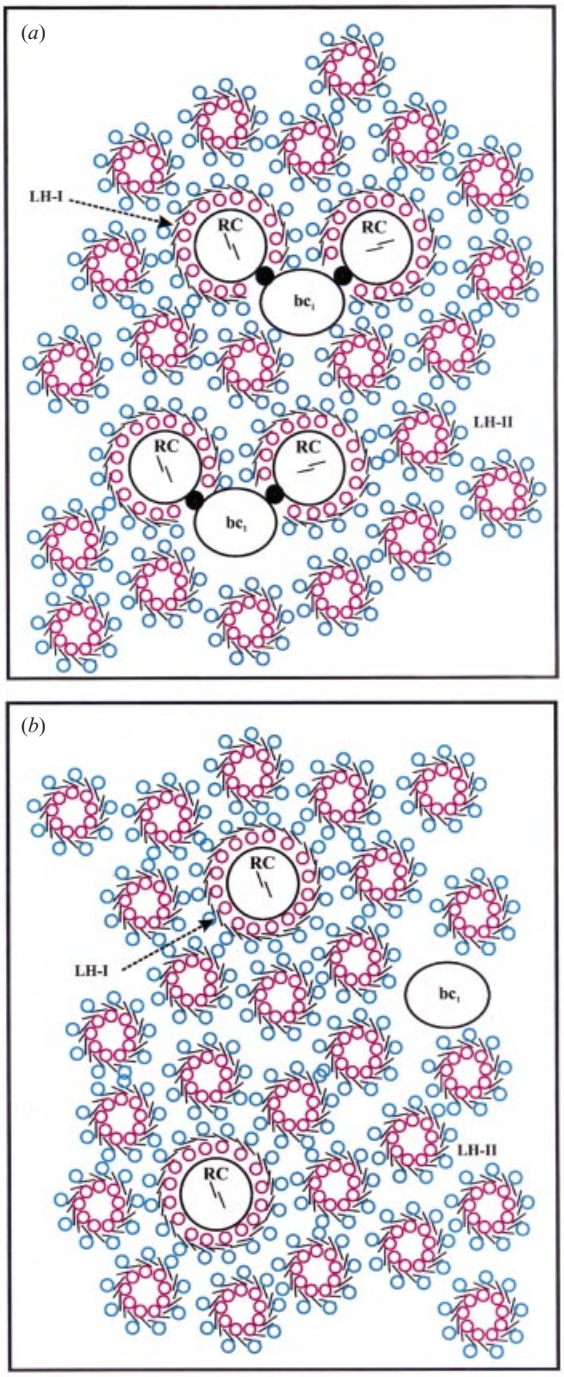

Fig. 3. Proposed models of the bacterial PSU. (*a*) Model A: PSU according to Niederman (Westerhuis *et al*. 1998) and Parson (Monger & Parson, 1977; Nagarajan & Parson, 1997). A pair of RCs, each surrounded by an open circle LH-I, associate with the cytochrome bc_1 complex (bc_1) to form the core of the PSU. The core is in turn surrounded by peripheral antenna complexes (LH-IIs). The small circles represent transmembrane helices with BChls sandwiched in between. Also shown is the PufX protein (solid dot) located between RC and bc_1. (*b*) Model B: PSU as proposed by Cogdell and colleagues (Papiz *et al*. 1996). An isolated RC is surrounded by a closed-circle LH-I complex to form the core of the PSU that is in a pool of LH-IIs. Also shown is the cytochrome bc_1 complex (bc_1).

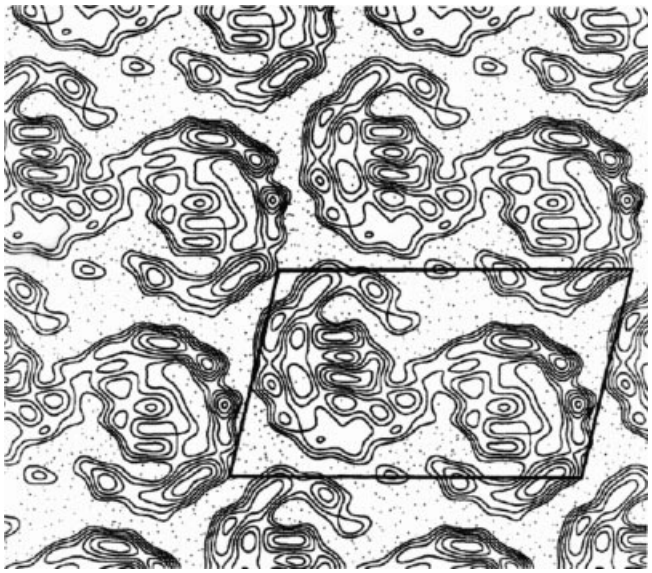

Fig. 4. Projection map of negatively stained native tubular flat membrane from *Rb. sphaeroides* at 20 Å resolution after processing and averaging (adapted from fig. 4B of Jungas *et al*. 1999). The unit cell ($a = 198$ Å, $b = 120$ Å and $\gamma = 103°$) is outlined in black. Positive density representing the protein is shown as solid lines and negative density as dotted lines.

electron microscopic projection maps and spectroscopic analyses (Papiz *et al*. 1996; Nagarajan & Parson, 1997; Westerhuis *et al*. 1998). The two models of bacterial PSU in the figure display significant differences in two major aspects: (1) the monomeric LH-I–RC complex is completely surrounded by LH-IIs in model B, whereas in model A pairs of RCs are clustered together; (2) in model A, LH-I forms an open-ring structure that allows shuffling of quinone between the RC and the cytochrome bc_1 complex, while in model B LH-I forms a closed circular structure.

Model A is based on fluorescence yield and singlet–singlet annihilation measurements of phospholipid-enriched *Rb. sphaeroides* chromatophores (Westerhuis *et al*. 1998). This model is in apparent agreement with the supercomplex model of the photosynthetic electron transfer chain in terms of the dimeric association of the RCs (Joliot *et al*. 1989). Evidence in favor of Model A appeared in newly reported electron micrographs of purified tubular membranes from *Rb. sphaeroides* (Jungas *et al*. 1999; Vermeglio & Joliot, 1999). It was found that the tubular membrane contains all the components of the photosynthetic apparatus, with a relative ratio of one cytochrome bc_1 complex: two RCs: $\sim$ 48 LH-I BChls (Jungas *et al*. 1999). Shown in Fig. 4 is the 20 Å resolution electron microscopic projection map of a negatively stained native tubular membrane from *Rb. sphaeroides* as reported in Jungas *et al*. (1999). The unit cell contains an elongated **S**-shaped supercomplex with a pseudo-twofold symmetry. Jungas *et al*. (1999) interpreted the map to mean that each supercomplex is composed of LH-Is that take the form of two **C**-shaped structures of $\sim$ 112 Å in external diameter, facing each other on the open side and enclosing the two RCs. Such a model allows shuffling of quinone between the RC and cytochrome bc_1 complex. Unfortunately, the location of the bc_1 complex can not be positively identified in this projection map due to a weak signal arising from a

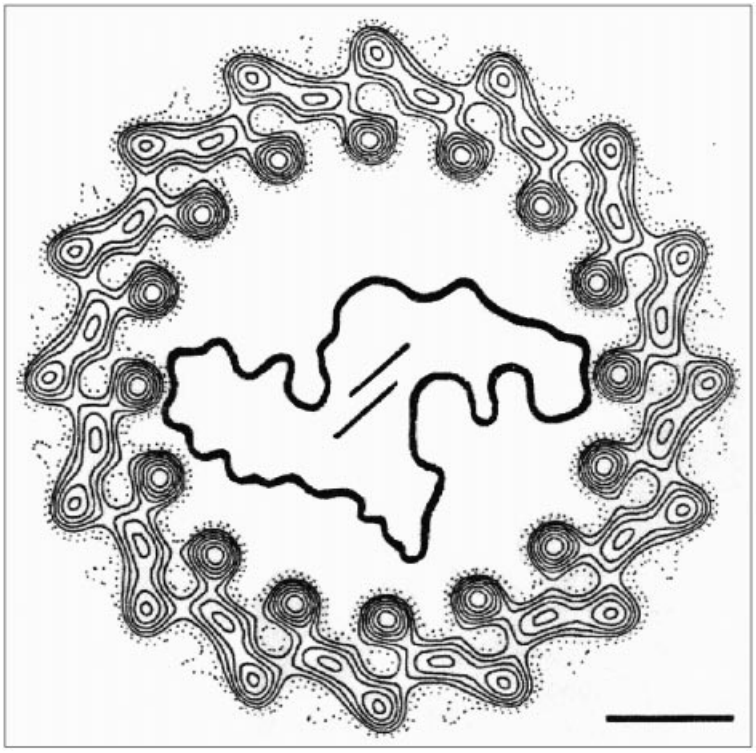

Fig. 5. The measured 8·5 Å electron microscopic projection map (black) of LH-I of *Rs. rubrum* (reproduced from Karrasch *et al*. 1995). Contours are in steps of 0·3 × r.m.s. density; scale bar represents 20 Å. The overall dimension of the cell is 120 × 120 Å.

technical difficulty: the stain used does not penetrate to the periplasmic side of the membrane where most of the extramembranous parts (Rieske protein and cyt C_1) of the bc_1 complex are located (Jungas *et al*. 1999).

Model B is based on spectroscopic observations (Deinum *et al*. 1991) and an 8.5 Å resolution electron micrograph for LH-I, which has been determined from a two dimensional (2D) crystal of the reconstituted LH-I of *Rs. rubrum* by Karrasch and colleagues (Karrasch *et al*. 1995; Papiz *et al*. 1996; Pullerits & Sundström, 1996; Hu *et al*. 1997). The electron microscopic electron density projection map, reproduced in Fig. 5, showed LH-I as a ring of 16 subunits. The ring has a diameter of 116 Å with a 68 Å hole in the center which, as pointed out by Karrasch *et al*. (1995), is large enough to incorporate a RC *in vivo*. A recent report of an electron micrograph of a 2D crystal of the LH-I–RC complex from *Rs. rubrum* further confirms the location of the RC in the center of LH-I (Walz & Ghosh, 1997). Questions have been raised as to whether the dissociation and reconstitution process employed, e.g. in Karrasch *et al*. (1995), introduces artifacts that render the reconstituted LH-Is of *Rs. rubrum* (Karrasch *et al*. 1995) an artificial variant of native LH-Is. These concerns were alleviated by the observation that the 2D crystal of the LH-I–RC complex, formed under much milder crystallization conditions under which no dissociation of the LH-I–RC complex can be detected, displayed the same LH-I ring size as the reconstituted LH-I (Walz & Ghosh, 1997). Furthermore, the gross morphology of the core PSU, which consists of a central core RC

surrounded by an LH-I ring, is consistent with earlier models of the PSU for both BChl *b*- and BChl *a*-containing bacteria based upon electron microscopy and image processing (Miller, 1982; Stark *et al*. 1984; Engelhardt *et al*. 1986; Meckenstock *et al*. 1992; Boonstra *et al*. 1994). Recently reported electron micrographs of the LH-I–RC complex from *Rp. viridis* and *Rb. sphaeroides* also indicated a single RC inside a closed ring of the LH-I (Ikeda-Yamasaki *et al*. 1998; Walz *et al*. 1998). However, the latest analysis of electron microscopic projection maps of 2D crystals of the LH-I–RC complex from *Rs. rubrum* by the Ghosh group suggested that, in carotenoid-less mutants, the LH-I–RC complex may have a non-circular symmetry (Stahlberg *et al*. 1998).

2.2 The crystal structure of the RC

The best known structural components of the bacterial PSU are LH-II and the RC. We will briefly outline the crystal structure of the RC from *Rb. sphaeroides* which is the only BChl *a*-containing species for which a high-resolution crystal structure of the RC is known (Chang *et al*. 1986; Allen *et al*. 1987; Ermler *et al*. 1994). The other known bacterial RC structure is from a BChl *b*-containing species *Rps. viridis* (Deisenhofer *et al*. 1985). As shown in Fig. 6, the RC from *Rb. sphaeroides* contains three protein subunits, known as L (light), M (medium), and H (heavy), respectively. The L- and M-subunits are homologous and are related by a pseudo-twofold circular symmetry. Multiple pigment molecules (cofactors) are bound to the L- and M-subunits, and are arranged accordingly in two symmetric branches, commonly referred to as A branch and B branch: two BChls which form a strongly interacting dimer constituting the so-called special pair (P_A, P_B), two accessory BChls in close proximity to the special pair (B_A, B_B), two bacteriopheophytins (H_A, H_B), and a pair of quinones (Q_A, Q_B) (Chang *et al*. 1986; Allen *et al*. 1987; Ermler *et al*. 1994).

Upon excitation of the RC special pair, a multi-step charge separation process is initiated. Since we are mainly concerned with the light-harvesting process and no further explanation of the electron transfer process will be attempted, we see it fit here to give a brief description of the electron transfer process. For readers interested in the subject, this primary process of charge separation has been studied extensively and was the subject of numerous review articles (Clayton, 1966, 1973; Deisenhofer & Michel, 1991; Breton & Verméglio, 1992; Deisenhofer & Norris, 1993; Fleming & van Grondelle, 1994; Lancaster *et al*. 1995; Parson & Warshel, 1995; Woodbury & Allen, 1995; Michel-Beyerle, 1996; Hoff & Deisenhofer, 1997; Bixon & Jortner, 1999).

It has been determined through X-ray crystallographic analysis and spectroscopic measurement that electron flow in the photosynthetic bacteria is cyclic. In addition to the photosynthetic RC, other electron carriers are involved in the cyclic flow, including a mobile quinone pool, a cytochrome bc_1 oxidoreductase, and a mobile cytochrome *c* molecule. Upon excitation, an electron within the special pair (P_A, P_B) is promoted to an excited state. This electron is transferred, through the accessory BChl (B_A), to the bacteriopheophytin (H_A) in 2–3 ps. The reduced bacteriopheophytin (H_A^{-1}) donates an electron to the adjacent quinone molecule (Q_A) in about 200 ps. The Q_A in turn passes an electron to the Q_B molecule in 200 μs, converting Q_B to a semiquinone radical. In the mean time, the positively charged special pair is neutralized by the transfer of an electron from a reduced cytochrome c_2 molecule on the periplasmic side of the membrane. A second photon is then absorbed by the special pair, and the flow of a second electron to Q_B takes place. With the acceptance of two

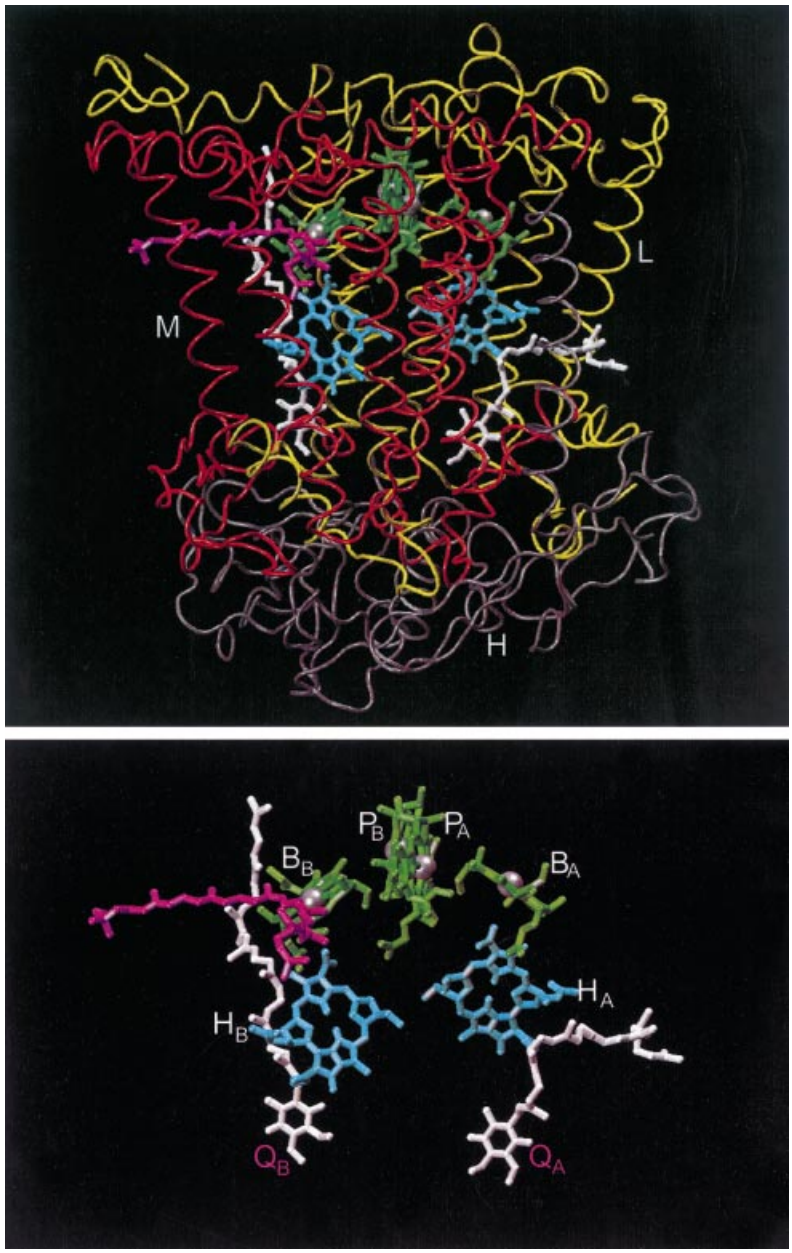

Fig. 6. Structure of the photosynthetic RC of *Rb. sphaeroides* (Ermler *et al.* 1994). (*a*) The protein subunits are represented as C_α traces with the L-, M- and H-subunits of the RC in yellow, red and gray, respectively. (*b*) Chromophores are represented in a licorice representation with the following label and color coding: RC special pair (P_A, P_B, green), accessory BChls (B_A, B_B, green), bacteriopheophytins (H_A, H_B, cyan), quinones (Q_A, Q_B, white), and a carotenoid molecule (magenta). The van der Waals spheres show the position of the central Mg^{2+} atoms of BChls. The phytol tails of BChls and bacteriopheophytin are omitted for clarity.

electrons by Q_B, the quinone molecule is reduced to the quinol form (H_2Q) by the simultaneous uptake of two protons from the cytoplasmic side of the membrane. This H_2Q molecule is then released from the RC into a mobile pool of quinones. The electron transfer

cycle is completed by the oxidation of quinol by the cytochrome bc_1 oxydoreductase, which results in the release of protons on the periplasmic side of the membrane and production of a reduced cytochrome c_2. Translocation of protons from the cytoplasmic side to the periplasmic side produces a proton gradient (proton-motive force) that drives ATP synthesis at the ATP synthase (Frenkel, 1954; Abrahams *et al*. 1994). These processes are also summarized in Fig. 1.

2.3 The crystal structures of LH-II

All the bacterial LHs are constructed in a remarkably similar fashion (Zuber, 1985; Zuber & Brunisholz, 1991). The basic structural unit is a heterodimer of two short peptides (transmembrane helices), commonly referred to as α-apoprotein and β-apoprotein; the two helices, in aggregating into the heterodimer, bind non-covalently BChls and carotenoids. Several heterodimers form the LHs in the form of large oligomers. The size of the complexes differs for LH-I and LH-II and is species dependent. LH-IIs from *Rps. acidophila* and *Rhodovulum sulfidophilum* were determined by electron microscopy (Savage *et al*. 1996) and X-ray crystallography (McDermott *et al*. 1995) to be nonamers of the $\alpha\beta$-heterodimers. The latest electron microscopy data suggest that LH-II from *Rb. sphaeroides* is also a nonamer (Walz *et al*. 1998). Sedimentation equilibrium experiments indicated that the LH-II complex from *Rs. molischianum* is an octamer (Kleinekofort *et al*. 1992), which is consistent with its crystal structure (Koepke *et al*. 1996).

The structures of LH-IIs from *Rps. acidophila* and *Rs. molischianum* had been determined by means of X-ray crystallography (Koepke *et al*. 1996) to 2·5 and 2·4 Å resolution, respectively. We will first describe the crystal structure of LH-II from *Rs. molischianum*, followed by a brief discussion of major differences between the two crystal structures. As shown in Fig. 7, the LH-II complex from *Rs. molischianum* is an octameric aggregate of $\alpha\beta$-heterodimers; the latter contains a pair of short peptides (α- and β-apoproteins) non-covalently binding three BChl *a* molecules and one lycopene (a specific type of carotenoid). Presumably, there exists a second lycopene for each $\alpha\beta$-heterodimer. The electron density map indeed contains a stretch of assignable density, but not long enough to positively resolve the entire lycopene (Koepke *et al*. 1996). Two concentric cylinders of α-helices, with the α-apoproteins inside and the β-apoproteins outside, form a scaffold for BChls and lycopenes.

Figure 8 depicts the arrangement of 24 BChl molecules in LH-II with all other components stripped away. Sixteen B850 BChl molecules form a continuous overlapping ring of 23 Å radius (based on central Mg^{2+} atoms of BChls) with each BChl oriented perpendicular to the membrane plane. Eight B800 BChls, forming another ring of 28 Å radius, are arranged with their tetrapyrrol rings nearly parallel to the membrane plane. The ligation sites for the B850 BChl are α-His34 and β-His35, while the B800 BChls ligate to α-Asp6.

The LH-II from *Rps. acidophilia* displays a similar ring shape aggregate of the $\alpha\beta$-heterodimers as that of *Rs. molischianum*, but differs in size of the ring. The LH-II from *Rps. acidophilia* contains nine $\alpha\beta$-heterodimers instead of eight as in the LH-II from *Rs. molischianum*. Essential differences are observed in the orientation of B800 BChl *a*. The Q_y-transition moment of B800 BChl *a* of *Rs. molischianum* is in an orientation parallel to the respective transition moment of the B850 BChl *a* attached to the same apoproteins, whereas the corresponding transition dipole moments are nearly perpendicular in *Rps. acidophila*. Binding sites of B800 BChl *a* in both LH-IIs are unique. Most frequently, the Mg^{2+} atoms

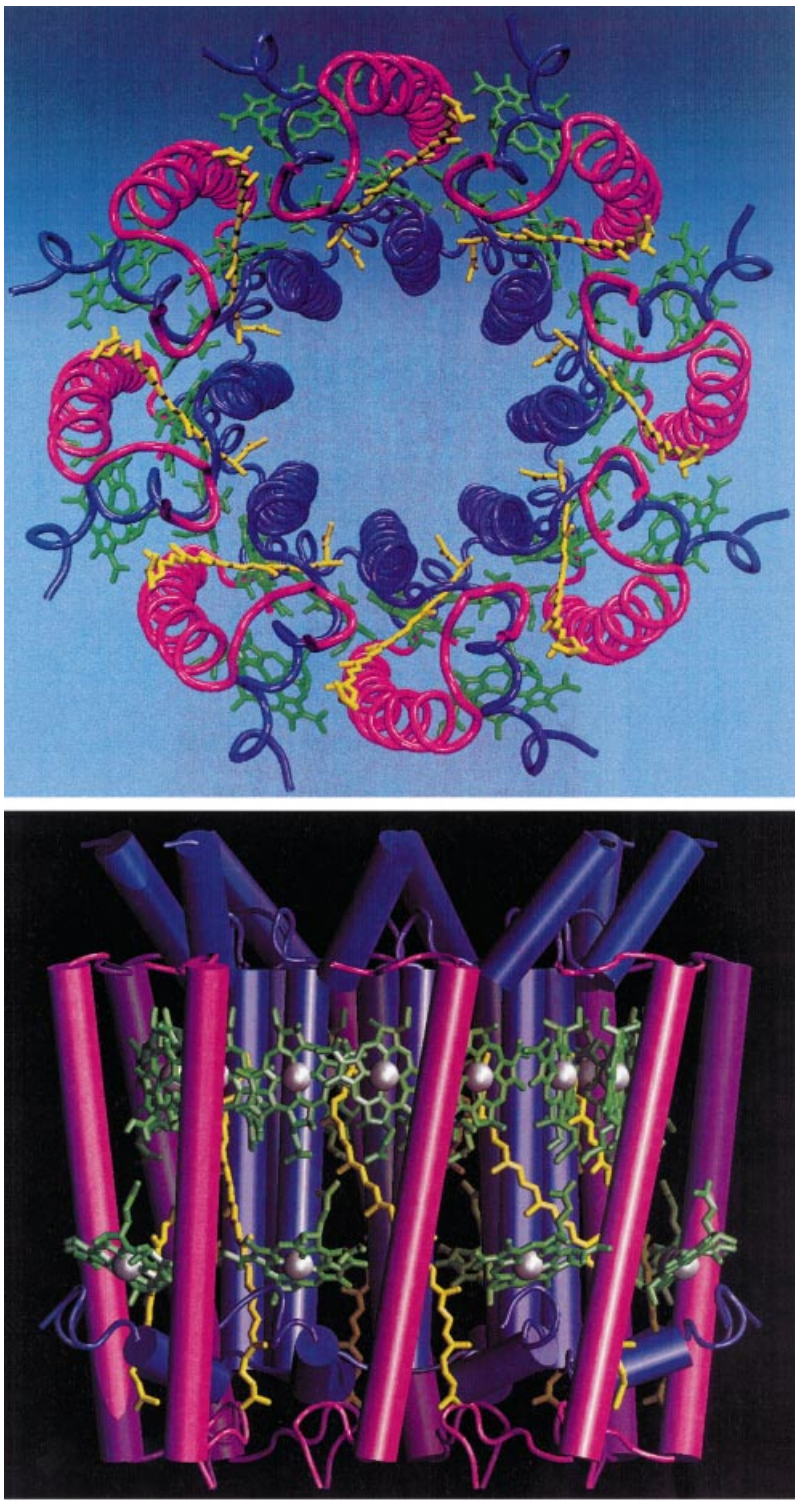

Fig. 7. The LH-II octameric complex from *Rs. molischianum*. (*a*) Top view with N-termini pointing upward, the apoproteins are represented as C_α tracing tubes with the α-apoproteins (inside) in blue and the β-apoprotein (outside) in magenta. The BChl *a* molecules are in green with phytyl tails truncated

of chlorophyll molecules are ligated by histidine residues. However, the B800 BChl *a* of LH-II from *Rs. molischianum* is ligated to $O_{\delta 1}$ of α-Asp6; in proximity (2·74 Å) to $O_{\delta 1}$, a water molecule is located. In the LH-II of *Rps. acidophila* the ligand of B800 BChl *a* was originally assigned to a formyl-methionine, but its final assignment awaits more analysis based on higher resolution data. Although two LH-IIs contain different carotenoid molecules (lycopene in *Rs. molischianum versus* rhodopin glucoside in *Rps. acidophila*), the overall arrangement of carotenoid molecules (orientation and position) in the respective crystal structures is very similar.

It is remarkable that LH-II, as an aggregate of multiple identical $\alpha\beta$-heterodimers, can adopt different ring sizes to fulfill its light-harvesting function in nearly the same manner. The absorption spectra of both LH-II of *Rps. acidophila* and LH-II of *Rs. molischianum* display similar characteristic B800 and B850 bands (Germeroth *et al*. 1993; Leguijt *et al*. 1992). Spectroscopic measurements suggest similar time constants for energy transfers involving LH-IIs of both *Rps. acidophila* and *Rs. molischianum* (Reddy *et al*. 1991; Wu *et al*. 1996; Ma *et al*. 1997). With its simple, symmetric architecture, LH-II constitutes an ideal model system for studying aggregate formation and adhesive interactions of proteins. Mechanical models reveal perfect self-complementarity of the $\alpha\beta$-heterodimers which interlock with each other forming a circular aggregate (Bailey *et al*. 1998).

2.4 Bacteriochlorophyll pairs in LH-II and the RC

BChls tend to form closely coupled aggregates in nature. The size of the aggregate varies, ranging from two in the RC special pair to 16 and 18 in the B850 BChl ring of the LH-IIs from *Rs. molischianum* and *Rps. acidophila*, respectively. The fundamental unit of the bacteriochlorophyll aggregate is the nearest-neighbor BChl pair. Given the circular aggregate of B850 BChls in LH-II, there are two types of BChl pairings, i.e. a intra-dimer BChl pair and a inter-dimer BChl pair. As shown in Fig. 8, each $\alpha\beta$-heterodimer contains three BChls: B800, B850a and B850b (in the ellipse enclosed by a solid line). We denote by B850a the B850 BChl binding to the α-apoprotein, and by B850b the B850 BChl binding to the β-apoprotein (see Fig. 8). BChl 850a′ is bound to the α-apoprotein of the (left) neighboring heterodimer. For the intra-dimer BChl pair (B850a and B850b) in the LH-II from *Rs. molischianum*, the Mg^{2+}–Mg^{2+} distances measure 9·2 Å. For the inter-dimer BChl pair (B850a′ and B850b), the Mg^{2+}–Mg^{2+} distances measure 8·9 Å.

Figure 9 compares the structural arrangement of the intra-dimer B850 BChl pair (top) with the inter-dimer B850 BChl pair of LH-II from *Rs. molischianum* (middle), as well as the RC special pair from *Rb. sphaeroides* (bottom). The three BChl pairs display distinctively different conformations. In the intra-dimer B850 BChl pair, ring III and ring V (see Fig. 8*b*) of one BChl overlap with those of the other BChl in the opposite direction. The tetrapyrrol planes of the two BChls are nearly parallel to each other with a crossing angle of 167·0° between the plane normals. The positive direction of the plane normal (white arrow in Fig. 9) is defined according to Fig. 8 such that the arrow of the plane normal points downwards in the direction perpendicular to the plane of paper. In the inter-dimer B850 BChl pair, ring I of one BChl

---

for clarity. The lycopenes are in yellow. (*b*) Side view, same color as in (*a*) with the α helical segments represented as cylinders. [Produced with the program VMD (Humphrey *et al*. 1996) and then rendered with Rayshade.]

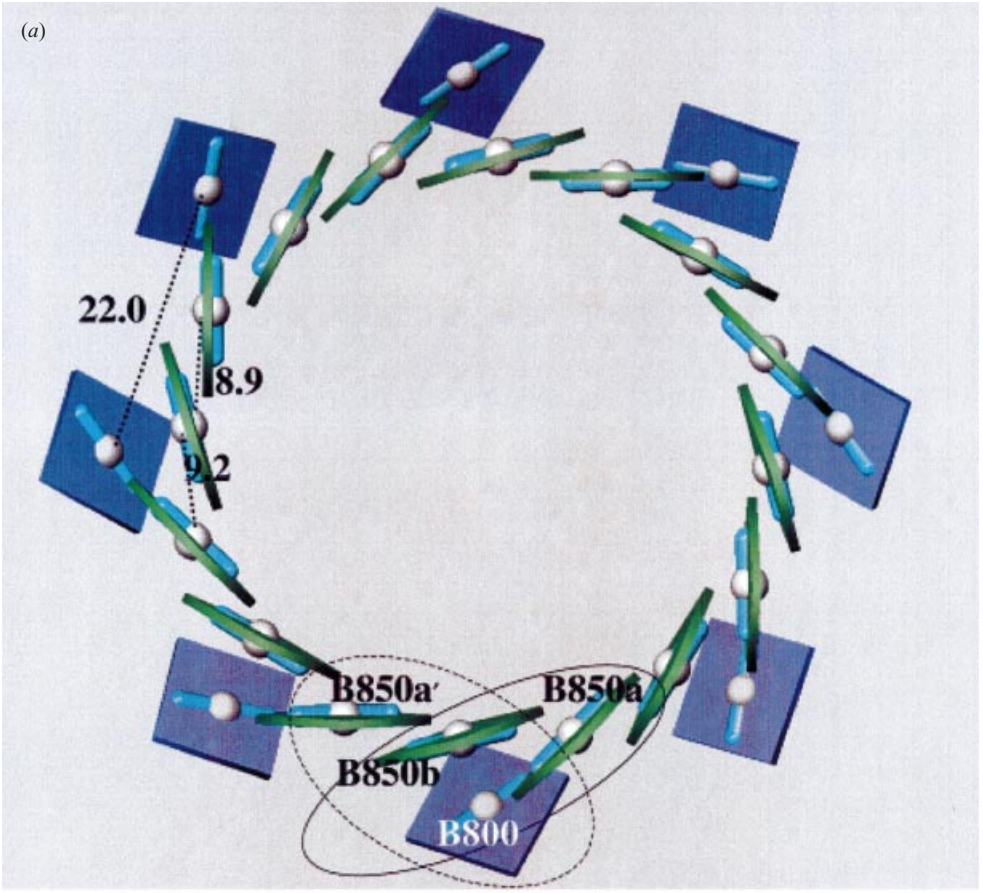

Fig. 8. For legend see opposite.

overlaps with that of the other BChl in the opposite direction. The tetrapyrrol planes of the two BChls are much more tilted against each other, with a crossing angle of 147·9° between the plane normals.

In the RC special pair, the tetrapyrrol planes of the two BChls are nearly parallel to each other with a crossing angle of 175·9°. Rings I of the two BChls overlap with each other with a much closer atom to atom distance in comparison with the ring I overlap of the inter-dimer B850 BChl pair. Furthermore, a careful examination of Fig. 9 indicates that binding of histidine residues to the central Mg^{2+} atoms of BChls in the RC special pair is totally different from the B850 BChls. Again, we use Fig. 8*b* as a reference. In the RC special pair, the histidine residues bind the BChl molecules from down under the plane of figure whereas in the B850 BChls the histidine residues bind the BChl molecules from on top of the plane of figure. The significance of this difference is not clear at the moment. One consequence of this difference in BChl ligand binding is that the hydrogen-bonding of the histidine residues in the RC special pair is sterically hindered. As noted before (Hu & Schulten, 1998), in LH-II from *Rs. molischianum* the two histidine residues α-His34 and β-His35, which bind the central Mg^{2+} atoms of the B850 BChls, can actually be involved in hydrogen bonding of the 13^1-keto group (see Fig. 8*b*) of the B850 BChls. As illustrated in Fig. 9, the distance between the $N_{\delta 1}$ atom of β-His35 and the 9-keto oxygen of B850a BChl measures 3·6 Å and the distance between the $N_{\delta 1}$ atom of α-His34 and the 13^1-keto oxygen of B850b BChl is also 3·6 Å.

2.5 Models of LH-I and the LH-I–RC complex

The current inability of the photosynthetic research community to resolve the differences between the two PSU models (see above) stems from the limitation of low-resolution electron microscopic data in resolving atomic level details (Karrasch *et al*. 1995; Walz & Ghosh, 1997; Walz *et al*. 1998; Ikeda-Yamasaki *et al*. 1998; Walz & Grigorieff, 1998). Although tremendous progress has been made in advancing the electron microscopy technique for macromolecular imaging in recent years (Walz & Grigorieff, 1998), this difficulty of limited resolution may not be easily overcome for many years to come.

Molecular modeling has proven to be a valuable tool in bridging this gap in structural resolution (Schlick *et al*. 1999; Hu *et al*. 1998). Modeling of the 3D structure of the photosynthetic membrane has complemented X-ray crystallography and electron microscopy in providing the structural organization of the pigment–protein complexes.

According to Model B, LH-I of *Rb. sphaeroides* has been modeled in Hu & Schulten (1998) as a hexadecamer of $\alpha\beta$-heterodimers; the modeling exploited a close homology of these heterodimers to those of LH-II from *Rs. molischianum*. The resulting LH-I structure yields an electron density projection map that is in agreement with an 8·5 Å resolution electron

---

Fig. 8. Arrangement of BChls in LH-II of *Rs. molischianum* (Koepke *et al*. 1996). BChls are represented as squares; 16 B850 BChls (gray) are arranged in the inner ring and 8 B800 BChls (black) in the outer ring. Bars connected with the BChls represent the Q_y transition dipole moments of individual BChls, and the van der Waals spheres show the position of the central Mg^{2+} atoms of BChls. Representative distances between central Mg^{2+} atoms of B800 BChl and B850 BChl are indicated (in Å). The Cartesian coordinate system is set up such that the eightfold symmetrical axis of the LH-II complex coincides with the z axis, and the x, y axes are in the plane of the paper. (*b*) Schematic drawing of BChl *a* with the phytyl tail (R) truncated for clarity. The carbon numbering system is that approved by IUPAC-IUB [IUPAC-IUB Joint Commission on Biochemical Nomenclature (JCBN), 1986]. [This figure has been produced with the program VMD (Humphrey *et al*. 1996).]

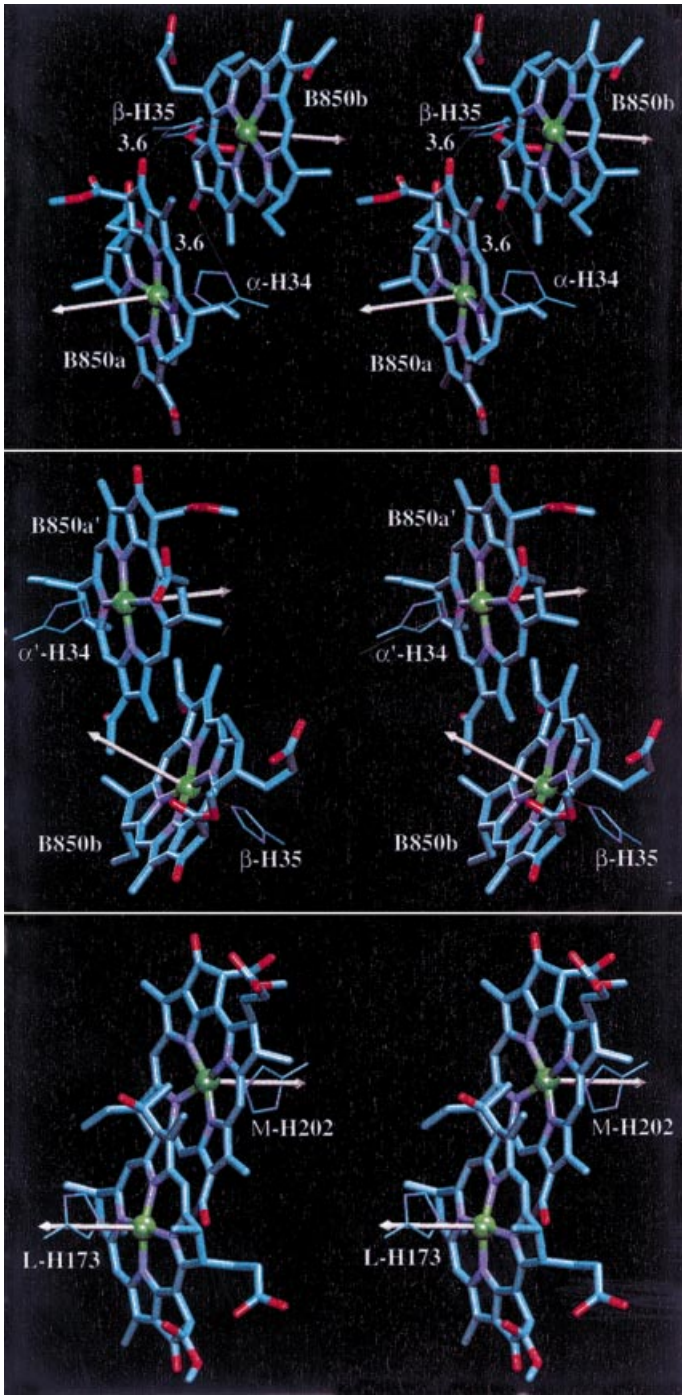

Fig. 9. Stereographic images of BChl *a* pairs based on the crystal structure of LH-II from *Rs. molischianum* and the crystal structure of the RC from *Rb. sphaeroides*. BChls are represented in a licorice representation with an atomic color coding scheme of C (cyan), N (Blue) and O (red). Green spheres represent the central Mg^{2+} atoms. Red dashed lines represent the metal ligation bond between Mg^{2+} and the N atom of histidine, and white dashed lines represent potential hydrogen bonds (see text). Also shown are histidine residues that are ligands of the central Mg^{2+} atoms of BChl *a*. The white arrow

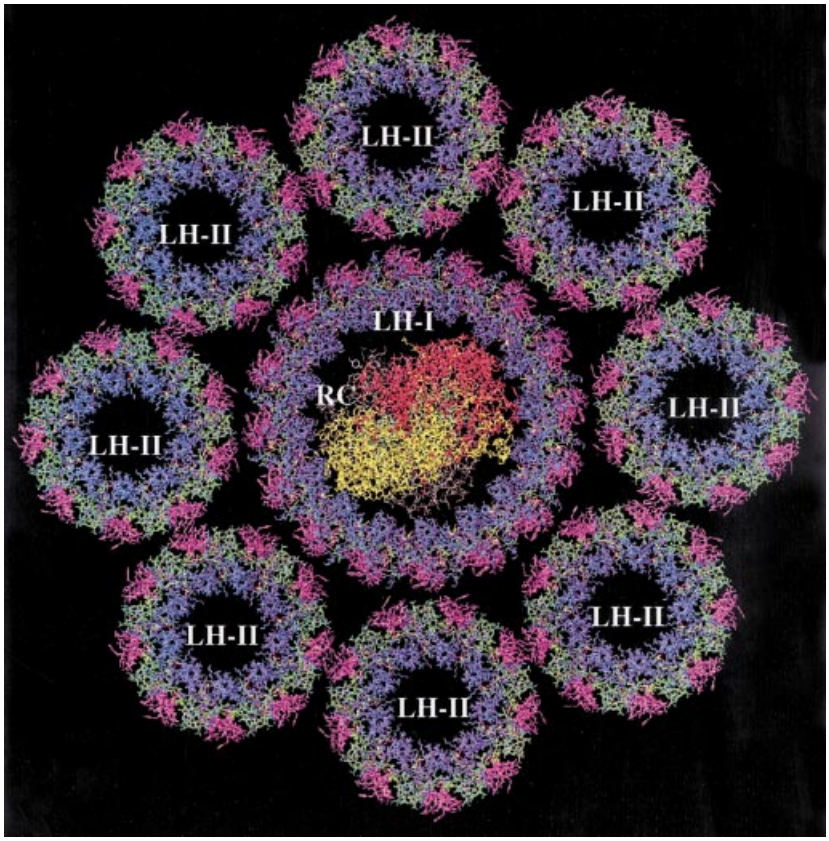

Fig. 10. Arrangement of pigment–protein complexes in the modeled bacterial photosynthetic unit (PSU) of *Rb. sphaeroides*. α-Apoproteins of both LH-I and LH-II are colored in blue and β-apoproteins in magenta, and the L-, M-, H-subunits of RC in yellow, red, gray, respectively. All the BChls are shown in green, and carotenoids in yellow. [Produced with the program VMD (Humphrey *et al.* 1996).]

microscopy projection map for the highly homologous LH-I of *Rs. rubrum* (Karrasch *et al.* 1995). The LH-I contains a ring of 32 BChls referred to as B875 BChls according to their main absorption band. The Mg^{2+}–Mg^{2+} distance between neighboring B875 BChls is 9·2 Å within the $\alpha\beta$-heterodimer and 9·3 Å between neighboring heterodimers.

The modeled LH-I has been docked to the photosynthetic RC of *Rb. sphaeroides* by means of a constrained conformational search (Hu & Schulten, 1998), employing for the latter the structure reported in (Ermler *et al.* 1994).

2.6 Model for the PSU

Figure 10 presents a model of the PSU for *Rb. sphaeroides*. Only eight LH-IIs are shown. The actual photosynthetic apparatus can contain up to about ten LH-IIs around each LH-I, with the number of LH-IIs varying according to growth conditions such as light intensity and

represents the normal of the BChl plane; the positive direction of the plane normal is defined according to Fig. 8 such that the arrow of the plane normal points downwards in the direction perpendicular to the plane of figure. *Top*: intra-dimer BChl *a* pair; *middle*: inter-dimer BChl *a* pair; *bottom*: RC special pair.

temperature. The unit has been constructed using the modeled LH-I–RC complex from *Rb. sphaeroides* (Hu & Schulten, 1997; Hu *et al*. 1997), and a model structure of LH-II from *Rb. sphaeroides*. Since electron microscopy observations suggest that the LH-II of *Rb. sphaeroides* contains nine $\alpha\beta$-heterodimers (Walz *et al*. 1998), instead of eight as in the LH-II of *Rs. molischianum*, LH-II of *Rb. sphaeroides*, as shown in Fig. 10, has been constructed as a nanomer of $\alpha\beta$-heterodimers by means of homology modeling using the $\alpha\beta$-heterodimer of LH-II from *Rp. acidophila* as a template. For this purpose, the modeling protocol developed and successfully applied previously (Hu *et al*. 1995a; Koepke *et al*. 1996; Hu & Schulten, 1998) was utilized.

3. Excitation transfer in the PSU

The PSU is a protein aggregate of overwhelming complexity. The task of connecting its structure to the light-harvesting/excitation funneling function, as depicted in Fig. 2, appears formidable. However, it is the chromophores that carry out the function of photon fueling and excitation transfer; the proteins in the PSU serve mainly a structural role, as a scaffold for the chlorophyll and carotenoid chromophores. In Fig. 11, the arrangement of chromophores without the surrounding protein components is shown for a minimal PSU, which contains the LH-I–RC complex and only three of the surrounding LH-IIs in the PSU. One can discern a hierarchical aggregate of the BChls, organized into rings of 18 closely coupled (B850) and nine loosely coupled (B800) BChls in the peripheral LH-IIs surrounding a large ring of 32 closely coupled (B875) BChls of LH-I which in turn surrounds four chlorophylls of the RC. Close proximity of carotenoids with BChls in LHs can also be recognized.

The two most prominent features of the pigment organization are the ring-like architecture of the BChl aggregate within individual pigment–protein complexes LH-II and LH-I, and the coplanar arrangement of the B850 BChls of LH-II, the B875 BChls of LH-I, as well as the RC special pair and the accessory BChls. An analysis of the LH-I and LH-II structures as reported in (Hu *et al*. 1997; Hu & Schulten, 1998) indicates that each BChl of the B850 ring of LH-II and of the B875 ring of LH-I is non-covalently bound to three side-chain atoms of the α- or β-apoprotein such that the BChls are held in a rigid orientation, underscoring the relevance of the arrangement shown in Fig. 11.

One may want to conclude at this point that the structural model implies an obvious answer to the question how photons are fueled into the BChl system and electronic excitation is funneled to the RC. The coplanar arrangement of the BChls and, consequently, of their transition dipole moments is optimal for excitation transfer between BChls. Pigments with higher excitation energies are located at the periphery of the system, thus ensuring the desired flow of electronic excitation LH-II $\rightarrow$ LH-I $\rightarrow$ RC. However, the intuitive appeal of the aggregate architecture in Fig. 11 can not be confused with a sound understanding, which requires that one applies the laws of physics to the chromophore aggregate shown, and investigates the emergent properties as well as their relationship to the function of the PSU. The efficient transfer of electronic excitation from the periphery to the center is hardly a foregone conclusion. The steps necessary to describe migration of excitation and to determine the overall efficiency of excitation trapping in the PSU are outlined in the following.

First, one must concede that the system of 200–300 BChls and about 100 carotenoids is too large to be described *ab initio* on the basis of quantum physics. The system needs to be divided

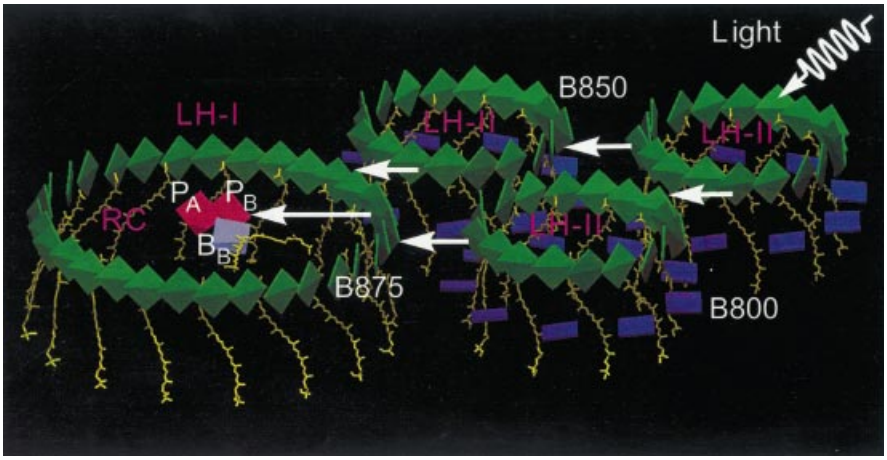

Fig. 11. Pigment organization in a minimum photosynthetic unit consisting of RC, LH-I and LH-II. BChls are represented as squares. LH-II contains two types of BChls, commonly referred to as B800 (dark blue) and B850 (green) which absorb at 800 and 850 nm, respectively. BChls in LH-I absorb at 875 nm and are labeled as B875 (green). P_A and P_B refer to the RC special pair, and B_A, B_B to the accessory BChls in the RC. The figure demonstrates the co-planar arrangement of the B850 BChl ring in LH-II, the B875 BChl ring of LH-I, and the RC BChls P_A, P_B, B_A, B_B [Produced with the program VMD (Humphrey *et al*. 1996).]

into components, with proper justification that the necessary division does not essentially alter relevant properties. Fortunately, the aggregate shown exhibits a distinct hierarchy of spatial and interaction energy scales. Chromophores within the individual LH-II, LH-I and RC units are spatially closer and likely more tightly coupled than are chromophores belonging to different units. If the latter assertion holds true, it allows one to separate excitation transfer between chromophores within one pigment–protein complex from excitation transfer between chromophores from different pigment–protein complexes. Thus, the individual pigment–protein complexes are natural components for a first division of the PSU. To divide these components into further subcomponents, one has to analyze the spatial arrangement of chromophores with a finer measure. In fact, only a part of the chromophores, the conjugated π-electron system, is directly involved in light absorption and excitation transfer. The relative arrangement of the conjugated systems, rather than that of the complete chromophores, is shown in Fig. 12 for the chromophores in LH-II.

One can discern that an individual pigment–protein complex can be divided in up to three types of subcomponents, namely B800 BChls (only present in LH-II), rings of BChls and carotenoids. The conjugated systems of B800 BChls are well separated from each other and from the ring of BChls and are likely well described as individual BChls. In contrast, the conjugated systems of BChls within the ring are in very close contact, as indicated by the overlapping surfaces in Fig. 12, suggesting that the entire ring of BChls should be described as a single system. The conjugated systems of carotenoids appear to be spatially separated far enough from BChls to justify their description as individual systems rather than as parts of a combined BChl–Car system. However, because of their close contact with several BChls, the resulting interaction requires a detailed description and the assumed separation of carotenoids from BChls requires special scrutinization. On the basis of the spatial arrangement depicted in Fig. 12, one can identify individual BChls, rings of BChls, and carotenoids as

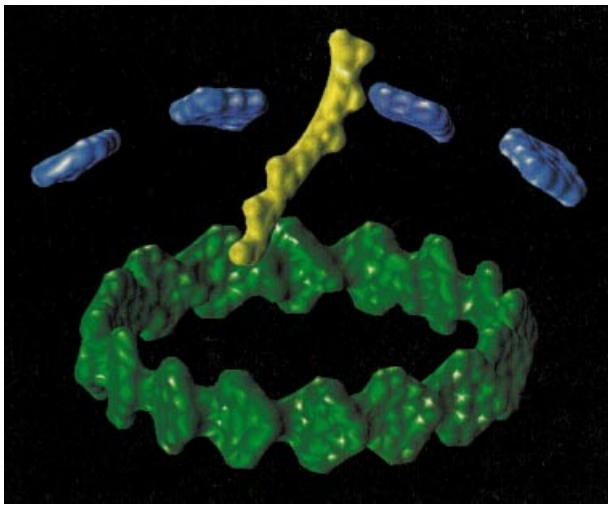

Fig. 12. Spatial arrangement of the conjugated π-electron systems of the chromophores within the LH-II complex from *Rs. molischianum*. The conjugated systems are represented in MSMS surface representation, generated with the program VMD (Humphrey *et al.* 1996). For clarity, only 4 of the 8 B800 BChls (blue) and 1 of the 8 carotenoids (yellow) present in LH-II are shown. The conjugated systems within the ring of B850 BChls (green) appear to be connected to each other. Conjugated systems of carotenoids are in close contact with B800 BChls and the B850 BChl ring. The spatial arrangement suggests that individual (B800) BChls, rings of BChls, and carotenoids can serve as three fundamental building blocks into which the PSU can be divided.

fundamental building blocks for the PSU. In the RC, the system of closely connected special pair BChls and accessory BChls can be considered to be a fourth kind of building block.

Having divided the PSU into the above-mentioned building blocks, one needs to describe their respective electronic excitations. However, even these building blocks are too large for a truly fundamental description. Rather, so-called semi-empirical descriptions need to be evoked or so-called *ab-initio* methods with a high degree of simplification, the choice of which implies also a strong empirical component. Since chlorophylls and carotenoids have been investigated intensely for decades by means of semi-empirical methods (Gouterman, 1961; Thompson & Zerner, 1991), one treads here on fairly safe ground. The most intriguing building blocks of the PSU are the rings of BChls. To understand the primary processes of light absorption and excitation transfer in the PSU, it is important to characterize the electronic and optical properties of the BChl rings upon electronic excitation. However, even the most extensive semi-empirical calculations can only describe excitations of the smaller B850 BChls rings in the PSU due to computational limitations. To overcome this limitation, one has to develop a less expensive description which recovers the essential features of electronic excitations in circular BChl aggregates. This can be achieved through a simple and intuitive effective Hamiltonian description (Hu *et al.* 1997).

With the knowledge of electronic excitations, the next step towards an understanding of the PSU is to describe the excitation transfer processes between the building blocks. An immediate problem arises. Radiationless excitation transfer processes, as they occur in the PSU, are mediated through the vibrational states of the participating molecules and thus require a description of the vibrational states associated with the respective electronic transitions. The computational and conceptual challenges involved in a description of the

vibrational states render a purely theoretical description difficult and such a description has been achieved only very recently (A. Damjanović *et al*. In Press). However, the application of the needed theory is very cumbersome. Fortunately, the theory of radiationless excitation transfer points to a way to circumvent the problem of describing the vibrational states. In determining the rate for an excitation transfer processes, one can separate the effect of the purely electronic transitions, described by an electronic coupling term, from the effect of the vibrational states, described by a spectral overlap integral. As shown by Förster (1965), the spectral overlap integral can be determined through measurement of the absorption and emission spectra of the participating molecules, which are both experimentally readily accessible quantities for chromophores. Such treatment assumes implicitly that excitation transfer processes are slow enough for the vibrational degrees of freedom to be in thermal equilibrium.

Theory can provide an estimate of the electronic coupling between chromophore moieties (chlorophylls, carotenoids), which is the essential quantity to describe the effect of geometries on the excitation transfer rates. The size of the couplings will also be a crucial test to determine whether the above division of the PSU into building blocks, based solely on observation of the structure, can be justified on theoretical grounds. As in the description of electronic excitations, the level of detail of the theory has to be adjusted to the size and spatial relation of the molecules involved. The most detailed theoretical description of electronic couplings is required for excitation transfer between the closely spaced carotenoids and BChls. For transfer between individual B800 BChls, the comparatively large distance between the chromophores allows one to evoke a multipolar approximation, leading to a much simplified description of electronic couplings. This description can then be extended to describe electronic couplings between rings of BChls.

With the theory to describe excitation transfer between all building blocks in the PSU, the description of their electronic excitations, the knowledge of the geometry, and spectroscopic information on absorption and emission, the rates for all excitation transfer steps in the PSU can be calculated (Damjanović *et al*. 1999). By combining the rates for all individual transfer steps into a Master equation, one can formulate a kinetic model of excitation migration in the PSU (Ritz *et al*. 2001). This kinetic model allows one to predict systemic properties of the complete PSU, such as the average time and the quantum yield of excitation trapping in the RC. The computational task involved in the suggested theoretical investigations is formidable and the results necessarily complex, but the investigations reported in (Damjanović *et al*. 1999; Ritz *et al*. 2001) have overcome the main obstacles. A further caveat lies in the fact that the structure shown in Figs 11 and 12 is a static, stroboscopic view, and a highly idealized one in regard to the symmetry of the individual units. The actual system may vary greatly from the crystal structures. For example, the LH-I ring surrounding the RC may actually be severely distorted in its shape by the RC or exhibit a **C**-shaped instead of a ring structure in some species (Jungas *et al*. 1999). Since LHs are most likely assembled in the membrane, a fraction of LHs may exhibit incomplete ring structures. Even complete rings may show static distortions from the idealized ring symmetry due to interactions with the membrane or neighboring LHs. The effect of static disorder on spectral properties of LHs has been described in (Sener & Schulten, In Press) and in the work referenced therein. Furthermore, the systems are subject to thermal motion which distort the imposed symmetries. The physical description achieved must be subjected to the above-mentioned distortions in order to discern what features of the description are robust against thermal motion and shape

changes. In a ground-breaking investigation (A. Damjanović *et al*. In Press) combining molecular dynamics simulations, quantum chemistry calculations, and an analysis in the framework of the polaron model with input from the afore-mentioned calculations, the spectral properties of a thermalized system of B850 BChls in LH-II from *Rs. molischianum* was successfully described.

3.1 Electronic excitations of BChls

3.1.1 Individual BChls

Electronic excitations of individual BChls have been determined through INDO-CIS calculations (Cory *et al*. 1998). The two lowest excitations are labeled Q_y and Q_x and are calculated to lie at 751 and 551 nm, respectively. The Q_y excitation is characterized by a strong transition dipole moment approximately along the so-called long *y*-axis which passes through the pyrrol rings I and III (cf. Fig. 8). A complete analysis of the INDO-CIS results reveals higher energy excitations corresponding to the Soret or B band. However, these states should not play a role for excitation migration since they are out of resonance with other relevant electronic excitations, but these states may absorb light and fuel its energy into the light-harvesting system. The INDO-CIS method had proved earlier to be satisfactory for the description of electronic excitations of chlorophylls (Thompson & Zerner, 1991). The energies of the Q-band excitations agree within 20 nm with those measured through absorption spectroscopy of BChls in solution. However, a shortfall of CIS methods is that they generally overestimate the size of Q_y transition dipole moments. For BChl *a*, the experimentally determined values of Q_y transition dipole moments range from 6·1 to 7·7 D (Sauer *et al*. 1966; Visscher *et al*. 1991; Pearlstein, 1992), the calculated value is 11 D (Cory *et al*. 1998). This error has to be taken into account when deriving conclusions about coupling strengths on the basis of CIS results, since coupling strengths are closely related to the transition dipole moments.

3.1.2 Rings of BChls

3.1.2.1 Exciton states

The B850 BChls of LH-II and the B875 BChls of LH-I can be represented as circular aggregates of $2N$ BChls where $N = 8$ for LH-II from *Rs. molischianum*, $N = 9$ for LH-II from *Rps. acidophila*, and $N = 16$ for LH-I from various species. Due to the dimerization of the BChls, reflected in the structures (McDermott *et al*. 1995; Koepke *et al*. 1996; Hu & Schulten, 1998) and interactions between electronic excitations of the individual BChls the BChl aggregates in LH-II exhibit only an N-fold symmetry.

Quantum chemical treatments of the B850 aggregate based on the coordinates of LH-II crystal structures have been carried out by several groups (Sauer *et al*. 1996; Alden *et al*. 1997; Cory *et al*. l998; A. Damjanović *et al*. In Press). For the most extensive calculation up to date, the semi-empirical INDO-CIS method (Cory *et al*. 1998) has been employed to describe the B850 hexadecamer from *Rs. molischianum* (Cory *et al*. 1998). Starting from the crystal structure, the phytyl tails of the BChls have been truncated to limit each BChl to 44 atoms. The B850 hexadecamer studied included 704 atoms and over 2000 electrons, the CI expansion included 4096 configurations.

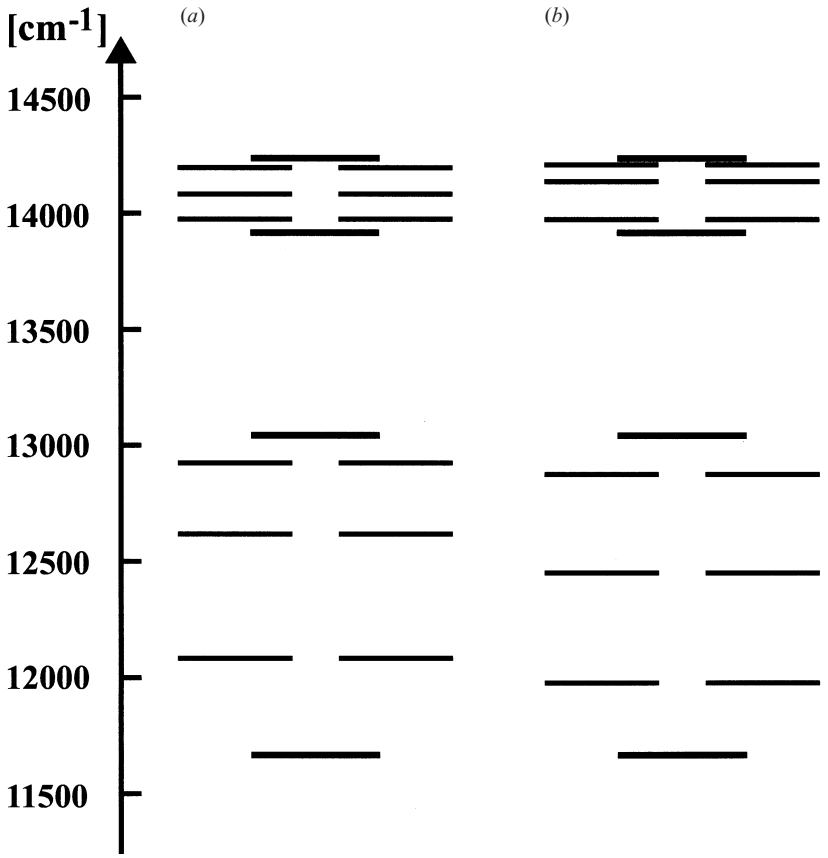

Fig. 13. (*a*) Low-energy part of the spectrum of the circular hexadecameric B850 BChl aggregate according to INDO-CIS calculations (Cory *et al.* 1998). (*b*) Spectrum of the same aggregate according to the effective Hamiltonian description (Hu *et al.* 1997).

The low energy part of the spectrum resulting for the ring of 16 B850 BChls is presented in Fig. 13(*a*). The energy levels are coherent superpositions of individual BChl excitations, so-called excitons (Knox, 1977). One can discern that the spectrum presented in Fig. 13 exhibits two bands of different width. The existence of two bands is due to the above mentioned dimerization of BChls, the difference in width is due to the influence of long-range interactions between non-neighboring BChls. The INDO-CIS calculation incorporated the influence of Q_y, Q_x and Soret excitations of individual BChls as well as of so-called charge resonance states. An analysis of the CI expansion of the states shows that the Q_y excitations of individual BChls have the dominating influence on the shape of the low-energy part of the spectrum displayed in Fig. 13. However, the interaction of Q_y excitations with the high-lying charge resonance states results in a noticeable depression of the lowest exciton state due to level repulsion.

The most significant characteristic of the exciton spectrum shown in Fig. 13 is the splitting of energy levels over a range of more than 2500 cm^{-1}. The presence of this so-called exciton splitting has far reaching implications for the excitation transfer properties of BChl rings. It enhances the spectral overlap of higher lying carotenoid or B800 excitations with the B850 or B875 BChl aggregates, and, thus, speeds up excitation transfer towards the BChl rings. The

excitation energies of individual BChls of the B850 system of LH-II from *Rs. molischianum* were calculated for every 2 fs time window of a molecular dynamics run (A. Damjanović *et al*. In Press). The resulting excitation energies and coupling energies were then used in a subsequent linear response theory as well as a polaron model description of the exciton system.

3.1.3 Effective Hamiltonian

Since the B850 BChl spectrum in Fig. 13(*a*) arises mainly from interactions between the BChl Q_y excitations of individual BChls, one may ask in how far a reduced description in terms of just these excitations would reproduce the INDO-CIS results in which thousands of other excitations have been accounted for. Such reduced description (Hu *et al*. 1997; Ritz *et al*. 1998b, 2001; Damjanović *et al*. 2000a; Sener & Schulten, In Press; A. Damjanović *et al*. In Press) can be formulated in terms of Q_y excitations of individual BChls,

$$|j\rangle = |\mathrm{BChl}_1\ \mathrm{BChl}_2 \cdots \mathrm{BChl}_j^* \cdots \mathrm{BChl}_{2N}\rangle \quad (j = 1, 2, \ldots, 2N), \tag{1}$$

Here, BChl_j^* describes the jth BChl being in the Q_y excited state, whereas all other BChls are in the electronic ground states.

An exciton state $\widetilde{|n\rangle}$ is then expressed as a linear superposition of the individual Q_y excitations $|j\rangle$,

$$\widetilde{|n\rangle} = \sum_{j=1}^{2N} c_{nj}|j\rangle. \tag{2}$$

The expansion coefficients c_{nj} are obtained by solving the eigenvalue problem of a $2N \times 2N$ effective Hamiltonian $\langle j|\hat{H}|k\rangle$. The diagonal elements $\langle j|\hat{H}|j\rangle = \epsilon$ account for the excitation energy of the Q_y state. For non-nearest-neighbor BChls j and k, associated interactions $\langle j|\hat{H}|k\rangle$ should be well approximated by dipole–dipole coupling terms

$$\langle j|\hat{H}|k\rangle = C\left(\frac{\mathbf{d}_j \cdot \mathbf{d}_k}{r_{jk}^3} - \frac{3(\mathbf{r}_{jk} \cdot \mathbf{d}_j)(\mathbf{r}_{jk} \cdot \mathbf{d}_k)}{r_{jk}^5}\right) \quad (k \neq j, \quad j \pm 1), \tag{3}$$

where $\mathbf{d}_j$ are unit vectors describing the direction of the transition dipole moments of the ground state $\rightarrow Q_y$ state transition of the jth BChl and $\mathbf{r}_{jk}$ is the vector connecting the centers of BChl j and BChl k. C is a parameter, yet unspecified, related to the dipole strength of the ground state $\rightarrow Q_y$ transition. The induced dipole–induced dipole coupling does not account well for interactions between neighboring BChls because the dipolar term is not the leading term for cases in which the extension of the molecules (5 Å) is only slightly smaller than the distance between the molecules (9 Å). Due to the N-fold symmetry of BChl aggregates, the respective matrix elements $\langle j|\hat{H}|j+1\rangle$ assume only two different values, namely, v_1 (v_2) for odd (even) j. The Hamiltonian is then specified through four parameters, ϵ, v_1, v_2, C. For the B850 hexadecamer of LH-II from *Rs. molischianum*, these parameters can be chosen such that the spectrum resulting from the matrix $\langle j|\hat{H}|k\rangle$ reproduces exactly the bandwidths, defined through the levels $\widetilde{|1\rangle}$, $\widetilde{|8\rangle}$, $\widetilde{|9\rangle}$, and $\widetilde{|16\rangle}$, from the spectrum of the full INDO-CIS calculation. The spectrum is shown in Fig. 13*b*. The corresponding parameters are $\epsilon = 13242\ \mathrm{cm}^{-1}$, $v_1 = 790\ \mathrm{cm}^{-1}$, $v_2 = 369\ \mathrm{cm}^{-1}$ and $C = 505644\ \text{Å}^3\ \mathrm{cm}^{-1}$.

It is not surprising that the effective Hamiltonian description does not reproduce the energy gap Δ between the lowest exciton state $\widetilde{|1\rangle}$ and the pair of degenerate exciton states $\widetilde{|2\rangle}$, $\widetilde{|3\rangle}$ well, since charge resonance states were not included in the description. The energy gap Δ measures only 225 cm^{-1} in the effective Hamiltonian picture, compared to 422 cm^{-1} in the INDO-CIS calculation. Apart from this feature, the spectrum from the INDO-CIS calculation is reproduced remarkably well by the effective Hamiltonian, especially if one takes into account that the effective Hamiltonian operates with a basis set which is almost three orders of magnitude smaller than that of the INDO-CIS Hamiltonian. It should be noted that the effective Hamiltonian description presented here is the minimal description which is required to reproduce the band widths from the INDO-CIS description. Effective Hamiltonian descriptions, in which the dimerization or non-nearest-neighbor interactions are neglected (Pearlstein & Zuber, 1985; Novoderezhkin & Razjivin, 1995; Hu *et al*. 1995b, Dracheva *et al*. 1996) will result in spectra with significant qualitative differences, such as the occurrence of only one band or of two symmetric bands. The effective Hamiltonian as described reflects the ideal symmetry of the B850 system of an LH-II ring at equilibrium. The effective Hamiltonian description can be naturally extended to account for non-symmetric LH-IIs. For example, one can assume an ensemble of LH-IIs, each described by effective Hamiltonians with different local excitation energies ϵ_j as done in Hu *et al*. (1997). One can assume random Hamiltonians in all matrix elements as studied systematically in Sener & Schulten (In Press). The latter study demonstrated that the spectral properties of random ensembles of effective Hamiltonians show universal properties, e.g. the resulting spectra depend only on the r.m.s. value of matrix elements, not on the type of randomness.

3.1.4 Optical properties

A key feature of the electronic excitations connected with the B850 BChl spectrum in Fig. 13 is the distribution of oscillator strength of the exciton states. The dipole strength is proportional to the square of the transition dipole moment of a state. The transition dipole moment associated with the exciton state $\widetilde{|n\rangle}$ is

$$\mathbf{D}_n = \sum_{j=1}^{2N} c_{nj}\mathbf{d}_j, \tag{4}$$

where $\mathbf{d}_j$ denotes the transition dipole moment of the single BChl transition $|j\rangle$, and c_{nj} are the expansion coefficients as defined in Eq. (2). It can be shown that in aggregates of $2N$ BChls with perfect $2N$-fold circular symmetry and coplanar arrangement of BChl transition dipole moments, only the energetically degenerate pair of exciton states $\widetilde{|2\rangle}$, $\widetilde{|3\rangle}$ carry non-zero dipole strength. Each of these two states carries equal dipole strength, namely N times the dipole strength of an individual BChl Q_y transition. The latter property reflects the sum rule that the sum of all dipole strengths of the exciton band system must be equal to the sum of dipole strength of the individual Q_y transitions (Hu *et al*. 1997).

The distribution of dipole strength can have important functional implications: excitation of the B850 BChl system would result, after thermal relaxation, in the preferential population of the energetically lowest exciton state $\widetilde{|1\rangle}$ which is optically forbidden due to its vanishing dipole strength and, hence, is prevented from wasteful fluorescence. One may, however, argue that this property is of lesser importance in the native photosynthetic unit because all excitation transfer processes (< 10 ps) are fast compared to the lifetime of the BChl Q_y state

(1 ns), so that fluorescence does not lead to a significant loss of energy. Nevertheless, the generation of an energy trap is a remarkable property of circular BChl aggregates and can be of importance under conditions in which excitation is not quenched efficiently.

We note that the theoretically predicted super-radiance, i.e., the enhancement of the dipole strength due to exciton delocalization, has been observed in recent measurements of the nonlinear absorption and of the differential optical density spectrum of LH-II from several species (Leupold *et al*. 1996, 2000; Stiel *et al*. 1997). Most notably, the B850 band of LH-II from *Rs. molischianum* has been shown to exhibit two perpendicular transition dipole moments, each of $17{\cdot}8 \pm 0{\cdot}9$ D (Leupold *et al*. 2000). For exciton delocalization over the entire circular aggregate of 16 B850 BChls, theory predicts that the transition dipole moments of the exciton states $\widetilde{|2\rangle}$, $\widetilde{|3\rangle}$ are perpendicular to each other and have a value of $\sqrt{8}|\mathbf{d}_j|$. Assuming a value for the individual transition dipole moments of 6·3 D, this would correspond to a value of 17·8 D for the exciton states, in perfect agreement with the experiment. Exciton delocalization over a large part of the BChl aggregate is also consistent with results of single-molecule fluorescence-excitation spectroscopy of isolated single LH-II complexes (van Oijen *et al*. 1999). Two broad and intense bands of the B850 BChl ring were observed in all fluorescence-excitation spectra. The transition dipole moments of these two bands were mutually orthogonal, as expected for exciton delocalization over a significant part of the aggregate. However, the extent of super-radiance found in the above-mentioned experiments could not be reproduced in all other experiments. Time-resolved nonlinear absorption spectroscopy measurements suggest considerably smaller super-radiance values (Monshouwer *et al*. 1997). The reason for this discrepancy is not clear.

3.1.5 The effect of disorder

The properties of the B850 BChl system outlined above hinge on the ideal eightfold symmetry axis of LH-II of *Rs. molischianum*. Distortions would alter the dipole strength distributions as well as the distribution of exciton levels. In particular, one expects that the degeneracy of the strongly allowed exciton states $\widetilde{|2\rangle}$, $\widetilde{|3\rangle}$ will be lifted when the ring symmetry is broken. Furthermore, some of the dipole strength of these states will be redistributed to other, originally optically forbidden transitions, in particular the lowest exciton state, and the exciton states $\widetilde{|6\rangle}$, $\widetilde{|7\rangle}$. In fact, a splitting of the states $\widetilde{|2\rangle}$, $\widetilde{|3\rangle}$ by (on average) 110 cm^{-1} has been observed in single molecule spectroscopy experiments (van Oijen *et al*. 1999; Ketelars *et al*. 2001) at low temperatures. The higher energetic of the two states has a weaker intensity with the intensity ratio between respective transitions ranging from 0·3–0·7 (Ketelars *et al*. 2001). Similarly, the results of nonlinear polarization spectroscopy in bacteria other than *Rs. molischianum* show a splitting between the dominating transitions, e.g., by 140 cm^{-1} in LH-II from *Rb. sphaeroides*. The intensity of the two respective bands is clearly different (Leupold *et al*. 2000).

The effect of breaking of the circular symmetry is also manifested in the exciton delocalization length; for ideal circular complexes this length would cover the entire aggregate (i.e. 16 BChls in case of *Rs. molischianum*). The effect of disorder is to reduce this delocalization length to smaller number of BChls, i.e. distribute dipole strength more equally among various excitonic levels. There have been vastly different estimates of exciton coherence length in LH-II reported in literature (Leupold *et al*. 1996; Pullerits *et al*. 1996; Chachisvilis *et al*. 1997; Jimenez *et al*. 1997; Kennis *et al*. 1997; Monshouwer *et al*. 1997;

Novoderezhkin *et al*. 1999), ranging from two BChls (Jimenez *et al*. 1997) to the full length of the ring (Leupold *et al*. 1996). A natural explanation for some of the different estimates of delocalization length is the temperature at which the experiment is performed, but no consensus on this problem has been reached yet.

One needs to ask which type of distortions can result in the observed intensity and energy differences of the dominating transitions, and explain the observed delocalization lengths. We will distinguish four types of distortions and describe their effects on the optical properties of BChl aggregates, in particular, on the distribution of dipole strength and energies of the originally degenerate and strongly allowed states $\widetilde{|2\rangle}$, $\widetilde{|3\rangle}$.

First, the native system can have a structure which deviates principally from the crystal structure. For some species of purple bacteria, e.g., *Rb. sphaeroides*, LH-I complexes in native, LH-II-less membranes are **C**-shaped and not ring-shaped (Jungas *et al*. 1999). Furthermore, the LHs in the membrane may be in a dynamical equilibrium between complete, ring-shaped, LHs and complexes in the process of being built, which consequently lack one or more of their subunits, or, while already containing all of their subunits, are not closed yet, i.e., that the distance between two of their subunits may be considerably larger than that between other subunits. In all of the latter cases as well as in the case of the **C**-shaped LH-Is, the respective BChl aggregates do not exhibit a full circular symmetry, but retain only one symmetry axis. One can easily adopt the effective Hamiltonian description to such cases. For example, if one assumes that the LH-I ring in *Rb. sphaeroides* consists of 24 BChls arranged on three quarters of a circle, as suggested in (Jungas *et al*. (1999), the effective Hamiltonian predicts a split of 122 cm^{-1} between the exciton levels $\widetilde{|2\rangle}$, $\widetilde{|3\rangle}$ and dipole strengths differing by a factor of 4. Details of the energy and dipole splitting vary, depending on the number of missing BChls (Hu *et al*. 1997), but the important fact is that disruptions of the nature described here result in a significant splitting of energies and dipole strengths of the originally degenerate and allowed exciton states which is consistent with the above-mentioned experimental observations.

The authors of the first single molecule spectroscopy experiments on LHs (Bopp *et al*. 1997, 1999; van Oijen *et al*. 1999) have proposed that BChl aggregates may be deformed into ellipses, i.e. a C_2 symmetrical deformation. Group theory shows that in BChl aggregates with a C_2 symmetry there will always be pairs of exciton states with identical intensity. Only a further breaking of the C_2 symmetry, so that not more than one symmetry axis is retained, will lead to the observed splittings in intensity of the $\widetilde{|2\rangle}$, $\widetilde{|3\rangle}$ levels. It is important to notice that the effect of an elliptical deformation will be different depending on the initial symmetry of the BChl aggregate. In a BChl aggregate with C_9 symmetry, such as the B850 BChl aggregate in LH-II from *Rps. acidophila*, the elliptically deformed aggregate will only retain one symmetry axis. However, for a BChl aggregate with C_8 symmetry, such as in LH-II from *Rs. molischianum*, the elliptically deformed aggregate will still be C_2 symmetric. If an elliptical deformation is the cause of the disorder, a difference in intensity of the allowed bands should therefore only be observed in *Rps. acidophila*, but not in *Rs. molischianum*, where the intensity of the respective bands should be the same. Single molecule spectroscopy experiments at low temperatures on LH-II from *Rs. molischianum* could shed light on the type of large-scale distortions present in LHs.

Calculations suggest that the size of the elliptical deformation must be at least $\delta r/r_0 = 7\,\%$ in order to explain the observed splittings in energy and intensity in LH-II from *Rps. acidophila* (Matsushita *et al*. 2001). While electron microscopy suggests that LH-Is can be

deformed into shapes with C_4 symmetry (Stahlberg *et al*. 1998), it yet remains to be seen whether the much more compact LH-IIs can be deformed into ellipses to the degree required by theory. Likewise, it remains to be seen whether an opening of LH-II rings can occur in the membrane.

The two types of distortions discussed above are static in nature and include a considerable rearrangement of the protein scaffold holding the chromophores. In contrast to these large-scale distortions, smaller distortions of the circular symmetry occur due to interaction of the molecular system with its environment, in this case the thermally agitated protein. These variations will result in a change of the BChl binding energies, positions and orientations, while retaining an approximate circular symmetry. A variation of binding energies results in variations of the effective Hamiltonian diagonal elements (diagonal disorder), a variation of BChl positions and orientations results in variations of the off-diagonal elements (off-diagonal disorder).

The effect of the environment on absorption properties and exciton dynamics depends on the timescale of protein motions and chromophore vibrations compared to the characteristic times for an observed dynamical process (absorption, fluorescence, excitation transfer). The slow modulating processes can be modeled as static. The static disorder has been modeled in Hu *et al*. (1997) by randomizing the diagonal elements of an effective Hamiltonian and carrying out an effective Hamiltonian description numerically for a large ensemble of randomized Hamiltonians. With increasing disorder, the energetic splitting of the exciton levels $\widetilde{|2\rangle}$, $\widetilde{|3\rangle}$ becomes significant. However, only for very large disorder is significant dipole strength redistributed to other exciton levels. In all cases, the dipole strength of the exciton levels $\widetilde{|2\rangle}$, $\widetilde{|3\rangle}$ is identical. Using a distribution consistent with the inhomogeneous broadening measured by hole-burning spectroscopy (Reddy *et al*. 1992), the effect of diagonal disorder on exciton delocalization and dipole strength distribution was found to be noticeable, but small. Static off-diagonal disorder shows similar effects (Wu *et al*. 1997; Wu & Small, 1998; Jang *et al*. 2001).

The picture presented so far treated the slowly changing, or static distortions, and is expected to hold at low temperatures. The dynamic (or often called thermal) disorder, due to its rapidly modulating nature requires a conceptually different and technically extremely difficult treatment. In addition to knowledge of the magnitude of variation of diagonal and off-diagonal matrix elements of effective Hamiltonian, the timescales of their fluctuations need to be determined. The modulation of the diagonal matrix elements of the Hamiltonian can be thought of as originating from several high-frequency intramolecular vibrational modes, as well as low-frequency modes which arise through the coupling to the protein surrounding. Here, each mode is characterized with its own coupling strength and timescale.

Due to extreme difficulties in parameterization of all of the vibrational modes, several approximate methods have been invoked; by representing the dynamic fluctuations as dichotomic Markov processes, Barvik *et al*. (1999) and Bakalis *et al*. (1999) have studied the combined effect of dynamic and static disorder on absorption line-shapes of circular molecular aggregates, for various model parameters describing coupling strengths and timescales of the disorder. A path integral approach (Ray & Makri, 1999), modeling the dynamic disorder as an Ohmic bath, suggested that the excitonic delocalization over the entire aggregate (and therefore distribution of dipole strength into only two excitonic levels) is lost, and that the excitons in LH-II are delocalized over 2–3 BChls.

Recently, a combined molecular dynamics/quantum chemistry approach (A. Damjanović

et al. In Press) has been used to identify the timescales and amplitudes of the fluctuations of the matrix elements of the Hamiltonian. Fluctuations of the off-diagonal matrix elements were modeled directly from molecular dynamics data. To describe variation of excitation energies of individual BChls (diagonal matrix elements), quantum chemistry calculations were performed, based on the structures emerging from molecular dynamics. The results showed that the fluctuations of diagonal matrix elements are two orders of magnitude larger than the largest fluctuations of the off-diagonal elements. The combined molecular dynamics/quantum chemistry approach allows one to directly determine coupling strengths and frequencies of all the chromophore and protein vibrational modes that are coupled to an electronic transition, without invoking any approximations. The obtained information is contained in a physical quantity called the spectral density. The authors in Damjanović *et al*. (In Press) have calculated the spectral density from molecular dynamics and quantum chemistry data, and in the framework of a polaron model determined the absorption spectrum of the B850 system in LH-II of *Rs. molischianum*. Furthermore, the authors found that the excitons are delocalized over 5 BChls.

3.2 Theory of excitation transfer

3.2.1 General theory

Excitation transfer between an initially excited donor D* and an initially unexcited acceptor A, $D^* + A \rightarrow D + A^*$, is a radiationless transition process (Förster, 1948). The excitation transfer occurs from a manifold of vibrational and bath states, associated with the excited electronic state of the donor, into a manifold of vibrational and bath states associated with the electronic ground state of the acceptor. The wavefunctions of the initial and the final states can be expressed, in the Born–Oppenheimer approximation, as a product of the electronic wavefuncion ψ and of the vibrational wavefunction χ,

$$\Psi_{D^*}\Psi_A = \psi_{D^*}\psi_A\chi(w_D^*)\chi(w_A), \tag{5}$$

$$\Psi_D\Psi_{A^*} = \psi_D\psi_{A^*}\chi(w_D)\chi(w_A^*). \tag{6}$$

Figure 14 presents a scheme of energy levels of a donor and of an acceptor molecule. The parameters w_D and w_D^* describe the continuum of vibrational and bath states associated with the donor ground and excited state, respectively. Similarly, w_A and w_A^* describe the continuum of vibrational and bath states associated with the acceptor ground and excited state, respectively. The energy E is transferred between the donor and the acceptor whose zero–zero transition energies are $E_D(0\text{–}0)$ and $E_A(0\text{–}0)$ respectively.

In the case that the electronic coupling V_{DA} is so weak that inter- and intramolecular relaxation processes occur on a timescale faster than excitation transfer, the rate of excitation transfer can be described according to the Golden Rule rate expression

$$k_{DA} = \frac{2\pi}{\hbar}\int_{E=0}^{\infty} dE \int_{w_A=0}^{\infty} dw_A \int_{\omega_D^*=0}^{\infty} dw_D^* \times \left[\frac{g_D^*(w_D^*)\exp(-w_D^*/k_BT)}{Z_D^*}\right]\left[\frac{g_A(w_A)\exp(-w_A/k_BT)}{Z_A}\right]\left|\tilde{U}_{DA}\right|^2. \tag{7}$$

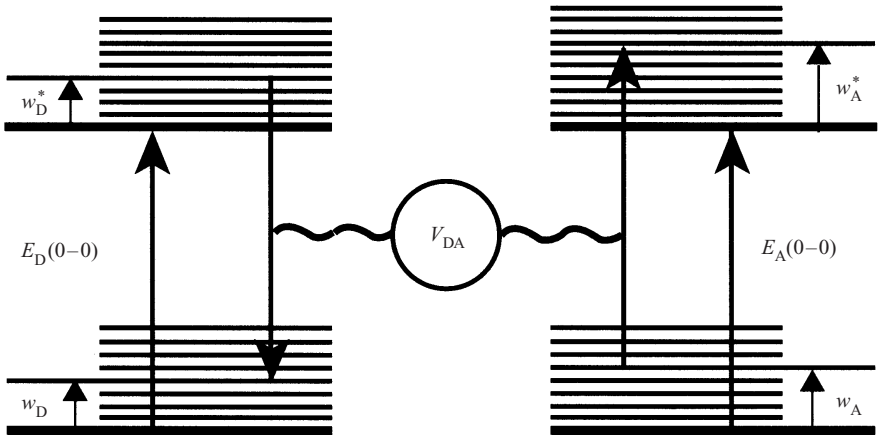

Fig. 14. Energy level scheme of a donor and of an acceptor molecule. The energies w_D, w_D^* w_A and w_A^* describe the continuum vibrational and bath states associated with the ground and the excited states of donor and acceptor, respectively. The energy that is transferred between the donor and the acceptor is denoted by E, while $E_D(0–0)$ and $E_A(0–0)$ label the zero–zero transition energies of donor and of acceptor respectively.

Here, $g_D^*(w_D^*)$ and $g_A(w_A)$ denote the multiplicity of the vibrational levels. It is assumed that the vibrational states are in thermal equilibrium, which is made explicit in Eq. (8) by weighting the vibrational state densities with Boltzmann factors and employing the partition functions Z_D^*, Z_A defined as

$$\left.\begin{aligned} Z_D^* &= \int_{w_{D=0}^*}^{\infty} \mathrm{d}w_D^* g_D^*(w_D^*) \exp(-w_D^*/k_B T), \\ Z_A &= \int_{w_{A=0}}^{\infty} \mathrm{d}w_A g_A^*(w_A) \exp(-w_A/k_B T). \end{aligned}\right\} \tag{8}$$

The interaction matrix $\tilde{U}_{DA}$ in Eq. (8) can be expressed as

$$\tilde{U}_{DA} = \langle \mathbf{\Psi}_{D^*} \mathbf{\Psi}_A | V_{DA} | \mathbf{\Psi}_D \mathbf{\Psi}_{A^*} \rangle. \tag{9}$$

Here, as above, V_{DA} represents the Coulomb interaction that causes the transition. The wavefunctions of the initial and the final states can be expressed, in the Born–Oppenheimer approximation, as a product of the electronic wavefunction ψ and of the vibrational wavefunction χ,

$$\mathbf{\Psi}_{D^*} \mathbf{\Psi}_A = \psi_{D^*} \psi_A \chi(w_D^*) \chi(w_A), \tag{10}$$

$$\mathbf{\Psi}_D \mathbf{\Psi}_{A^*} = \psi_D \psi_{A^*} \chi(w_D) \chi(w_A^*). \tag{11}$$

The interaction matrix $\tilde{U}_{DA}$ can in turn be approximated by a product of the purely electronic transition matrix element and two vibrational overlap terms, the Franck–Condon factors,

$$\tilde{U}_{DA} \approx U_{DA} \langle \chi(w_D^* | \chi(w_D) \rangle \langle \chi(w_A | \chi(w_A^*) \rangle, \tag{12}$$

where

$$U_{DA} = \langle \psi_{D^*} \psi_A | V_{DA} | \psi_D \psi_{A^*} \rangle \tag{13}$$

denotes the purely electronic part of the coupling. This simplification is known as the Condon approximation. It is possible whenever the electronic transition matrix elements depend only weakly on the nuclear degrees of freedom.

The rate for excitation transfer k_{DA} can now be rewritten as

$$k_{DA} = \frac{2\pi}{\hbar} |U_{DA}|^2 J_{DA}, \tag{14}$$

where all parameters related to the vibrational states are combined in the integral J_{DA}, defined as

$$J_{DA} = \int_{E=0}^{\infty} \mathrm{d}E G_D(E) G_A(E). \tag{15}$$

$G_D(E)$ and $G_A(E)$ are defined as

$$\left.\begin{aligned} G_D(E) &= \int_{w_D^*=0}^{\infty} \mathrm{d}w_D^* \left[\frac{g_D^*(w_D^*) \exp(-w_D^*/k_B T) |\langle \chi(w_D^*) | \chi(w_D) \rangle|^2}{Z_D^*} \right], \\ G_A(E) &= \int_{w_A=0}^{\infty} \mathrm{d}w_A \left[\frac{g_A(w_A) \exp(-w_A/k_B T) |\langle \chi(w_A) | \chi(w_A^*) \rangle|^2}{Z_A^*} \right], \end{aligned}\right\} \tag{16}$$

where

$$\left.\begin{aligned} w_D &= E_D(0\text{–}0) + w_D^* - E, \\ w_A^* &= -E_A(0\text{–}0) + w_A + E. \end{aligned}\right\} \tag{17}$$

By virtue of definition, $G_D(E)$ and $G_A(E)$ are normalized to unity on an energy scale. $G_D(E)$ and $G_A(E)$ are lineshape functions that can be understood as densities of states which combine the respective ground and excited states. They are often called the Franck–Condon weighted and thermally averaged combined densities of states.

Förster (1965) showed that the lineshape functions $G_D(E)$ and $G_A(E)$ can be related to the molar extinction coefficient $\epsilon_A(E)$ and the fluorescence spectrum $f_D(E)$ according to

$$\left.\begin{aligned} \epsilon_A(E) &= \frac{2\pi N_0}{3 \ln 10 \hbar^2 n c} |\mathbf{D}_A|^2 E G_A(E), \\ f_D(E) &= \frac{3\hbar^4 c^3 \tau_0}{4n} |\mathbf{D}_D|^2 E^3 G_D(E). \end{aligned}\right\} \tag{18}$$

Here, $N_0 = 6{\cdot}022 \times 10^{20}$ is the number of molecules per cm^3 per mol, n denotes the refractive index of the molecule sample, c is the speed of light in vacuum, and τ_0 is the radiative lifetime of the donor excited state. $\mathbf{D}_D$, $\mathbf{D}_A$ denote the transition dipole moments for the transition between ground and excited state of the donor and acceptor molecule, respectively. The occurrence of the factors E, E^3 in Eq. (18) derives from the condition that excited and ground state of a molecule must be populated such that the rate of transitions from ground to excited state induced by the radiation field (absorption) equals the rate of transitions from excited to ground state (spontaneous emission). Assumption of a blackbody radiation law leads to the functional form of the expressions in Eq. (18) (Einstein, 1917). With the normalized spectral functions

$$\left.\begin{aligned} \tilde{\epsilon}_A(E) &= \frac{\epsilon_A(E)}{\int_{E=0}^{\infty} \mathrm{d}E \epsilon_A(E)/E}, \\ \tilde{f}_D(E) &= \frac{f_D(E)}{\int_{E=0}^{\infty} \mathrm{d}E f_D(E)/E^3} \end{aligned}\right\} \tag{19}$$

one can rewrite the integral J_{DA} in Eq. (14) as

$$J_{\mathrm{DA}} = \int_{E=0}^{\infty} \mathrm{d}E \frac{\tilde{f}_{\mathrm{D}}(E)\tilde{\epsilon}_{\mathrm{A}}(E)}{E^4}. \tag{20}$$

Apart from the factor E^{-4}, the integral here represents the overlap of the normalized fluorescence spectrum of the initially excited donor D with the absorption spectrum of the finally excited acceptor A. The spectral overlap integral J_{DA} can thus be determined from spectroscopic measurements, whenever absorption and fluorescence can be observed.

3.2.2 Mechanisms of excitation transfer

The electronic coupling U_{DA} in Eq. (14) arises from the Coulomb interaction in the donor–acceptor pair. This interaction can be expressed

$$V_{\mathrm{DA}} = \frac{1}{2} \sum_{\substack{m,n,p,q \\ \in I_{\mathrm{D}} \cup I_{\mathrm{A}}}} \sum_{\sigma,\sigma'} (\phi_m \phi_n \,|\, \phi_p \phi_q)\; c^{\dagger}_{m\sigma} c^{\dagger}_{p\sigma'} c_{q\sigma'} c_{n\sigma}, \tag{21}$$

where $c^{\dagger}_{m\sigma}$, $c_{n\sigma'}$ denote the fermion creation and annihilation operators which create and annihilate, respectively, electrons with spins σ and σ' in the mutually orthogonal atomic orbitals ϕ_m and ϕ_n. I_{D}, I_{A} denote the set of atomic orbital indices of the donor and acceptor molecules, and $(\phi_m\phi_p|\phi_n\phi_q)$ denotes the Coulomb integral

$$(\phi_m\phi_p|\phi_n\phi_q) = \iint \mathrm{d}\mathbf{r}_1\, \mathrm{d}\mathbf{r}_2 \phi^{*}_m(\mathbf{r}_1)\; \phi_p(\mathbf{r}_1)\, \frac{e^2}{|\mathbf{r}_1 - \mathbf{r}_2|}\, \phi^{*}_n(\mathbf{r}_2)\phi_q(\mathbf{r}_2). \tag{22}$$

The intramolecular contributions to Eq. (21), arising from the sums $\boldsymbol{\Sigma}_{m,n,p,q\in I_{\mathrm{D}}}$ and $\boldsymbol{\Sigma}_{m,n,p,q\in I_{\mathrm{A}}}$ are accounted for in determining the intramolecular (donor, acceptor) electronic excitations; the intermolecular contributions, e.g. $\boldsymbol{\Sigma}_{m,p\in I_{\mathrm{D}},n,q\in I_{\mathrm{A}}}$ and $\boldsymbol{\Sigma}_{m,q\in I_{\mathrm{D}},n,p\in I_{\mathrm{A}}}$ are the perturbations which induce the electronic excitation transfer as described by Eq. (14). These contributions can be written, exploiting the anti-commutation properties of fermion operators,

$$V_{\mathrm{DA}} = \sum_{\substack{i,j,\in I_{\mathrm{D}} \\ \sigma}} \sum_{\substack{\mathrm{R,S},\in I_{\mathrm{A}} \\ \sigma'}} [(\phi_i\phi_j \,|\, \phi_{\mathrm{R}}\phi_{\mathrm{S}}) c^{\dagger}_{i\sigma} c_{j\sigma} c^{\dagger}_{\mathrm{R}\sigma'} c_{\mathrm{S}\sigma'} - (\phi_i\phi_{\mathrm{S}} \,|\, \phi_{\mathrm{R}}\phi_j) c^{\dagger}_{i\sigma} c_{j\sigma'} c^{\dagger}_{\mathrm{R}\sigma'} c_{\mathrm{S}\sigma}]. \tag{23}$$

From Eq. (23) follows immediately that the purely electronic Coulomb coupling $U_{\mathrm{DA}} = \langle \psi_{\mathrm{D}^*}\psi_{\mathrm{A}} | V_{\mathrm{DA}} | \psi_{\mathrm{D}}\psi_{\mathrm{A}^*} \rangle$ can be split into two contributions,

$$U_{\mathrm{DA}} = U_{\mathrm{C}} + U_{\mathrm{EX}}, \tag{24}$$

where

$$U_{\mathrm{C}} = \sum_{i,j\in I_{\mathrm{D}}} \sum_{\mathrm{R,S}\in I_{\mathrm{A}}} (\phi_i\phi_j \,|\, \phi_{\mathrm{R}}\phi_{\mathrm{S}})\, \langle \boldsymbol{\Psi}^{*}_{\mathrm{D}} | \sum_{\sigma} c^{\dagger}_{i\sigma} c_{j\sigma} | \boldsymbol{\Psi}_{\mathrm{D}} \rangle\, \langle \boldsymbol{\Psi}_{\mathrm{A}} \sum_{\sigma'} c^{\dagger}_{\mathrm{R}\sigma'} c_{\mathrm{S}\sigma'} | \boldsymbol{\Psi}^{*}_{\mathrm{A}} \rangle \tag{25}$$

describes the direct Coulomb interaction and where

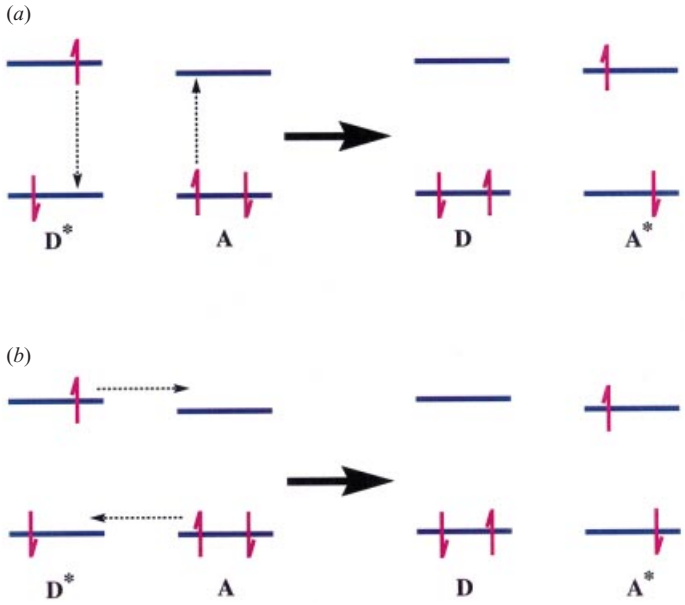

Fig. 15. Mechanisms of excitation transfer. (*a*) Coulomb mechanism; (*b*) electron exchange mechanism.

$$U_{\mathrm{EX}} = -\sum_{i,j\in I_{\mathrm{D}}}\sum_{\mathrm{R,S}\in I_{\mathrm{A}}}\sum_{\sigma,\sigma'}(\phi_i\phi_{\mathrm{S}}\,|\,\phi_{\mathrm{R}}\phi_j)\,\langle\Psi^*_{\mathrm{D}}|c^\dagger_{i\sigma}c_{j\sigma'}|\Psi_{\mathrm{D}}\rangle\,\langle\Psi_{\mathrm{A}}|c^\dagger_{\mathrm{R}\sigma'}c_{\mathrm{S}\sigma}|\Psi^*_{\mathrm{A}}\rangle \tag{26}$$

describes the exchange interaction which is well-known in multi-electron systems.

Depicted in the following drawing (Fig. 15) are the transfer mechanisms (*a*) due to the Coulomb term, as suggested by Oppenheimer (1941) and Förster (1948) (Coulomb mechanism), and (*b*) due to the electron exchange term, suggested by Dexter (1953) (Dexter mechanism). In case of the Coulomb mechanism, multipole–multipole Coulomb interaction de-excites an initially excited electron on the donor molecule D and simultaneously excites an electron on the acceptor molecule A. In case of the Dexter mechanism, excitation is transferred between a donor D and an acceptor A when an excited electron, initially belonging to D, is exchanged for a non-excited electron initially belonging to A.

As a consequence of selection rules, the Coulomb mechanism applies only to transfer of singlet excitations (assuming singlet ground states D and A), whereas the electron exchange mechanism is applicable also to transfer of triplet excitations. The Coulomb and electron exchange mechanisms for excitation transfer differ significantly in their operative range. While the Coulomb mechanism can be effective over distances of up to 50 Å , the exchange mechanism is effective only in case of sufficient overlap of the wavefunctions D* and A, i.e. for distances of a few Å.

Equations (25) and (26) describe Coulomb and exchange interaction exactly. Approximations are introduced in the description of the electronic excitations. As stated in the previous section, semi-empirical methods are required for a description of the excitations in case of Car–BChl transfer, while effective Hamiltonian descriptions can be applied to evaluate electronic excitations for BChl–BChl transfers involving BChl aggregates. Further approximations are required to evaluate the Coulomb integrals in Eqs. (25) and (26). The details and justification of these approximations are beyond the scope of this review and can be found in (Damjanović *et al*. 1999).

Equations (25) and (26) together with the spectral overlap integral allow one to evaluate the rate of excitation transfer through the Coulomb mechanism

$$k_{\mathrm{C}} = \frac{2\pi}{\hbar}|U_{\mathrm{C}}|^2 \int_{E=0}^{\infty} \mathrm{d}E \frac{\tilde{f}_{\mathrm{D}}(E)\tilde{\epsilon}_{\mathrm{A}}(E)}{E^4}, \tag{27}$$

where $\tilde{f}_{\mathrm{D}}(E)$, $\tilde{\epsilon}_{\mathrm{A}}$ denotes the normalized spectral functions as defined in Eq. (19).

Analogously, the excitation transfer rate through electron exchange coupling is

$$k_{\mathrm{EX}} = \frac{2\pi}{\hbar}|U_{\mathrm{EX}}|^2 \int_{E=0}^{\infty} \mathrm{d}E \frac{\tilde{f}_{\mathrm{D}}(E)\tilde{\epsilon}_{A}(E)}{E^4}. \tag{28}$$

It should be noted that the original Dexter rate expression (Dexter, 1953) is an approximation to the electron exchange rate in Eq. (28), lacking the factor E^{-4} in the spectral overlap integral. This omission has been transferred to several other articles. However, a correct representation of transition moments requires the use of the factor E^{-4} which is evident from the above derivation.

3.2.3 Approximation for long-range transfer

In case that the distance between the edges of D and A is much larger than the overall size of the molecules themselves, the Coulomb term U_{C} can be expanded into a multipole series. The first non-vanishing term in the multipole–multipole expansion of U_{C} is a dipole–dipole term, representing the interaction between the transition dipole moments $\mathbf{D}_{\mathrm{A}}$, $\mathbf{D}_{\mathrm{D}}$ of molecules D and A. If these transitions are allowed and the intermolecular distance r_{DA} is much larger than the overall size of the molecules, higher multipole contributions may be neglected and the Coulomb term in Eq. (25) can be approximated by

$$U_{\mathrm{C}} \approx U_{\mathrm{D-D}} = \frac{\mathbf{D}_{\dot{\mathrm{D}}}\mathbf{D}_{\mathrm{A}}}{r_{\mathrm{DA}}^3} - \frac{3}{r_{\mathrm{DA}}^5}(\mathbf{D}_{\dot{\mathrm{D}}}\mathbf{r}_{\mathrm{DA}})(\mathbf{D}_{\dot{\mathrm{A}}}\mathbf{r}_{\mathrm{DA}}) = \frac{\kappa}{r_{\mathrm{DA}}^3}|\mathbf{D}_{\mathrm{D}}||\mathbf{D}_{\mathrm{A}}|. \tag{29}$$

The orientation factor κ is defined by

$$\kappa = \cos\alpha - 3\cos\beta_{\mathrm{D}}\cos\beta_{\mathrm{A}}, \tag{30}$$

where α is the angle between the two transition moments of D and A, i.e. $\mathbf{D}_{\mathrm{D}}$ and $\mathbf{D}_{\mathrm{A}}$; β_{D} is the angle between the position vector $\mathbf{r}_{\mathrm{DA}}$ (connecting the centers of D and A) and $\mathbf{D}_{\mathrm{D}}$, and β_{A} is the angle between $\mathbf{r}_{\mathrm{DA}}$ and $\mathbf{D}_{\mathrm{A}}$.

Inserting the expression for the dipole–dipole coupling [Eq. (29)] into the rate equation [Eq. (14)], and identifying the spectral functions in Eq. (18), results in the famous Förster rate formula for excitation transfer through purely dipolar coupling (Förster, 1948)

$$k_{\mathrm{D-D}} = \frac{9\ln 10\hbar^5 c^4}{8n\tau_0}\frac{\kappa^2}{r_{\mathrm{DA}}^6}\int_{E=0}^{\infty} \mathrm{d}E \frac{f_{\mathrm{D}}(E)\epsilon_{\mathrm{A}}(E)}{E^4}. \tag{31}$$

One realizes that the rate of transfer between two optically allowed states has a R^{-6} distance dependence in the limit of large distances.

For calculations of the dipolar coupling $U_{\mathrm{D-D}}$ between BChls, we assume a size of 6·3 D for the Q_y transition dipole moments $|\mathbf{D}_{\mathrm{D}}|$, $|\mathbf{D}_{\mathrm{A}}|$. When the geometries of the molecules allows one to approximate the Coulomb coupling by the purely dipolar term $U_{\mathrm{D-D}}$, one arrives at very accurate predictions of transfer rates with Förster's formula.

When the stated geometrical criterium is not met, non-vanishing $|D_D|$ and $|D_A|$ values are not a precondition for excitation transfer and even optically forbidden transitions can be effective participants in the process. For a general description one cannot, therefore, rely on a multipole expansion, but rather needs to account in a numerical calculation for the complete Coulomb coupling between donor and acceptor electronic states according to Eqs. (25) and (26).

3.2.4 Transfer to exciton states

So far, excitation transfer has been considered to occur from an individual donor chromophore to an individual acceptor chromophore. This description can be extended to the case that either acceptor or donor, or both, are BChl exciton states. As described above, an exciton state $\widetilde{|n\rangle}$ can be approximated well as a linear superposition of single excited BChl states $|j\rangle$ with expansion coefficients c_{nj} [cf. Eqs. (2), (3)]. The electronic coupling from a single donor molecule $D = i$ to an exciton state $\widetilde{|n\rangle}$ of the BChl ring as acceptor, i.e. $A = \tilde{n}$, can then be expressed as

$$\tilde{U}_{i,n} = \sum_{j=1}^{2N} c_{nj} U_{i,j}, \tag{32}$$

where $U_{i,j}$ denotes the coupling between the individual donor molecules $D = i$ and the individual acceptor molecule $A = j$ and $2N$ is number of exciton states in the respective aggregate.

In case that the geometrical criterium for the application of the dipolar approximation is met, $U_{i,j}$ can be calculated according to Eq. (29). In the PSU, this is the case for transfer between B800 BChls and the B850 exciton. In case that the stated criterium is not met, one has to evaluate $U_{i,j}$ according to Eq. (25). In the PSU, this applies to transfer between carotenoids and B850 or B875 excitons.

For energetically degenerate exciton states $\widetilde{|n_1\rangle}$, $\widetilde{|n_2\rangle}$, excitation can be absorbed into any linear combination $\cos\gamma\widetilde{|n_1\rangle} + \sin\gamma\widetilde{|n_2\rangle}$ of these two states. We choose that combination which renders the resulting coupling

$$\tilde{U}_{i,(n_1,n_2)} = \cos\gamma\tilde{U}_{i,n_1} + \sin\gamma\tilde{U}_{i,n_2} \tag{33}$$

maximal. This combination is defined through the angle γ specified through

$$\tan 2\gamma = \frac{2\tilde{U}_{i,n_1}\tilde{U}_{i,n_2}}{\tilde{U}^2_{i,n_1} - \tilde{U}^2_{i,n_2}}. \tag{34}$$

In the following we introduce a single index m to enumerate the degenerate exciton states $\widetilde{|n_1\rangle}$ and $\widetilde{|n_1\rangle}$ and replace $\tilde{U}_{i,(n_1,n_2)}$ by $\tilde{U}_{i,m}$. In this manner we will relabel the states such that only one index labels a linear combination [with γ as defined in Eq. (34)] of two degenerate states, i.e. we will count subsequently only states with different energy. For the B850 exciton in LH-II from *Rs. molischianum*, the $2N = 16$ exciton states would thus be reduced to $M = 10$ states with different energies.

The rate of excitation transfer from an individual donor $D = i$ into exciton state $A = \tilde{m}$ as acceptor is

$$\tilde{k}_{i,m} = \frac{2\pi}{\hbar}|\tilde{U}_{i,m}|^2 \int S_i(E) S_m(E) \mathrm{d}E, \tag{35}$$

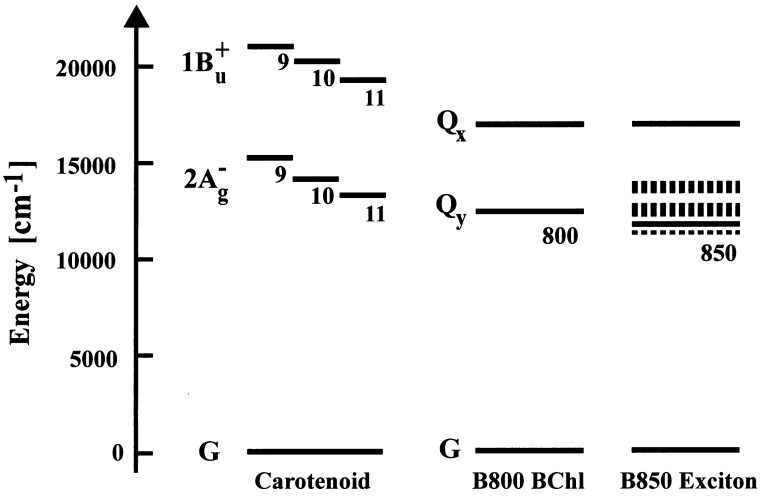

Fig. 16. Singlet excitation energies of carotenoid and BChl states. The carotenoid states are labeled according to their approximate C_{2h} and alternancy symmetry. Next to the carotenoid states, the location of the B800 BChl states and of the exciton states of the B850 band are shown. Solid lines represent spectroscopically measured energy levels for neurosporene ($n = 9$), spheroidene ($n = 10$), and lycopene ($n = 11$) (Zhang *et al.* 2000); dashed lines indicate the excitation energies of the symmetry forbidden exciton states of the B850 band calculated according to the effective Hamiltonian description.

while the total excitation transfer rate is a sum

$$k_{\mathrm{DA}} = \sum_{m=1}^{M} \tilde{k}_{i,m}. \tag{36}$$

In complete analogy, the electronic coupling for transfer between a donor exciton state, D $= \tilde{n}$, and an acceptor exciton state, A $= \tilde{m}$, is

$$\tilde{U}_{m,n} = \sum_{i} \sum_{j} c_{mi} c_{nj} U_{i,j}, \tag{37}$$

with expansion coefficients c_{mi} defined by Eq. (2). The rate of excitation transfer between the donor exciton state, D $= \tilde{m}$, and acceptor exciton state, A $= \tilde{n}$, is

$$\tilde{k}_{m,n} = \frac{2\pi}{\hbar} |\tilde{U}_{m,n}|^2 \int S_m(E) S_n(E) \mathrm{d}E, \tag{38}$$

To calculate the total excitation transfer rate, it is assumed that equilibrium between the donor exciton states E_{m} has been established, so that the donor exciton states are populated according to the Boltzmann distribution. The total excitation transfer rate between two ring aggregates is then

$$k_{\mathrm{DA}} = \sum_{m} \sum_{n} \frac{\mathrm{e}^{-E_m/kT}}{\sum_{m} \mathrm{e}^{-E_m/kT}} \tilde{k}_{m,n}. \tag{39}$$

3.3 Rates for transfer processes in the PSU

3.3.1 Car → BChl transfer

Carotenoids absorb radiation in the visible region inaccessible to (bacterio-)chlorophylls and transfer the absorbed energy in the form of electronic excitations to (bacterio-)chlorophylls. Figure 16 compares the energy levels of the carotenoid and BChl states involved in excitation transfer in various purple bacteria. The absorbing $S_2(1B_u^+)$ state energy decreases with an increase in the number of conjugated double bonds n. The indicated energies have been determined through fluorescence spectroscopy of neurosporene ($n = 9$) in LH-II from *Rb. sphaeroides* GIC, of spheroidene ($n = 10$) in LH-II from *Rb. sphaeroides* 2.4.1, and of lycopene of LH-II from *Rs. molischianum* (Zhang *et al*. 2000). The S_2 ($1B_u^+$) state relaxes via internal conversion within 130 fs ($n = 11$) to 320 fs ($n = 9$) into a low-lying, optically forbidden S_1 ($2A_g^-$) state. The discovery of the latter state dates back 30 years (Hudson & Kohler, 1972; Schulten & Karplus, 1972), however only very recently did several experimental groups succeed in measuring the $2A_g^-$ state energy of carotenoids with $n > 9$ directly (Fujii *et al*. 1998; Sashima *et al*. 1998; Krueger *et al*. 1999b, Polivka *et al*. 1999; Frank *et al*. 2000). The energies indicated in Fig. 16 stem from a steady-state fluorescence measurement of neurosporene, spheroidene, and lycopene in an *n*-hexane solution (Zhang *et al*. 2000). Theory had suggested the existence of a further optically forbidden $1B_u^-$ state between the $1B_u^+$ and $2A_g^-$ state for carotenoids with six or more conjugated double bonds (Tavan & Schulten, 1987), which has very recently been observed in experiments (Sashima *et al*. 1999, 2000). It has been suggested that the $1B_u^-$ state plays a role in speeding up $1B_u^+ \rightarrow 2A_g^-$ internal conversion (Sashima *et al*. 1999; Ritz *et al*. 2000), but for lack of adequate spectroscopic information the role of the $1B_u^-$ state remains obscure and we will not consider it here.

Noting that the carotenoid S_2 ($1B_u^+$) state is absorbing at a similar wavelength as the Q_x BChl state and that the S_1 ($2A_g^-$) state is close in energy to the Q_y state of BChl, two natural pathways of excitation transfer arise: excitation transfer $S_2 \rightarrow Q_x$ and excitation transfer $S_1 \rightarrow Q_y$, the latter preceded by the internal conversion $S_2 \rightarrow S_1$. Excitation transfer from lycopene could proceed to both B800 and B850 BChls. In the latter case, any of the exciton states of the B850 band ranging in energy from 710 to 865 nm can act as the accepting state for excitation transfer.

The $S_2 \rightarrow Q_x$ transfer time has been measured directly or estimated from lifetime measurements to lie between 57 fs ($n = 11$) and 300 fs ($n = 9$) (Shreve *et al*. 1991; Macpherson *et al*. 2001). In estimating transfer times from lifetime measurements, one measures the S_2 state lifetime in solution (τ_{solv}) and in the protein environment ($\tau_{\mathrm{LH\text{-}II}}$). Assuming that the difference in lifetimes is only due to excitation transfer one can then estimate the transfer time (τ_{ET}) according to $1/\tau_{\mathrm{ET}} = 1/\tau_{\mathrm{LH\text{-}II}} - 1/\tau_{\mathrm{solv}}$. Analogously, the $S_1 \rightarrow Q_y$ transfer time has been estimated to lie between 1·4 ps ($n = 9$) and 12·3 ps ($n = 11$) (Zhang *et al*. 2000). The questions arise by which mechanisms the excitation transfers can be mediated and how one can explain the differences in excitation transfer times between different species and carotenoids. These questions can be addressed through calculations of the transition density matrix elements of the carotenoid and BChl singlet states and of the electronic couplings between carotenoids and BChls. The results of these calculations are very sensitive to geometrical changes and thus require atomic resolution structural information of the Car–Chl system. Currently, three Car–Chl systems are resolved to atomic resolution, the lycopene ($n = 11$) – BChl *a* system of LH-II from *Rs. molischianum* (Koepke *et al*. 1996), the rhodopin

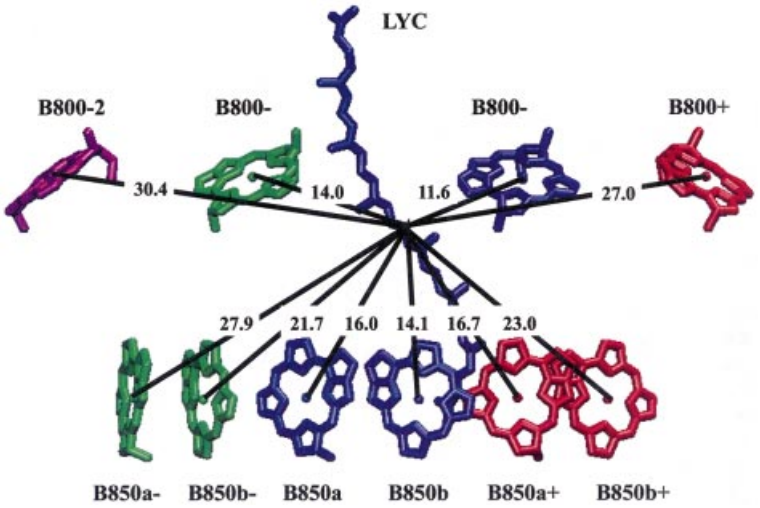

Fig. 17. Arrangement of lycopene and its neighboring BChls in LH-II from *Rs. molischianum* with coordinates taken from the X-ray crystallographic structure (Koepke *et al.* 1996). Lycopene, B800, B850a, and B850b belong to one monomer subunit as defined in Koepke *et al.* (1996). The structure of a monomer subunit is repeated with eightfold symmetry. BChls from other monomer subunits are indexed with reference to the subunit containing the lycopene depicted. Center-to-center distances are indicated in Ångstroms. [The figure has been produced with the program VMD (Humphrey *et al.* 1996).]

glucoside ($n = 11$) – BChl *a* system of LH-II from *Rps. acidophila* (McDermott *et al.* 1995), and the peridinin ($n = 9$) – Chl *a* system of PCP from *A. carterae* (Hofmann *et al.* 1996). Investigating the geometry of the Car–BChl systems in these LHs reveals that the geometrical criterion for the application of the dipolar approximation [Eq. (29)] is not met. The extension of the molecules (approximately 20 Å for carotenoids) is about as large as the distance between the molecule centers (approximately 15 Å) and larger than the distance between the closest atoms (cf. Fig. 17) for the center-to-center distances between lycopene and BChls in LH-II from *Rs. molischianum*. One needs to evaluate the electronic couplings including all orders of multipoles, according to Eqs. (25) and (26).

Several groups have developed methods to calculate the full Coulomb coupling; e.g. in Nagae *et al.* (1993). The transition density cube method of the Fleming group (Krueger *et al.* 1998a, b; Scholes *et al.* 1999) and the evaluation of transition density matrix elements developed independently by the Schulten group (Ritz *et al.* 1998a; Damjanović *et al.* 1999) are both recent methods that follow the spirit of the work of Nagae *et al.* (1993). With these methods it is now possible to evaluate the geometry dependence of the electronic coupling without the approximations inherent in Förster theory.

The full Coulomb coupling theory is less intuitive than the Förster theory since one has to take into account many different transition matrix elements that partly cancel each other. Even in the case of transfer between optically allowed states, the orientation of transition dipole moments does not allow any predictions about the strength of the coupling, since the dipole–dipole term does not necessarily give the leading contribution to the couplings. As an analysis in Krueger *et al.* (1998 b) shows, the full Coulomb coupling can differ by up to a factor of 4 from the Förster dipole–dipole coupling term, i.e. an estimate of the transfer rate based solely on the transition dipole contribution would differ up to 16 times from the correct transfer rate evaluated on the basis of the full Coulomb coupling.

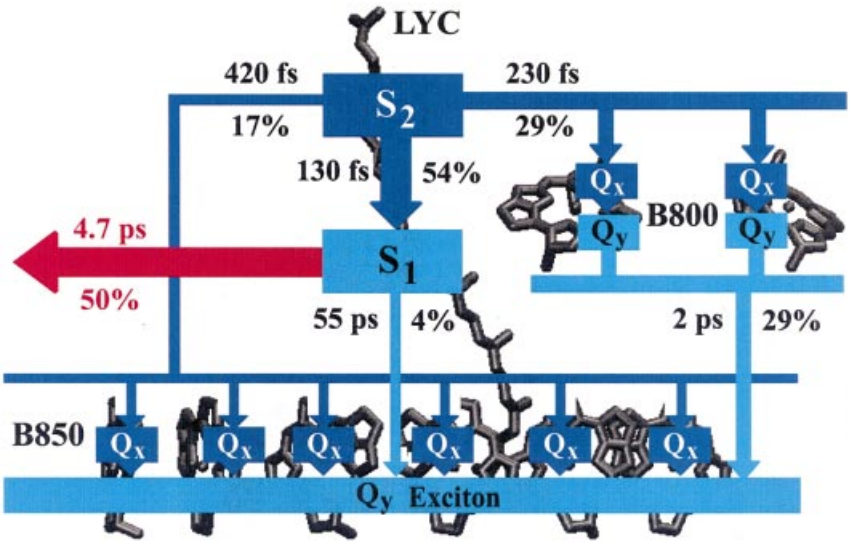

Fig. 18. Scheme of singlet excitation transfer and energy funneling in LH-II from *Rs. molischianum*. Shown are lycopene and representative BChls. The S_2 and S_1 lifetimes are experimental values. All lycopene → BChl transfer times are calculated with a full Coulomb coupling method (Ritz, 2001). B800 BChl → B850 BChl times are calculated as described below. Excitation transfer from S_2 competes with internal $S_2 \rightarrow S_1$ conversion, which occurs on the same timescale. Transfer via B800 BChls is the major pathway of $S_2 \rightarrow$ B850 Q_x transfer. Only a very small portion of S_1 excitation is transferred to BChl Q_y states, most of the S_1 excitation relaxes into the ground state. Due to the inefficiency of the $S_1 \rightarrow Q_y$ pathway, the overall lycopene → BChl excitation transfer occurs with an efficiency of only about 50 %.

3.3.1.1 Mechanism of Car → BChl transfer

Transfer from the optically forbidden S_1 state cannot occur via the Förster mechanism which requires the participating states to be allowed. It had been suggested that excitation transfer from this state can occur via the Coulomb mechanism (Thrash *et al*. 1979). Alternatively, the electron exchange (Dexter) mechanism (Dexter, 1953) had been suggested to mediate transfer through the S_1 state (Naqvi, 1980; Gillbro *et al*. 1988). The relative sizes of the couplings through the electron exchange and through the Coulomb interaction term have been evaluated with all of the above-mentioned full Coulomb coupling methods. These calculations show that the Dexter mechanism depends sensitively on edge-to-edge chromophore distances and is inefficient compared to the full Coulomb coupling mechanism even if the forbidden S_1 state is involved. This result has been ascertained for Car–Chl contacts in the range found in light harvesting, regardless of the details of the calculation method and has been found valid not only for a systematic study of hypothetical Car–Chl arrangements (Nagae *et al*. 1993), but also for the calculations based on the crystal structures of LH-II from *Rps. acidophila* (Krueger *et al*. 1998b), of LH-II from *Rs. molischianum* (Damjanović *et al*. 1999), and PCP from *A. carterae* (Damjanović *et al*. 2000b). The Dexter coupling describes a simultaneous exchange of electrons. An alternative to the Dexter exchange coupling is an exchange coupling that is mediated through successive virtual one-electron transfers to and from an intermediate ionic configuration. It has been suggested by several authors (Scholes *et al*. 1995, 1997, 1999) that the latter exchange coupling is larger than the Dexter exchange coupling; however, it was still found to be smaller than the Coulomb coupling.

3.3.1.2 Pathways of Car → BChl transfer

The arrangement of a carotenoid with its closest B800 and B850 BChls is shown in Figure 17 for the lycopene–BChl system of LH-II from *Rs. molischianum*. On the basis of the geometry and employing a full Coulomb coupling method (Damjanović *et al*. 1999), Car → BChl transfer rates for all possible pathways have been evaluated (Damjanović *et al*. 1999; Ritz, 2001). The latest calculations (Ritz, 2001), which include the effect of symmetry breaking through polar sidegroups as well as the effect of exciton delocalization in the B850 BChl system, show that about half of the excitation from the S_2 state of carotenoids relaxes into the S_1 state, while the other half is transferred within 150 fs to BChls. As shown in Fig. 18, most of the excitation is transferred within 150 fs to BChls. As shown in Fig. 18, most of the excitation is transferred to the B800− BChl (29 %) and the B850a+ BChl (13 %). It is worth noting that the center-to-center distance between carotenoids and BChls shown in Fig. 17 does not correlate well with the strength of the coupling. B800 BChl or B850b BChl, which both exhibit shorter center-to-center distances to lycopene than B800− BChl and B850a+ BChl, are both coupled much more weakly (Ritz *et al*. 2001). This property reflects the breakdown of the dipolar approximation in case of the closely spaced Car–BChl system and corroborates the necessity of a full Coulomb coupling evaluation for a reliable prediction of transfer rates.

Transfer from the S_1 state is largely ineffective; the major part of excitation is lost through dissipation, resulting in a low overall Car → BChl transfer efficiency of about 50 % in LH-II from *Rs. molischianum*.

In LH-II from *Rps. acidophila*, rhodopin glucoside, a carotenoid which is structurally very similar to lycopene, is employed. Calculations of Car → BChl show that transfer from the S_1 state of rhodopin glucoside is also inefficient, and, thus, the overall Car → BChl efficiency is low in LH-II from *Rps. acidophila* as well. An interesting difference occurs in the pathways of excitation transfer from the S_2 state. In LH-II from *Rps. acidophila*, the major part of the excitation is transferred directly to B850 BChls (35 %), only about 8 % are transferred to B800 BChls. Thus the removal of B800 BChls should have little effect on the Car → BChl transfer kinetics in LH-II from *Rps. acidophila* whereas the calculations predict a change on the transfer kinetics in LH-II from *Rs. molischianum* when B800 BChls are removed (Ritz, 2001).

3.3.2 Efficiency of Car → BChl transfer

The transfer steps discussed above reveal how purple bacteria can control the flow of excitation through variations in excitation energies and geometries of the BChl systems. Purple bacteria show also a great variability in the use of carotenoids, which fuel excitation energy with different efficiency to BChl, depending on the species and LH involved. The overall Car → BChl transfer efficiency has been measured to be close to 100 % in *Rb. sphaeroides* (Cogdell *et al*. 1981; van Grondelle *et al*. 1982; Kramer *et al*. 1984; Trautmann *et al*. 1990), between 38 and 75 % in *Rps. acidophila* (Angerhofer *et al*. 1986; Chadwick *et al*. 1987; Cogdell *et al*. 1992), and as low as 30 % in LH-I of *Rs. rubrum* (Frank, 1993).

The calculations on the three structurally solved systems suggest an explanation for the observed variations. Excitation transfer from the S_2 state occurs at best on the same timescale as internal conversion from the S_2 to the S_1 state, which means that the overall Car → Chl transfer efficiency can not exceed 30–70 % if it were solely based on $S_2 \rightarrow Q_x$ transfer. Species near unit transfer efficiencies will have to utilize the $S_1 \rightarrow Q_y$ transfer pathway in addition. The

Table 1. *Electronic couplings* U_{DA} (*in* cm^{-1}), *spectral overlaps* (*in* 10^{-6} *cm*), *and lifetimes for carotenoid* S_2 *states*, τ_{S2}, (*in fs*), *and for carotenoid* S_1 *states*, τ_{S1} (*in ps*)

	U_{DA}	J_{DA}	τ_{S2}
S_2–Q_x			
Neurosporene ($n = 9$)	118	27	320
Spheroidene ($n = 10$)	150	76	250
Lycopene ($n = 11$)	242	145	130
S_1–Q_y			
Neurosporene ($n = 9$)	41	189	21·2
Spheroidene ($n = 10$)	16	293	9·3
Lycopene ($n = 11$)	14	210	4·7

These factors determine the transfer efficiencies for the three Car–BChl systems investigated, the neurosporene–BChl system of LH-II from *Rb. sphaeroides* G1C, the spheroidene–BChl system of LH-II from *Rb. sphaeroides* 2.4.1, and the lycopene–BChl system of LH–II from *Rs. molischianum*. The carotenoids in these systems have an increasing number of conjugated double bonds *n*.

question arises why transfer through the optically forbidden S_1 state is efficient in some species but not in others.

There are, in principle, three factors that can account for the differences in transfer efficiencies for different Car–Chl systems: the electronic coupling U_{DA} between the donor carotenoid and acceptor Chl state, the spectral overlap J_{DA} of donor emission and acceptor absorption spectra, and the lifetime of the donor state in the absence of energy transfer. The first two factors determine the energy transfer rate k_{DA} according to Eq. (14), which depends quadratically on the electronic coupling and linearly on the spectral overlap. The third factor, the lifetime of a state S, influences the transfer efficiency according to

$$\eta_S = \frac{\tau_S}{\tau_S + \tau_{ET}}, \tag{40}$$

where τ_S is the lifetime of state S in the absence of excitation transfer and $\tau_{ET} = 1/k_{DA}$ is the time constant of excitation transfer.

In (Ritz *et al*. 2000) have been considered all three factors that determine excitation transfer efficiencies for three Car–BChl systems of purple bacteria, the neurosporene ($n = 9$)–BChl system of LH-II from *Rb. Sphaeroides* G1C, the spheroidene ($n = 10$)–BChl system of LH-II from *Rb. Sphaeroides*, and the lycopene ($n = 11$)–BChl system of LH-II from *Rs. molischianum*. Spectral overlaps (with B850 BChls) and lifetimes have been measured through fluorescence spectroscopy of the respective pigment–protein complexes and are listed in Table 1. To evaluate electronic couplings we employed perfect polyenes with $n = 9$–11 as carotenoid analogs and treated all carbon atoms with identical parameters ('symmetric' carotenoid model). Carotenoid wavefunctions were evaluated with a self-consistent configuration interaction calculation including all single and double excited configurations. A symmetric analog has been employed for BChl as in the previous sections. Since the structure of *Rb. sphaeroides* G1C and *Rb. sphaeroides* are not known, we choose to arrange the polyenes such that their center of mass matches the center of mass of lycopene in LH-II from *Rs. molischianum* and their axis is aligned at the same angle as the axis of lycopene. Obviously, the placement of the shorter carotenoid analogs may result in geometries that are different from the actual Car–BChl geometries in the respective native systems. The couplings listed

in Table 1 correspond to couplings between the respective carotenoid analog and B850a BChl. No scaling of the couplings has been employed.

The results presented in Table 1 allow a comprehensive discussion of the efficiencies of Car → BChl transfer processes involved in light harvesting through carotenoids.

The light-harvesting process through carotenoids is initiated through absorption into the S_2 ($1B_u^+$) state. In this state, direct excitation transfer to the Q_x state competes with internal conversion to the S_1 ($2A_g^-$) state, involving likely the S_2 ($1B_u^-$) state. The $S_2 \rightarrow Q_x$ excitation transfer speeds up considerably with an increase in the number of conjugated double bonds. From our calculations, we predict a transfer time ratio of 20:5:1 for $n = 9:10:11$. The shortening in transfer times is controlled mainly by the increase in spectral overlaps and, secondarily, by the increase in electronic couplings.

Once energy has relaxed to the S_1 state, again two processes compete, excitation transfer to the Q_y state of BChls, and internal conversion to the ground state. Unlike for the transfer from the S_2 state, no clear trend for the transfer rates with an increase in n can be established. The results of the above presented Coulomb coupling calculations for peridinin and lycopene, based on the crystal structures and including the effect of sidegroup variations, suggest that the controlling factor for the S_1–Q_y electronic couplings is not the length of conjugated system, but the degree of symmetry breaking. The effect of symmetry breaking is to increase the electronic coupling. This effect can be induced either by the use of an asymmetric carotenoid, such as peridinin, in which case the effect is strong, or by geometric distortion of a symmetric carotenoid, such as lycopene, in the protein environment, in which case the effect is weaker. A strong effect of symmetry breaking has been suggested to result from a non-C_{2h}-symmetrical arrangement of the functional (methyl, carbonyl) groups in peridinin (Damjanović *et al*. 2000b). Although the calculated $S_1 \rightarrow Q_y$ couplings for peridinin may be an overestimate, because of the uncertainties in parameterization, the large differences in electronic couplings for the asymmetric peridinin compared to the symmetric lycopene suggest nevertheless that the different symmetries with their effect on the electronic couplings are a dominant factor in explaining why transfer from the S_1 state is highly efficient for peridinin, and not efficient for lycopene.

Compared to the effects of symmetry breaking on electronic couplings which have a quadratic effect on the transfer rates, the effect of spectral overlaps on the $S_1 \rightarrow Q_y$ transfer rates is very small and cannot be considered as a dominant factor. It is interesting to note, though, that the spectral overlap is maximized for carotenoids with n between 9 and 11, the range in which most carotenoids in light harvesting can be found.

A second factor contributing to the efficiencies of $S_1 \rightarrow Q_y$ transfer is the strong decrease of S_1 lifetimes with increase in n. The S_1 lifetime for neurosporene ($n = 9$), 21·2 ps, is almost five times longer than the S_1 lifetime for lycopene ($n = 11$), 4·7 ps. This in itself is a sufficient difference to explain why transfer from the S_1 state in neurosporene is efficient, while it is inefficient in lycopene.

Summarizing this discussion, we note that the experimentally observed overall Car → Chl transfer efficiencies can be explained in systems for which theoretical and experimental data are available. The overall transfer efficiency is determined mainly by the efficiency of transfer through the S_1 state. Light-harvesting systems with a low overall efficiency, such as LH-II from *Rs. molischianum* and *Rps. acidophila*, employ long, symmetric carotenoids (lycopene, rhodopin glucoside). Their resulting small S_1–Q_y electronic couplings and short S_1 lifetimes render transfer through the S_1 state inefficient. Excitation transfer in these light-harvesting

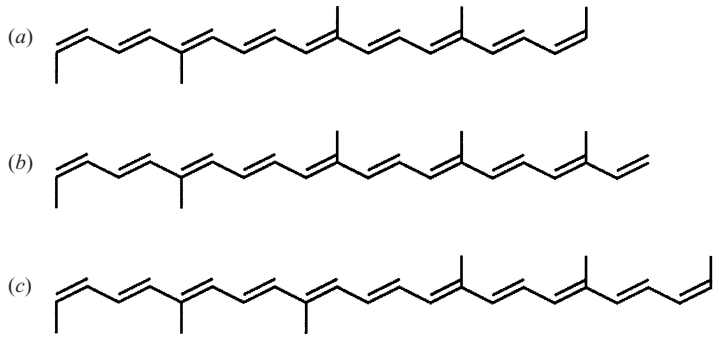

Fig. 19. Structure of conjugated systems with methyl side groups of neurosporene, spheroidene, and lycopene. The C_{2h} symmetry is broken for neurosporene and spheroidene, since 5 methyl side groups cannot be arranged such that the structure is invariant under rotation by 180°. In contrast, the 6 methyl side groups on lycopene are arranged in C_{2h} symmetric fashion. Symmetry breaking enhances couplings to the S_1 state, and, thus, excitation transfer rates. The structures suggest that transfer through the lycopene S_1 is slower than through the neurosporene or spheroidene S_1 state, which is consistent with experimental data.

systems occurs through the $S_2 \rightarrow Q_x$ pathway. Because of the short S_2 lifetime, the efficiency of this transfer is low.

In contrast, systems with near unit transfer efficiencies, such as PCP from *A. carterae* and LH-II from *Rb. Sphaeroides* G1C, employ short ($n = 9$) carotenoids (peridinin, neurosporene). In case of the symmetric neurosporene, the long S_1 lifetime renders transfer through the S_1 state efficient. In peridinin, the effect of symmetry breaking, through asymmetrical arrangement of methyl side groups and the presence of a carbonyl group, vastly increases S_1–Q_y electronic couplings. This increase, in conjunction with an additional effect of the carbonyl group on the spectroscopic properties of peridinin renders transfer through the S_1 state efficient.

A particular interesting system is LH-II from *Rb. sphaeroides* 2.4.1, which employs the carotenoid spheroidene ($n = 10$). Its S_1 lifetime is only a factor 2 longer than the lycopene S_1 lifetime in *Rs. molischianum* and therefore not sufficient as an explanation for the near unit efficiency observed in *Rb. sphaeroides* 2.4.1 as opposed to the 50 % efficiency in the lycopene–BChl system in *Rs. molischianum*. The conjugated systems of neurosporene, spheroidene and lycopene are shown in Fig. 19. An inspection of the spheroidene structure shows that spheroidene (as well as neurosporene) exhibits a non C_{2h}-symmetrical arrangement of its methyl side groups, unlike lycopene, in which the methyl groups are arranged in a C_{2h}-symmetrical fashion. On the basis of the electronic coupling calculations reviewed here, we suggest that this difference in symmetries can be a dominant factor in explaining why transfer through the S_1 state is efficient in spheroidene, but not in lycopene. We note the symmetry properties can provide an explanation for the experimentally estimated $S_1 \rightarrow Q_y$ transfer times, which are very similar for the equally asymmetrical neurosporene and spheroidene (1·4 and 2·1 ps, respectively), but significantly longer for lycopene (12·1 ps). Additional support for this suggestion comes from a reconstitution study (Noguchi *et al.* 1990), in which the efficiency for Car → Chl transfer was found to drop from 72 to 43 % when spheroidene ($n = 10$) was replaced by rhodopin ($n = 11$) in LH-I from *Rb. sphaeroides*, whereas a substitution by neurosporene ($n = 9$) had no effect on the efficiency. Since the conjugated system of rhodopin is identical to that of lycopene and thus exhibits C_{2h} symmetry, the above-mentioned symmetry breaking effect can account for the observed differences in efficiencies.

However, we caution against conclusions in the absence of structural information. The above calculations of electronic couplings for LH-II from *Rs. molischianum* in comparison to LH-II from *Rps. acidophila* (Ritz, 2001) show that the exact geometrical arrangement has a significant effect on the coupling. While the strong dependence of electronic couplings on the geometries may invalidate some of our conclusions and suggestions for the effect of electronic couplings, it also means that nature can employ this dependence to control energy transfer efficiencies. To say the least, it can be misleading to analyze excitation transfer efficiencies solely on the basis of spectral overlap and lifetimes, assuming that electronic couplings are similar between different species of light-harvesting systems.

3.3.3 B800–B850 transfer

B800 BChls play a role in enhancing the absorption cross-section of the PSU. They are oriented such that they absorb light in a direction perpendicular to that of the B850 BChls and the B875 BChls. The individual B800 BChls can transfer the resulting excitation energy to the B850 ring through the Förster mechanism (Oppenheimer, 1941; Förster, 1948). The experimentally determined transfer rate is 700 fs at room temperature (Shreve *et al*. 1991). Quantum chemical calculations in Cory *et al*. (1998) have demonstrated that the B800 BChls are only weakly coupled with each other and with the B850 BChls. If one assumes that B850 BChls are only weakly coupled among each other and do not form exciton states, Förster theory would predict a B800 → B850 BChl transfer time of 6·6 ps. This value, as do the following transfer rate values, assumes a size of 6·3 D for the transition dipole moment of BChls. If one takes the exciton nature of the B850 BChl states into account, the exciton splitting will result in a shortening of transfer times due to improved spectral overlap (Damjanović *et al*. 1999). Employing the effective Hamiltonian model and evaluating the transfer rate according to Eq. (36) then predicts a transfer time of 2·3 ps, which is closer to the experimentally observed value, but still more than a factor of 3 too long. In the case of B800 → B850 transfer, one would expect the best agreement between theory and experiment, because the geometry allows the use of the dipolar approximation and the description of B800 is unproblematic, it being a single molecule. One reason for the remaining discrepancy may lie in an underestimation of the transition dipole moments in the protein environment. The transfer time scales with the factor $(|\mathbf{D}_{\mathrm{real}}|/6{\cdot}3)^4$. Another reason may lie in the still unexplained influence of the carotenoids which are in close contact with both B800 and B850 BChls. It has been shown that changes in carotenoid absorption correlate with the dynamics of B800 → B850 BChl excitation transfer (Herek *et al*. 1998), indicating a considerable interaction between carotenoids and BChls. Scholes & Fleming, (2000) have estimated through quantum chemical calculations that the perturbation of BChl transition dipole moments through the presence of the carotenoids results in a speed-up of B800 → B850 BChl transfer by a factor of 1·7, which would indeed result in a close agreement of experimental and predicted transfer times.

3.3.4 LH-II → LH-II transfer

Excitation transfer from B800 BChls and carotenoids fuels the delocalized ring systems of LH-IIs (in case of carotenoids also of LH-I) with photons. Due to the use of high-lying exciton states in case of B800 → B850 transfer and due to the large energy gap in case of Car → BChl transfer, excitation transfer from these auxiliary pigments to the B850 system occurs

only forward; back-transfer is negligible. In case of transfer between the BChl systems of LH-II, LH-I, and the RC, excitation energies are very similar, resulting in similar transfer rates for forward and back-transfer between these BChls systems. In the following sections, we will investigate in which way the excitation energy landscape of the BChl systems can allow a purple bacterium to control the flow of excitation and to adapt to different light conditions.

Transfer rates between LH-IIs have not been observed experimentally. We evaluate a transfer time of 10·0 ps. This time is longer than the calculated transfer time for LH-II → LH-I transfer (see below). If the number of LH-IIs is significantly larger than the number of LH-Is in the native membrane, back-and-forth transfer processes within a 'lake' of LH-IIs may slow down transfer towards the RC. In this regard it is interesting to note (see also below) that under low-light conditions, LH-IIs are replaced by structurally very similar LH-IIIs, with a BChl aggregate absorbing at 820 nm instead of 850 nm (Gardiner *et al*. 1993). The introduction of LH-IIIs creates an energy funnel instead of the lake of LH-IIs and can thus enhance excitation trapping.

3.3.5 LH-II → LH-I transfer

The time constant for LH-II → LH-I excitation transfer has been measured to be 3·3 ps in *Rb. sphaeroides* (Hess *et al*. 1995). Calculations show (Ritz, 2001; Ritz *et al*. 2001) that excitation transfer originates from several B850 exciton states, mostly from the degenerate pair of second and third B850 exciton states, but also from the lowest B850 exciton state and the degenerate pair of fourth and fifth B850 exciton states. The calculated transfer time is 7·7 ps, which is a factor of 2 longer than the measured time. It should be noted that the population of the donor exciton states depends on the calculated energy gap between the lowest exciton levels, which is not predicted well by the effective Hamiltonian description. The low-lying exciton states couple with very different strength to the acceptor states, so that an error in the evaluation of the population will result in a considerable error in the transfer time. Given the simplicity of the effective Hamiltonian used, the theoretical result is in remarkable agreement with the experimental value, suggesting that the effective Hamiltonian captures the essential physics of the transfer process.

Forward LH-II → LH-I transfer has to compete with backwards LH-I → LH-II transfer. In the absence of an exciton, the ratio K between forward and backward transfer would relate to the energy difference of individual donor and acceptor BChl molecules according to $e^{-[E_D - E_A/kT]}$. In this two-level description one would obtain a value of $K = 5{\cdot}4$ when considering $E_D =$ 850 nm and $E_A = 875$ nm. This ratio would correspond to a back-transfer time of 42 ps. However, due to the formation of an exciton involving multiple BChls, the calculated back transfer time from LH-I to LH-II is considerably shorter than the one estimated from the simplistic two-level description, namely 15·5 ps. This fast back transfer may be of advantage under high-light conditions when an RC cannot turn over the excitation provided. Then, excitation could be transferred back to LH-IIs and from there transferred on to other LH-Is with open RCs. As discussed above, the introduction of higher-energetic LH-IIIs can act as a control mechanism to increase forward transfer to LH-I under low-light conditions.

3.3.6 LH-I → RC transfer

The time-determining step in the excitation funnel is transfer from the LH-I ring to the RC. Because of the ring symmetry, the lowest lying, optically forbidden B875 exciton state is only

very weakly coupled to the RC BChls. Symmetry breaking through the accessory BChls in the RC leads to an increase in coupling (Hu *et al*. 1997), but the coupling remains small compared to the strongly coupled second and third B875 exciton states. Transfer originates therefore from this degenerate pair of exciton states (Damjanović *et al*. 2000a). The calculated transfer time of 16 ps (Damjanović *et al*. 2000a) is in excellent agreement with measured LH-I–RC transfer times of 35–37 ps at 77 K (Bergström *et al*. 1989; Visscher *et al*. 1989), from which one can estimate a transfer time of about 25 ps at room temperature (van Grondelle *et al*. 1994).

The use of the higher-lying LH-I exciton states as a main transfer pathway leads to an interesting phenomenon. In forward (LH-I $\rightarrow$ RC) transfer, only about 42 % (Boltzmann population of the $\widetilde{|2\rangle}$, $\widetilde{|3\rangle}$ LH-I exciton states) of the excitation is transferred from the higher-lying LH-I exciton states to the lowest exciton state of the RC, whereas 58 % of excitation is transferred between the weakly coupled lowest exciton states of LH-I and RC. In contrast, back (RC $\rightarrow$ LH-I) transfer occurs from the almost 100 % populated, lowest exciton state of the RC to the higher-lying LH-I exciton states. Therefore back transfer is always faster than forward transfer. This design can have a photoprotective role. Excitation that is not used towards the initial electron transfer step will be transferred back towards the LH-I ring rather than being dissipated in the RC which might result in an overheating of the RC. The calculated time for back transfer is 8·1 ps (Damjanović *et al*. 2000a). A back-transfer time of 7–9 ps has been estimated from the experimentally measured decay kinetics after excitation of the RC (Timpmann *et al*. 1993). The back-transfer time is slower than the initial electron transfer step occurring in 3 ps, which means that excitation energy trapping by the RC is efficient. However the calculated back-transfer time constant has the same order of magnitude as the initial electron transfer step, suggesting that the geometrical arrangement with a distance of about 40 Å between RC and LH-I BChl may be necessary in order to balance the transfer-time constants. If the LH-I BChls were closer to the RC, back transfer would be faster than the initial electron-transfer step in the RC; if the LH-I BChls were more distant, the forward-transfer step would become slower, resulting in a decrease of efficiency.

3.3.7 Excitation migration in the PSU

We summarize the previous sections within Fig. 20. Figure 20, presenting the complete set of transfer rates, demonstrates a remarkable conceptional achievement, as it shows that a complex molecular machinery involving hundreds of pigments and tens of thousands of atoms can be described with high accuracy through the application of the laws of quantum physics. The calculated rates agree well, although not perfectly, with experimental results, indicated in parentheses in Fig. 20. Likely reasons for the remaining discrepancy include, as discussed above, an underestimation of the BChl *a* Q_y transition dipole moment in the protein environment of purple bacteria and an overestimation of the exciton delocalization, in particular for LH-I.

Figure 20 reveals an important principle in the organization of the PSU. Forward- and back-transfer rates between the different pigment–protein complexes are very similar, and thus the transfer reactions are not biased strongly in any particular direction. In particular there exists no strong bias of excitation transfer towards the RC. It is therefore inappropriate to describe the BChl aggregates as forming an excitation funnel with the RC at the center. Only the accessory pigments, carotenoids and B800 BChls funnel their excitation energy into the respective BChl aggregates. The system of BChl aggregates is better described as a

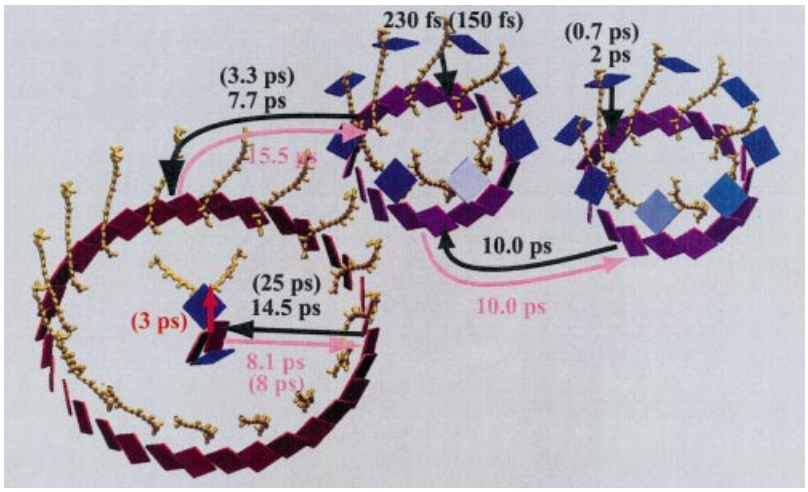

Fig. 20. Excitation transfer times in the photosynthetic unit of purple bacteria. Times for all possible excitation transfer steps have been calculated as indicated in the figure. Experimental times, if available, are shown in parentheses. [Produced with the program VMD (Humphrey *et al*. 1996).]

reservoir in which excitation is distributed more or less evenly throughout the whole system. The organization appears to be rather inefficient. However, kinetic calculations based on the rates shown in Fig. 20 show that excitation is trapped within 200 ps or less at the RC, for a large variety of PSU architectures (Ritz *et al*. 2001). This trapping time is small compared to the BChl decay time of 1000 ps, so that the yield of the PSU remains high, i.e. above 85%.

The rationale for this organization becomes clear when one considers that RCs exist in two spectral forms. In the 'open' form, the RC special pair is neutral and can utilize excitation towards an electron transfer. After the electron transfer, the RC is in the closed form with the active special pair BChl being in a cation state and unable to utilize further excitation until it is reduced by the uptake of an electron. If the BChl aggregates in LH-Is and LH-IIs were forming an excitation funnel towards the RC, all of the excess excitation arriving while the RC is closed would be dissipated in the RC special pair which could result in an overheating of the special pair. By lifting the energy of the RC above that of the B875 BChl aggregate in LH-I, the back-transfer rate from the RC to LH-I becomes faster than the forward-transfer rate from LH-I to the RC. If the RC is closed, excitation is returned to LH-I, and, thus dissipation can be spread over a much larger area. Dissipation is spread over an even larger area due to transfer from LH-Is to LH-IIs and subsequent transfer between LH-IIs. As the calculations in Ritz *et al*. (2001) show, the dissipation is effectively spread out over the entire BChl system. Under normal light conditions, it appears to be more important for a purple bacterium to protect its PSU against damage from overheating by spreading out dissipation than to achieve a higher efficiency. However, under low-light conditions, the purple bacterium *Rps. acidophila* changes the organization of its PSU. LH-IIs are replaced gradually by LH-IIIs which absorb at a higher energy. Under continuous low irradiation, all LH-IIs are replaced by LH-IIIs (Gardiner *et al*. 1993; McLuskey *et al*. 2001). The insertion of LH-III changes the excitation reservoir to an excitation funnel towards LH-I. This change results in a reduction of the trapping time by approximately a factor of 2, and, consequently in a higher quantum yield. The price for the rise in yield is a more uneven distribution of dissipation with most of the excitation being dissipated in LH-I and RC. It is worth noting that replacing LH-

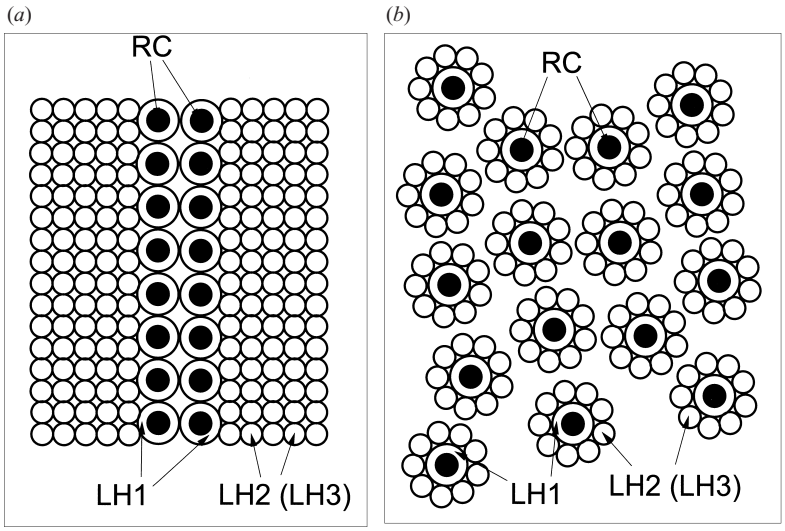

Fig. 21. Schematic figures of the model architectures described in the text. (*a*) Stripe architecture; (*b*) circular architecture.

II by LH-III molecules increases the yield by not more than 3–6%, depending on the architecture of the PSU (Ritz *et al*. 2001).

As discussed above, it is still unknown how the LHs are organized within the photosynthetic membrane. However, the availability of all rates for intra- and inter-complex transfer processes allows one to address the question of how much the functionality of the photosynthetic apparatus is influenced, and possibly controlled by the large-scale organization of the PSU. Two extreme model architectures of the PSU, as displayed in Fig. 21, have been considered.

In the circular architecture, the distance from any LH-II to the RC is minimized, since each LH-II is in direct contact with LH-I. In the stripe architecture, a similar number of LH-IIs are arranged in such a fashion that LH-IIs extend as far as possible away from the LH-I–RC complex. One requires that the architecture is densely filling the membrane. Thus, LH-IIs were arranged (Ritz *et al*. 2001), not in a single file but in a file of pairs extending up to five steps away from the LH-I–RC complex. The trapping time in the circular architecture of about 110 ps is approximately a factor of 2 smaller than the trapping time in the stripe architecture. Consequently, the yield in the circular architecture is about 6–8% higher than in the stripe architecture. On the other hand, excitation is dissipated more evenly in the stripe architecture (Ritz *et al*. 2001).

The changes observed from the stripe to the circular architecture are similar in quality and size as the changes that occur when LH-IIs are replaced by LH-IIIs in any of the two architectures. Since the latter changes are important enough to be coded in the genome, we must conclude that the changes observed due to differences in architectures are also functionally important to the bacterium.

This conclusion immediately raises the question of how a bacterium can control the organization of the PSU. To answer this question, one must understand how a bacterium controls the generation of the various pigment–protein complexes in the desired stoichoimetry and by which mechanism the pigment–protein complexes are assembled into

the multi-protein machinery of the PSU. It is at this point that structural information alone is no longer sufficient to understand the biological function, but that genetic and structural information need to be considered together.

3.3.8 Genetic basis of PSU assembly

The PSUs of purple bacteria need to achieve a high enough efficiency to provide sufficient energy for the bacteria to survive while at the same time the PSUs need to be protected against photooxidative damage. This precarious balance is maintained for a large range of environmental conditions. Bacteria adapt to changes in environmental conditions by rebuilding the complete photosynthetic apparatus on a timescale of minutes to at most a few hours.

Two environmental factors, oxygen tension and light intensity, have been shown to regulate the synthesis of PSU proteins (Cohen-Bazire *et al*. 1957). Oxygen at atmospheric levels (21 %) represses the photopigment production almost completely and the cell obtains its energy from respiration and substrate-level phosphorylation. In contrast, under anaerobic conditions (< 1 %) intracytoplasmatic membrane invaginations are formed which house the photosynthetic apparatus for the conversion of light energy into chemical energy. Light regulates synthesis of the antenna light-harvesting complexes, LH-II, which are synthesized at a rate inversely proportional to environmental light intensity.

Most of the factors responsible for the expression of the photosynthetic apparatus of purple bacteria have been characterized genetically, leading to the discovery of several proteins of unknown function and structure that play a role in controlling and supporting PSU assembly (Farchaus & Oesterhelt, 1989; Wong *et al*. 1996; Young *et al*. 1998; Young & Beatty, 1998; Aklujkar *et al*. 2000; Frese *et al*. 2000).

The structural genes required for PSU synthesis in *Rb. capsulatus* (Bauer *et al*. 1993) are located in a 46 kb region of the chromosome termed the photosynthesis gene cluster (GeneBank accession no. Z11165) which is shown in Fig. 22.

The central region contains a clustering of BChl and carotenoid biosynthesis genes flanked by the LH-I and RC structural genes. The latter are organized in the *puf* and *puh* operons. The *puf* operon encodes the LH-I apoproteins (α and β) and the L- and M-subunit of the RC (cf. Fig. 6 for the structure of the RC). In addition to these there are two further genes, *pufQ* and *pufX*, the structural roles of which are not clear. The protein PufX has been best characterized for *Rb. sphaeroides* where it is essential for photosynthetic growth and required for ubiquinone/ubiquinol shuttling between the RC quinone-binding site and the cytochrome bc_1 complex (Farchaus & Oesterhelt, 1989). PufX is either closely associated with or integrated into the LH-I ring and might be responsible for the long-range supraorganization of the photosynthetic unit (Frese *et al*. 2000). PufQ has been suggested to act as a regulator for BChl a synthesis levels (Bauer *et al*. 1993).

The *puh* operon contains the gene *puhA* encoding the H-subunit of the RC and five open reading frames (ORFs) located downstream of the *puhA* gene (Alberti *et al*. 1995). Recently, it has been shown in both *Rb. capsulatus* (Wong *et al*. 1996) and *R. rubrum* (Cheng *et al*. 2000; Lupo & Ghosh, unpublished observations) *puhA* that H-subunit deletion mutants were incapable of photosynthetic growth. The mutants in both studies contain no photosynthetic apparatus in the membrane, despite normal expression of the RC L and M proteins and LH-I polypeptides on the *puf* operon. These experimental results suggest that RC-H is required

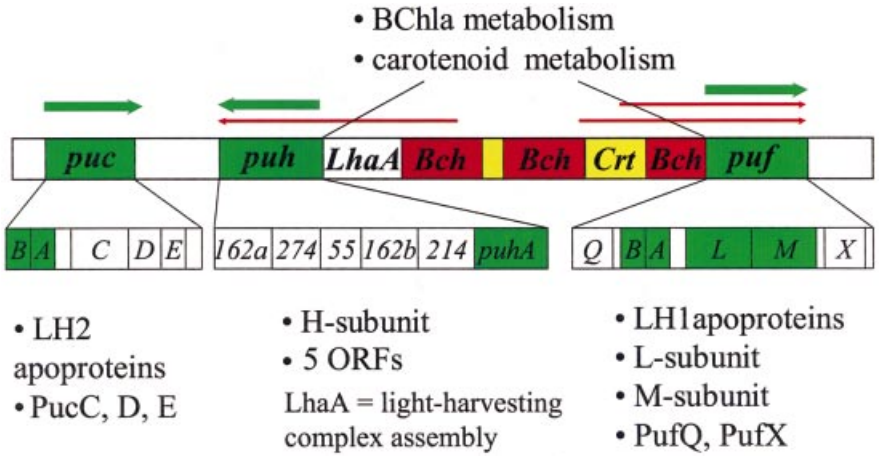

Fig. 22. Schematic overview of the photosynthesis gene cluster of *Rb. capsulatus* containing the genes for BChl *a* metabolism (red) and carotenoid metabolism (yellow) flanked by the *puf* and *puh* operons (green). The structurally characterized gene products are depicted as green fields and the non-characterized gene products as white fields (ORFs, open reading frames). The transcripts arising from the superoperons are depicted as red arrows. The *puf* and *puh* operon transcripts are depicted as green arrows. The longer transcripts are weakly repressed by oxygen, whereas the *puf* and *puh* operons are under control of strong oxygen-regulated promoters and are expressed at high levels under anaerobic conditions.

for the normal formation of the PSU in the photosynthetic membrane and that the assembly process is unstable or inefficient in the absence of RC-H. H-subunit deletion mutants of *R. rubrum* are still capable of forming LH-1 complexes in certain growth media (Lupo and Ghosh, unpublished observations), but can not assemble L and M subunits. Furthermore, in *Rb. capsulatus* the first two ORFs (ORF214 and ORF162b) transcribed after *puhA* possess a crucial role for photosynthetic growth and have been proposed to be assembly factors (Wong *et al*. 1996; Aklujkar *et al*. 2000). The more downstream located ORFs (ORF274, ORF55 and ORF162a) have not been genetically characterized at present.

Immediately upstream of the *puh* operon, a large gene encoding a protein that consists of 477 residues is located on the photosynthesis gene cluster of *Rb. capsulatus* (Young *et al*. 1998; Young & Beatty, 1998). This gene product is termed LhaA, for light-harvesting complex assembly, and is a major factor in LH-I assembly. Gene disruptions in *lhaA* lead to mutant strains deficient in LH-I. A theoretical 2D LhaA membrane topology model has been presented and it has been proposed that this protein might interact with LH components to enhance membrane insertion and stabilization of these complexes in the intracytoplasmic membrane (Young & Beatty, 1998).

The LH-II apoproteins (α and β) are encoded by the *puc* operon, which is unlinked to other parts of the photosynthesis gene cluster (cf. Fig. 22). In *Rb. capsulatus*, the *puc* operon contains a further gene, *pucC*, and two additional genes. *PucC* deletion mutants which completely lack the LH-II complex have been described in *Rb. capsulatus*. Due to its high degree of amino-acid conservation compared to LhaA (47 %) a similar functional role of PucC for the assembly of LH-II has been proposed (Young & Beatty, 1998).

In addition to these interesting features, which can be observed by single gene approach studies, regulation patterns for PSU synthesis on the transcriptional and post-transcriptional level have been investigated. The most intriguing feature of the photosynthesis gene cluster

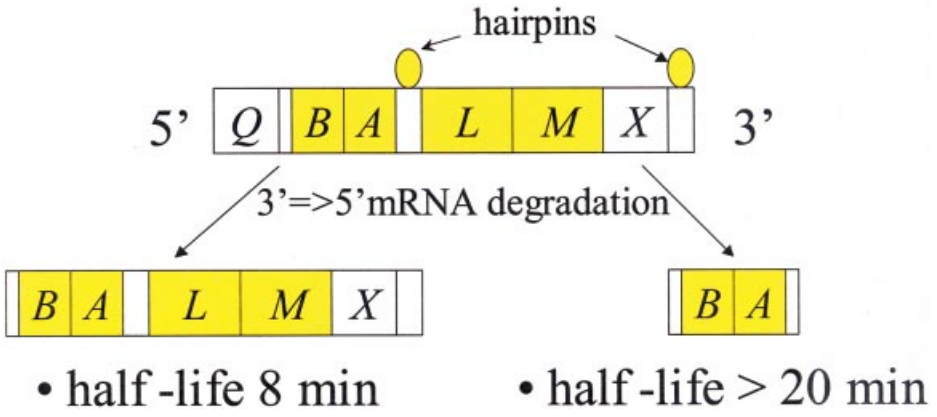

Fig. 23. Schematic overview of the mRNA processing events of the *puf* primary transcript. The *pufQBALMX* gets rapidly 5′ degraded to *pufBALMX* which gets degraded to *pufBA*. Further 3′→5′ degradation is halted by a hairpin region between *pufA* and *pufL*. The shorter *pufBA* message exhibits a longer half-life leading to an accumulation of *pufBA*.

is that its genes are organized into superoperons (Alberti *et al*. 1995). The superoperon organization produces several overlapping transcripts extending from the pigment biosynthesis genes into the *puf* and *puh* operons. Of these, the biosynthesis genes are weakly repressed by oxygen, whereas *puf* and *puh* operons are strongly repressed by oxygen. The advantage of this transcriptional system is that the synthesis of enzymes involved in photopigment biosynthesis is tightly coupled to synthesis of the structural polypeptides that bind the photopigments. The second advantage is that this floppy superoperon control allows aerobically grown cells a rapid adaption to photosynthetic growth conditions because a basic level of structural components for the PSU is always present in the cell. Under anaerobic conditions the *puf* and *puh* operons are expressed at high levels providing the high protein levels necessary for PSU formation. Recently it has been shown (Cheng *et al*. 2000) that the *puh* promoter can be expressed under semi-aerobic conditions and is more tolerant to oxygen than the *puf* promoter. Under anaerobic conditions RC-H is therefore present at high levels prior to the expression of RC-L, RC-M and LH-I polypeptides suggesting that the gene products can serve as foundation proteins for RC–LH-I assembly.

A further feature in expression of the photosynthetic gene cluster is that each of the different operons are encoded by one mRNA transcript. This so-called polycistronic organization allows the coordinated expression of all *puf* and *puh* genes for PSU formation. However an immediate problem arises when considering the expression of the *puf* gene. The stoichiometry of *pufAB* genes, encoding LH-I apoproteins, to *pufLM* genes, encoding the RC L- and M-subunits, is 1:1, but building of the RC–LH-I supercomplex requires 16 times more LH-I apoproteins than RC proteins. Nature has solved this problem by a post-transcriptional mRNA-processing event, illustrated in Fig. 23, which has been characterized for *Rb. capsulatus* in Klug (1995).

The complete *pufBALMX* message of *Rb. capsulatus* consisting of the RC L- and M-subunit, PufX and the LH-I apoproteins (α and β) is shortened by partial 3′→5′ degradation to a *pufBA* message consisting only of the LH-I apoproteins (α and β). The degradation only affects the *pufLMX* genes because of a hairpin sequence between *pufA* and *pufL*. Removal of the hairpin sequence results in severe changes of LH-I:RC stoichoimetries. Both mRNAs lack *pufQ* due to a rapid 5′ processing event of the primary transcript *pufQBALMX*. An

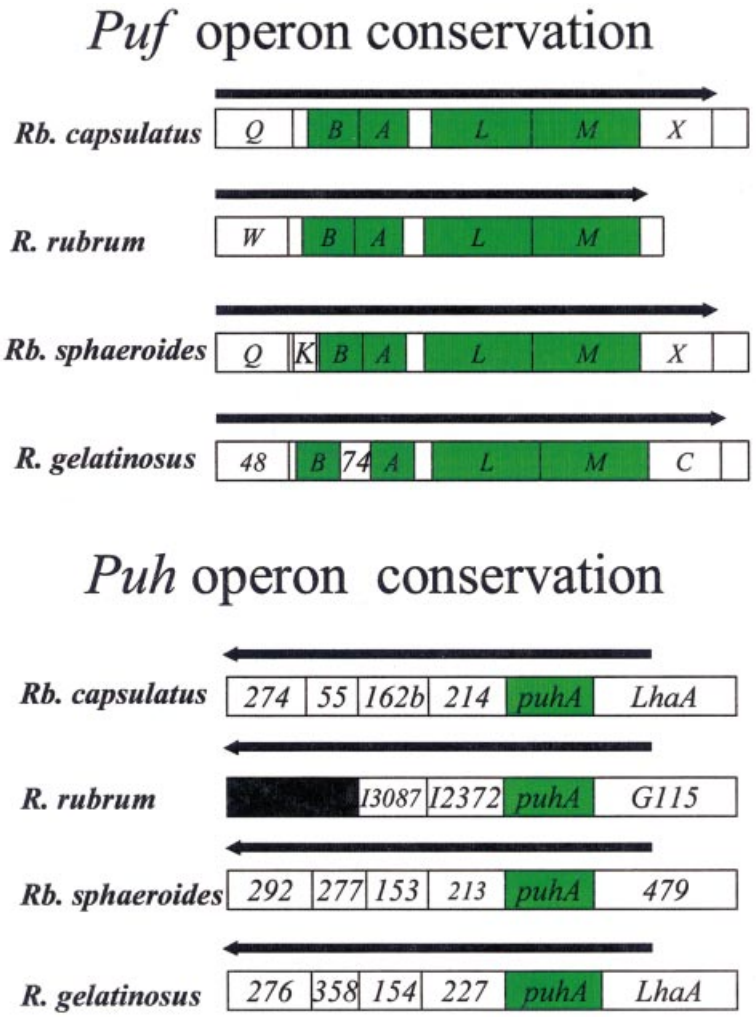

Fig. 24. Conservation of the *puf* and *puh* operons in various purple bacteria. The structurally characterized gene products are depicted as green fields and the structurally non-characterized genes as white fields.

important difference between the two mRNAs is their stability against further degradation. The *pufBALMX* message has a half-life of 8 min and the shorter *pufBA* message possesses a half-life greater than 20 min. As a consequence of the different stabilities *pufBA* accumulates compared to *pufBALMX*, leading to a 10- to 20-fold excess of LH-I synthesis relative to RC protein synthesis. This intriguing explanation of how nature achieves the needed stoichoimetry of LH-I and RC proteins underscores the necessity of adopting a systemic view when studying cellular machineries. The structure of the RC–LH-I supercomplex is determined by many factors, including the transcription mechanism of the photosynthesis gene cluster, the post-transcription processes leading to various mRNA segments, the different stability of these mRNA segments, the assembly mechanism of the expressed protein components in the membrane, and possibly further, yet unidentified, factors. Only the correct interplay of these many factors will result in the creation of a PSU capable of carrying out its essential functions.

The photosynthesis gene cluster has been best studied in *Rb. capsulatus* (Bauer *et al.* 1993; Alberti *et al.* 1995; Klug, 1995) but it is remarkable how the overall organization, the regulation patterns and even the homology of individual proteins and ORFs are conserved among many different species of purple bacteria.

In Fig. 24, we compare the gene organization of the *puf* operon and the *puh* operon of four different species, namely *Rb. capsulatus*, *R. rubrum*, *Rb. sphaeroides* and *R. gelatinosus*, exhibiting a high degree of conservation. Two possibilities for achieving this high degree of conservation can be discussed. Either the purple bacteria have acquired the photosynthesis genes recently by lateral gene transfer or selective pressure forced various species to retain these organizational patterns. The latter appears more likely as suggested by sequence comparative studies in which phylogenetic trees constructed from RC sequences mirror the phylogeny from 16S rRNA of the same species (Blankenship, 1992). According to this result it seems to be very likely that the photosynthesis gene cluster of purple bacteria is a very ancient gene organization form retained by selective pressure.

4. Concluding remarks

The pigment–protein complexes in the bacterial PSU are responsible for the absorption of light energy and its conversion to electronic excitation that drives the primary charge separation process. All the pigment–protein complexes bind both BChls and carotenoids; with a typical number of 10 LH-IIs, 1 LH-I and 1 RC the PSU contains approximately 300 BChls. The observed stoichiometric ratio BChl:Car of 3:2 implies the presence of 200 carotenoids. Out of all these pigments, only very few BChls in the RC directly take part in photochemical reactions; most BChls serve as light-harvesting antennae capturing the sunlight and funneling electronic excitation towards the RC. A wealth of evidence has accumulated now which proves that the organization of PSUs, to surround an RC with aggregates of chlorophylls and associated carotenoids, is universal in photosynthetic bacteria, higher plants and other photosynthetic organisms (Cogdell *et al.* 1996; Fromme, 1996; Hankamer *et al.* 1997; Hu & Schulten, 1997).

The flow of excitation from the outer antenna complexes to the RC is controlled by differences in excitation energies between the various chromophores in the PSU. Each of the antenna systems contains accessory chromophores with high excitation energies, e.g. carotenoids and B800 BChls (in LH-II). These accessory chromophores collect high-energy light, thereby extending the spectral cross-section of the PSU and funnel the light energy, in form of electronic excitation, to the BChl ring systems in the antenna complexes. Once excitation has reached one of the BChl ring systems, it flows more or less undirected between the BChl ring systems and is thereby spread over a large area of the PSU. In this architecture, an excitation reservoir is created, from which the RC drains excitation as needed, and in which excess excitation is dissipated over a large area. The flow of excitation in this reservoir can be regulated by fine-tuning the relative excitation energies of the BChl ring systems, e.g. by replacing LH-II with LH-III. During billions of years of evolution, nature has adopted a variety of ways to shift the spectral maxima for light absorption. A direct way of shifting the spectrum is to use different kinds of pigments that absorb maximally at different wavelength (Scheer, 1991). A more elegant way of doing this is achieved in the bacterial PSU. LH-II, LH-I and RC all contain BChl *a* as the major pigment. Absorption spectra of monomeric BChl *a* peaks at 772 nm in organic solvent. In the PSU, the peak positions red-shift to various

extents (i.e. 800 ~ 900 nm), yielding absorption maxima of 800 and 850 nm for LH-II and 875 nm for LH-I, respectively. The observed spectral shifts result mainly from intrinsic properties of BChls and excitonic interactions (Hu *et al*. 1997; Cory *et al*. 1998). Excitonic coupling splits the excited state energies, thus improving the overlap between donor and acceptor spectra in the excitation cascade (Hu *et al*. 1997; Cory *et al*. 1998; Damjanović *et al*. 1999). It has also been suggested that the spectra of BChls are tuned to a limited degree through interaction with the protein environment, e.g. through formylmethionine–Mg^{2+} ligation in case of B800 of LH-II from *Rps*. *acidophila* (McDermott *et al*. 1995) or through an Asp–Mg^{2+} ligation in case of B800 of LH-II from *Rs*. *molischianum* (Koepke *et al*. 1996).

The efficient flow of excitation through the chromophore system requires highly ordered aggregates, the geometry of which is adapted to the needed interactions; carotenoids must be in close (van der Waals) contact with BChls for triplet quenching and must be proximate within a few Ångstroms for transfer of optically forbidden excitations. Chlorophylls, in order to achieve significant exciton splitting, must have Mg^{2+}–Mg^{2+} distances of about 10 Å; for energy transfer on a picosecond timescale, Mg^{2+}–Mg^{2+} distances must be of the order of 20 Å. Exciton splitting facilitate photon fueling into the BChl funnel due to an increase in spectral overlap with higher-energetic chromophores. It is possible that BChls form aggregates to achieve coherence over many chromophores, and thus, significant exciton splitting.

A multi-protein architecture displayed by the bacterial PSU is necessary to provide a large enough scaffold for the number of chromophores employed in light harvesting. Due to this architecture, antenna systems employ a hierarchy of chromophore aggregates; the chromophores are closer and more tightly coupled in the individual pigment–protein complex, e.g. in LH-II, and more loosely coupled between different pigment–protein complexes. The control of the overall aggregation of the multi-protein system is in itself an impressive achievement worthy of study (Bailey *et al*. 1998).

In summary, the bacterial PSU constitutes an ideal model system of the photosynthetic apparatus which, due to its smaller size, is more amenable to study (Clayton & Sistrom, 1978; Blankenship *et al*. 1995). The properties of the antenna systems of purple bacteria discussed here may potentially serve an understanding of a broader class of photosynthetic life forms since the underlying physical principles governing the light-harvesting and electron-transfer processes are most likely similar for all the photosynthetic organisms (Borisov, 1978; Grossman *et al*. 1995; Green & Durnford, 1996; Gantt, 1996; Nugent, 1996; Larkum & Howe, 1997; Hu & Schulten 1997). In this regard, it is worth mentioning that momentous progress has been achieved recently in structural determination of pigment–protein complexes of other photosynthetic organisms. Among others, Photosystem I (PS I) of cyanobacterium *Synechococcus elongatus* has very recently been resolved at 2·5 Å resolution by X-ray crystallography (Jordan *et al*. 2001). PS II from higher plants (spinach), green alga *Chlamydomonas reinhardtii* and cyanobacterium *Synechococcus elongatus* have been imaged by electron microscopy (Rhee *et al*. 1998; Nield *et al*. 2000), and a 3·8 Å structure for PS II of the cyanobacterium *Synechococcus elongatus* has recently been determined by X-ray crystallography (Zouni *et al*. 2001); the structure of the plant light-harvesting complex LHCII, located within the thylakoid membrane in the vicinity of PS II, was resolved at 3·4 Å (Kühlbrandt, 1994); and the peridinin–chlorophyll–protein (PCP), an extra-membrane LH in the photosynthetic unit of dinoflagellates, has been resolved at 2·0 Å resolution (Hofmann *et al*. 1996). Also, the structure of the water-soluble BChl *a* protein (BChl protein) from the green photosynthetic bacterium *Prosthecochloris aestuarii* has been determined at 1·9 Å

resolution in 1986 (Tronrud *et al*. 1986). The availability of more integrated light-harvesting systems from various photosynthetic organisms furnishes the unique opportunity for a comparative study of the light harvesting process.

5. Acknowledgments

The authors acknowledge financial support from the National Institutes of Health (P41RR05969), the National Science Foundation (NSF BIR 9318159 and NSF BIR-94-23827(EQ)), the deArce Fund for Medical Research and Development, and the Carver Charitable Trust.

6. References

Aagaard, J. & Sistrom, W. (1972). Control of synthesis of reaction center bacteriochlorophyll in photosynthetic bacteria. *Photochem. Photobiol.* **15**, 209–225.

Abrahams, J., Leslie, A., Lutter, R. & Walker, J. (1994). Structure at 2·8 Å resolution of F_1-ATPase from bovine heart mitochondria. *Nature* **370**, 621–628.

Aklujkar, M., Harmer, A., Prince, R. & Beatty, J. (2000). The *orf162b* sequence of *Rhodobacter capsulatus* encodes a protein required for optimal levels of photosynthetic pigment–protein complexes. *J. Bacteriol.* **182**, 5440–5447.

Alberti, M., Burke, D. & Hearst, J. (1995). Structure and sequence of the photosynthesis gene cluster. In *Anoxygenic Photosynthetic Bacteria* (eds. R. Blankenship, M. Madigan & C. Bauer), pp. 1083–1106. Dordrecht: Kluwer Academic Publishers.

Alden, R., Johnson, E., Nagarajan, V., Parson, W., Law, C. & Cogdell, R. (1997). Calculations of spectroscopic properties of the LH2 bacteriochlorophyll-protein antenna complex from *Rhodopseudomonas acidophila*. *J. phys. Chem.* (*B*), **101**, 4667–4680.

Allen, J., Yeates, T., Komiya, H. & Rees, D. (1987). Structure of the reaction center from *Rhodobacter sphaeroides* R-26: the protein subunits. *Proc. natn. Acad. Sci. USA* **84**, 6162–6166.

Angerhofer, A., Cogdell, R. & Hipkins, M. (1986). A spectral characterization of the light-harvesting pigment–protein complexes from *Rhodopseudomonas acidophila*. *Biochim. Biophys. Acta* **848**, 333–341.

Arnold, W. & Kohn, H. I. (1934). The chlorophyll unit in photosynthesis. *J. gen. Physiol.* **18**, 109–112.

Bailey, M., Schulten, K. & Johnson, J. E. (1998). The use of solid physical models for the study of macromolecular assembly. *Curr. Opin. struct. Biol.* **8**, 202–208.

Bakalis, L. D., Coca, M. & Knoester, J. (1999). Optical line shapes of dynamically disordered aggregates. *J. chem. Phys.* **110**, 2208–2218.

Barnes, C. R. (1893). On the food of green plants. *Bot. Gaz.* **18**, 403–411.

Barvik, I., Warns, C., Neidlinger, T. & Reineker, P. (1999). Simulation of excitonic optical line shapes of cyclic molecular aggregates with 9 and 18 units: influence of quasi-static and dynamic disorder. *Chem. Phys.* **240**, 173–189.

Bauer, C., Buggy, J. & Mosley, C. (1993). Control of photosystem genes in *Rhodobacter capsulatus*. *Trends Genet.* **9**, 56–60.

Bergström, H., van Grondelle, R. & Sundström, V. (1989). Characterization of excitation energy trapping in photosynthetic purple bacteria at 77 K. *FEBS Lett.* **250**, 503–508.

Bixon, M. & Jortner, J. (1999). Electron transfer – from isolated molecules to biomolecules. *Adv. chem. Phys.* **106**, 35–202.

Blankenship, R. (1992). Origin and early evolution of photosynthesis. *Photosyn. Res.* **33**, 91–111.

Blankenship, R. E., Madigan, M. T. & Bauer, C. E. (1995). *Anoxygenic Photosynthetic Bacteria*. Dordrecht: Kluwer Academic Publishers.

Boonstra, A., Germeroth, L. & Boekema, E. (1994). Structure of the light harvesting antenna from *Rhodospirillum molischianum* studied by electron microscopy. *Biochim. Biophys. Acta* **1184**, 227–234.

Bopp, M., Yiwei, J., Li, L., Cogdell, R. & Hochstrasser, R. (1997). Fluorescence and photobleaching dynamics of single light-harvesting complexes. *Proc. natn. Acad. Sci. USA* **94**, 10630–10635.

Bopp, M., Sytnik, A., Howard, T., Cogdell, R. & Hochstrasser, R. (1999). The dynamics of structural deformations of immobilized single light-harvesting complexes. *Proc. natn. Acad. Sci. USA* **96**, 11271–11276.

Borisov, A. Y. (1978). Energy-migration mechanisms in antenna chlorophylls. In *The Photosynthetic Bacteria* (ed. R. Sistrom), pp. 323–331. New York: Plenum Press.

Borisov, A. Y. & Godik, V. I. (1973). Excitation energy transfer in photosynthesis. *Biochim. Biophys. Acta* **301**, 227–248.

Breton, J. & Verméglio, A. (1992). *The Photosynthetic Bacterial Reaction Center II*. New York: Plenum Press.

Chachisvilis, M., Kühn, O., Pullerits, T. & Sundström, V. (1997). Excitons in photosynthetic purple bacteria: wavelike motion or incoherent hopping? *J. phys. Chem.* (*B*), **101**, 7275–7283.

Chadwick, B., Zhang, C., Cogdell, R. & Frank, H. (1987). The effects of lithium dodecyl sulfate and sodium borohydride on the absorption spectrum of the B800–850 light harvesting complex from *Rhodopseudomonas acidophila* 7750. *Biochim. Biophys. Acta* **893**, 444–451.

Chang, C. H., Tiede, D., Tang, J., Smith, U., Norris, J. & Schiffer, M. (1986). Structure of *Rhodopseudomonas sphaeroides* R-26 reaction center. *FEBS Lett.* **205**, 82–86.

Cheng, Y., Brantner, C., Tsapin, A. & Collins, M. (2000). Role of the H protein in assembly of the photochemical reaction center and intracytoplasmic membrane in *Rhodospirillum rubrum*. *J. Bacteriol.* **182**, 1200–1207.

Clayton, R. & Sistrom, W. (Eds.) (1978). *The Photosynthetic Bacteria*. New York: Plenum Press.

Clayton, R. K. (1966). The bacterial photosynthetic reaction center. *Brookhaven Symp. Biol.* **19**, 62–70.

Clayton, R. K. (1973). Primary processes in bacterial photosynthesis. *Annu. Rev. biophys. Bioeng.* **2**, 131–156.

Cogdell, R., Andersson, P. & Gillbro, T. (1992). Carotenoid singlet states and their involvement in photosynthetic light-harvesting pigments. *J. Photochem. Photobiol.* (*B*), **15**, 105–112.

Cogdell, R., Fyfe, P., Barrett, S., Prince, S., Freer, A., Isaacs, N., McGlynn, P. & Hunter, C. (1996). The purple bacterial photosynthetic unit. *Photosyn. Res.* **48**, 55–63.

Cogdell, R., Hipkins, M., MacDonald, W. & Truscott, T. (1981). Energy transfer between the carotenoid and the bacteriochlorophyll within the B-800–850 light-harvesting pigment–protein complex of *Rhodopseudomonas sphaeroides*. *Biochim. Biophys. Acta* **634**, 191–202.

Cogdell, R. J., Isaacs, N. W., Howard, T. D., McLuskey, K., Fraser, N. J. & Prince, S. M. (1999). How photosynthetic bacteria harvest solar energy. *J. Bacteriol.* **181**, 3869–3879.

Cohen-Bazire, G., Sistrom, W. & Stanier, R. (1957). Kinetic studies in pigment synthesis by non-sulfur bacteria. *J. Cellular comp. Physiol.* **49**, 25–68.

Cory, M. G., Zerner, M. C., Hu, X. & Schulten, K. (1998). Electronic excitations in aggregates of bacteriochlorophylls. *J. phys. Chem.* (*B*), **102**, 7640–7650.

Damjanović, A., Kosztin, I., Kleinekathoefer, U. & Schulten, K. (In Press). Excitons in a photosynthetic light-harvesting system: a combined molecular dynamics, quantum chemistry and polaron study. *Phys. Rev.* (*E*).

Damjanović, A., Ritz, T. & Schulten, K. (1999). Energy transfer between carotenoids and bacteriochlorophylls in a light harvesting protein. *Phys. Rev.* (*E*), **59**, 3293–3311.

Damjanović, A., Ritz, T. & Schulten, K. (2000a). Excitation energy trapping by the reaction center of *Rhodobacter sphaeroides*. *Int. J. Quantum Chem.* **77**, 139–151.

Damjanović, A., Ritz, T. & Schulten, K. (2000b). Excitation transfer in the peridinin–chlorophyll–protein of *Amphidinium carterae*. *Biophys. J.* **79**, 1695–1705.

Deinum, G., Otte, S., Gardiner, A., Aartsma, T., Cogdell, R. & Amesz, J. (1991). Antenna organization of *Rhodopseudomonas viridis* in relation to the redox state of the primary electron donor. *Biochim. Biophys. Acta* **1060**, 125–131.

Deisenhofer, J., Epp, O., Mikki, K., Huber, R. & Michel, H. (1985). Structure of the protein subunits in the photosynthetic reaction centre of *Rhodopseudomonas virdis* at 3 Å resolution. *Nature* **318**, 618–624.

Deisenhofer, J. & Michel, H. (1991). High-resolution structures of photosynthetic reaction centers. *Annu. Rev. Biophys. biophys. Chem.* **20**, 247–266.

Deisenhofer, J. & Norris, J. R. (Eds.) (1993). *The Photosynthetic Reaction Center. Volumes I and II*. San Diego: Academic Press.

Dexter, D. (1953). A theory of sensitized luminescence in solids. *J. chem. Phys.* **21**, 836–850.

Dracheva, T., Novoderezhkin, V. & Razjivin, A. (1996). Exciton delocalization in the antenna of purple bacteria – exciton spectrum using X-ray data and experimental site inhomogeneity. *FEBS Lett.* **387**, 81–84.

Duysens, L. N. M. (1952). Transfer of excitation energy in photosynthesis. PhD thesis, Utrecht.

Duysens, L. N. M. (1964). Photosynthesis. *Progr. Biophys. molec. Biol.* **14**, 1–104.

Duysens, L. N. M. (1988). The discovery of the two photosynthetic systems: a personal account. *Photosyn. Res.* **21**, 61–79.

Einstein, A. (1917). Zur Quantentheorie der Strahlung. *Physik. Zeitschrift* **18**, 121–128.

Emerson, R. & Arnold, A. (1932). The photochemical reaction in photosynthesis. *J. gen. Physiol.* **16**, 191–205.

Engelhardt, H., Engel, A. & Baumeister, W. (1986). Stoichiometric model of the photosynthetic unit of *Ectothiorhodospira halochloris*. *Proc. natn. Acad. Sci. USA* **83**, 8972–8976.

Ermler, U., Fritzsch, G., Buchanan, S. & Michel, H. (1994). Structure of the photosynthetic reaction center from *Rhodobacter sphaeroides* at 2·65 Å resolution: cofactors and protein-cofactor interactions. *Structure* **2**, 925–936.

Farchaus, J. & Oesterhelt, D. (1989). A *Rhodobacter sphaeroides puf* L, M, and X deletion mutant and its complementation in trans with a 5·3 kb *puf* operon shuttle fragment. *EMBO J.* **8**, 47–54.

Fleming, G. & van Grondelle, R. (1994). The primary steps of photosynthesis. *Physics Today* **47**, 48–55.

Fleming, G. R. & van Grondelle, R. (1997). Femtosecond spectroscopy of photosynthetic light-harvesting systems. *Curr. Opin. struct. Biol.* **7**, 738–748.

Förster, T. (1948). Zwischenmolekulare Energiewanderung und Fluoreszenz. *Ann. Phys.* (*Leipzig*) **2**, 55–75.

Förster, T. (1965). *Delocalized Excitation and Excitation Transfer*, pp. 93–137. New York: Academic Press.

Francke, C. & Amesz, J. (1995). The size of the photosynthetic unit in purple bacteria. *Photosyn. Res.* **46**, 347–352.

Frank, H. (1993). Carotenoids in photosynthetic bacterial reaction centers: structure, spectroscopy, and photochemistry. In *The Photosynthetic Reaction Center*, vol. 2, pp. 221–237. San Diego: Academic Press.

Frank, H. A., Bautista, J. A., Josue, J., Pendon, Z., Hiller, R. G., Sharples, F. P., Gosztola, D. & Wasielewski, M. R. (2000). Effect of the solvent environment on the spectroscopic properties and dynamics of the lowest excited states of carotenoids. *J. phys. Chem.* (*B*), **104**, 4569–4577.

Freiberg, A. (1995). Coupling of antennas to reaction centers. In *Anoxygenic Photosynthetic Bacteria* (eds. R. E. Blankenship, M. T. Madigan & C. E. Bauer), pp. 385–398. Dordrecht: Kluwer Academic Publishers.

Frenkel, A. (1954). Light-induced phosphorylation by cell-free preparations of photosynthetic bacteria. *J. Am. chem. Soc.* **76**, 5568–5569.

Frese, R., Olsen, J., Branvall, R., Westerhuis, W., Hunter, C. & van Grondelle, R. (2000). The long-range supraorganization of the bacterial photosynthetic unit: a key role for PufX. *Proc. natn. Acad. USA* **97**, 5197–5202.

Fromme, P. (1996). Structure and function of photosystem I. *Curr. Opin. struct. Biol.* **6**, 473–484.

Fujii, R., Onaka, K., Kuki, M., Koyama, Y. & Watanabe, Y. (1998). The A_g^- energies of all-trans-neurosporene and spheroidene as determined by fluorescence spectroscopy. *Chem. Phys. Lett.* **288**, 847–853.

Fyfe, P. K. & Cogdell, R. J. (1996). Purple bacterial antenna complexes. *Curr. Opin. struct. Biol.* **6**, 467–472.

Gantt, E. (1996). Pigment protein complexes and the concept of the photosynthetic unit: chlorophyll complexes and phycobilisomes. *Photosyn. Res.* **48**, 47–53.

Gardiner, A., Cogdell, R. & Takaichi, S. (1993). The effect of growth conditions on the light-harvesting apparatus in *Rhodopseudomonas acidophila*. *Photosyn. Res.* **38**, 159–168.

Germeroth, L., Lottspeich, F., Robert, B. & Michel, H. (1993). Unexpected similarities of the B800–850 light-harvesting complex from *Rhodospirillum molischianum* to the B870 light-harvesting complexes from other purple photosynthetic bacteria. *Biochemistry* **32**, 5615–5621.

Gest, H. (1993). History of concepts of the comparative biochemistry of oxygenic and anoxygenic photosyntheses. *Photosyn. Res.* **35**, 87–96.

Gillbro, T., Cogdell, R. J. & Sundström, V. (1988). Energy transfer from carotenoid to bacteriochlorophyll a in the B800–820 antenna complexes from *Rhodopseudomonas acidophila* strain 7050. *FEBS Lett.* **235**, 169–172.

Gouterman, M. (1961). Spectra of porphyrins. *J. molec. Spectrosc.* **6**, 138–163.

Govindjee, (Ed.) (1982). *Photosynthesis*. New York: Academic Press.

Green, B. R. & Durnford, D. G. (1996). The chlorophyll-carotenoid proteins of oxygenic photosynthesis. *Annu. Rev. Plant. Physiol.* **47**, 685–714.

Grossman, A. R., Bhaya, D., Apt, K. E. & Kehoe, D. M. (1995). Light-harvesting complexes in oxygenic photosynthesis: diversity, control, and evolution. *Annu. Rev. Genet.* **29**, 231–288.

Hankamer, B., Barber, J. & Boekema, E. J. (1997). Structure and membrane organization of photosystem II in green plants. *Annu. Rev. Plant. Physiol.* **48**, 641–671.

Hawthornthwaite, A. M. & Cogdell, R. J. (1991). Bacteriochlorophyll binding proteins. In *Chlorophylls* (ed. H. Scheer), pp. 493–528. Boca Raton: CRC Press.

Herek, J., Polivka, T., Pullerits, T., Fowler, G., Hunter, C. & Sundström, V. (1998). Ultrafast carotenoid band shifts probe structure and dynamics in photosynthetic antenna complexes. *Biochemistry* **37**, 7057–7061.

Hess, S., Chachisvilis, M., Timpmann, K., Jones, M., Fowler, G., Hunter, C. & Sundström, V. (1995). Temporally and spectrally resolved subpicosecond energy transfer within the peripheral antenna complex (LH2) and from LH2 to the core antenna complex in photosynthetic purple bacteria. *Proc. natn. Acad. Sci. USA* **92**, 12333–12337.

Hoff, A. J. & Deisenhofer, J. (1997). Photophysics of photosynthesis. Structure and spectroscopy of reaction centers of purple bacteria. *Phys. Rep.* **287**, 1–247.

Hofmann, E., Wrench, P., Sharples, F., Hiller, R., Welte, W. & Diederichs, K. (1996). Structural basis of light harvesting by carotenoids: peridinin-chlorophyll-protein from *Amphidinium carterae*. *Science* **272**, 1788–1791.

Hu, X., Damjanović, A., Ritz, T. & Schulten, K. (1998). Architecture and function of the light harvesting apparatus of purple bacteria. *Proc. natn. Acad. Sci. USA* **95**, 5935–5941.

Hu, X., Ritz, T., Damjanović, A. & Schulten, K. (1997). Pigment organization and transfer of electronic excitation in the purple bacteria. *J. phys. Chem.* (*B*), **101**, 3854–3871.

Hu, X. & Schulten, K. (1997). How nature harvests sunlight. *Physics Today* **50**, 28–34.

Hu, X. & Schulten, K. (1998). A model for the light-harvesting complex I (B875) of *Rhodobacter sphaeroides*. *Biophys. J.* **75**, 683–694.

Hu, X., Xu, D., Hamer, K., Schulten, K., Koepke, J. & Michel, H. (1995a). Predicting the structure of the light-harvesting complex II of *Rhodospirillum molischianum*. *Protein Sci.* **4**, 1670–1682.

Hu, X., Xu, D., Hamer, K., Schulten, K., Koepke, J. & Michel, H. (1995b). Prediction of the structure of an integral membrane protein – the light-harvesting complex II of *Rhodospirillum molischianum*. In *Biological Membranes: A Molecular Perspective from Computation and Experiment* (eds. K. Merz. & B. Roux), pp. 503–533. Cambridge, MA: Birkhäuser.

Hudson, B. & Kohler, B. (1972). A low-lying weak transition in the polyene α,ω-diphenyloctatetraene. *Chem. Phys. Lett.* **14**, 299–304.

Humphrey, W. F., Dalke, A. & Schulten, K. (1996). VMD – Visual Molecular Dynamics. *J. molec. Graphics* **14**, 33–38.

Hunter, C. N., van Grondelle, R. & Olsen, J. D. (1989). Photosynthetic antenna proteins – 100 ps before photochemistry starts. *Trends Biochem. Sci.* **14**, 72–75.

Ikeda-Yamasaki, I., Odahara, T., Mitsuoka, K., Fujiyoshi, Y. & Murata, K. (1998). Projection map of the reaction center-light harvesting 1 complex from *Rhodopseudomonas viridis* at 10 angstrom resolution. *FEBS Lett.* **425**, 505–508.

IUPAC–IUB Joint Commission on Biochemical Nomenclature (JCBN) (1986). Nomenclature of tetrapyrroles, recommendations. *Eur. J. Biochem.* **178**, 277–328.

Jang, S, Dempster, S. E. & Silbey, R. J. (2001). Characterization of the static disorder in the B850 band of LH2. *J. phys. Chem.* (*B*). **105**, 6655–6665.

Jimenez, R., van Mourik, F., Yu, J. Y. & Fleming, G. R. (1997). Three-pulse photon echo measurements on LH1 and LH2 complexes of *Rhodobacter sphaeroides*: a nonlinear spectroscopic probe of energy transfer. *J. phys. Chem.* (*B*), **101**, 7350–7359.

Joliot, P., Vermeglio, A. & Joliot, A. (1989). Evidence for supercomplexes between reaction centers, cytochrome c_2 and cytochrome bc_1 complex in *Rhodobacter sphaeroides* whole cells. *Biochim. Biophys. Acta* **975**, 336–345.

Jordan, P., Fromme, P., Witt, H., Klukas, O., Saenger, W. & Krauss, N. (2001). Three-dimensional structure of cyanobacterial photosystem I at 2·5 Å resolution. *Nature* **411**, 909–917.

Jungas, C., Ranck, J., Rigaud, J., Joliot, P. & Vermeglio, A. (1999). Supramolecular organization of the photosynthetic apparatus of *Rhodobacter sphaeroides*. *EMBO J.* **18**, 534–542.

Kaplan, S. & Arntzen, C. (1982). Photosynthetic membrane structure and function. In *Photosynthesis, Energy Conversion by Plants and Bacteria* (ed. Govindjee), vol. 1, pp. 65–151. New York: Academic Press.

Karrasch, S., Bullough, P. & Ghosh, R. (1995). 8·5 Å projection map of the light-harvesting complex I from *Rhodospirillum rubrum* reveals a ring composed of 16 subunits. *EMBO J.* **14**, 631–638.

Kennis, J., Strltsov, A., Permentier, H., Aartsma, T. & Amesz, J. (1997). Exciton coherence and energy transfer in the LH2 antenna complex of *Rhodopseudomonas acidophila* at low temperature. *J. phys. Chem.* (*B*), **101**, 8369–8374.

Ketelars, M., van Oijen, A., Matsushita, M., Köhler, J., Schmidt, J. & Aartsma, T. (2001). Spectroscopy of the B850 band of individual light-harvesting 2 complexes of *Rhodopseudomonas acidophila* I. Experiments and Monte Carlo simulations. *Biophys. J.* **80**, 1591–1603.

Kleinekofort, W., Germeroth, L., van der Broek, J., Schubert, D. & Michel, H. (1992). The light-harvesting complex II (B800/850) from *Rhodospirillum molischianum* is an octamer. *Biochim. Biophys. Acta* **1140**, 102–104.

Klug, G. (1995). Post-transcriptional control of photosynthesis gene expression. In *Anoxygenic Photosynthetic Bacteria* (eds. R. Blankenship, M. Madigan & C. Bauer), pp. 1235–1244. Dordrecht: Kluwer Academic Publishers.

Knox, R. S. (1977). Photosynthetic efficiency and exciton transfer and trapping. In *Primary Process of Photosynthesis* (ed. J. Barber), pp. 55–97. Amsterdam: Elsevier.

Koepke, J., Hu, X., Münke, C., Schulten, K. & Michel, H. (1996). The crystal structure of the light harvesting complex II (B800–850) from *Rhodospirillum molischianum*. *Structure* **4**, 581–597.

Kramer, H., van Grondelle, R., Hunter, C. N., Westerhuis, W. & Amesz, J. (1984). Pigment organization of the B800–850 antenna complex of *Rhodopseudomonas sphaeroides*. *Biochim. Biophys. Acta* **765**, 156–165.

Krueger, B., Scholes, G., Yu, J. & Fleming, G. (1999a). The light harvesting process in purple bacteria. *Acta. Phys. Pol.* (*A*), **95**, 63–83.

Krueger, B., Scholes, G., Gould, I. & Fleming, G. (1999b). Carotenoid mediated B800–B850 coupling in LH2. *Phys. chem. Comm.* **8**, 9/03172C.

Krueger, B., Scholes, G., Jimenez, R. & Fleming, G. (1998a). Electronic excitation transfer from carotenoid to bacteriochlorophyll in the purple bacterium *Rhodopseudomonas acidophila*. *J. phys. Chem.* (*B*), **102**, 2284–2292.

Krueger, B. P., Scholes, G. D. & Fleming, G. R. (1998b). Calculation of couplings and energy-transfer pathways between the pigments of LH2 by the *ab initio* transition density cube method. *J. phys. Chem.* (*B*) **102**, 5378–5386.

Kühlbrandt, W. (1994). High-resolution electron crystallography of membrane proteins. In *Membrane Protein Structure: Experimental Approaches* (ed. S. White), pp. 206–223. New York: Oxford University Press.

Lancaster, C., Ermler, U. & Michel, H. (1995). The structure of photosynthetic reaction centers from purple bacteria as revealed by X-ray crystallography. In *Anoxygenic Photosynthetic Bacteria* (eds. R. Blankenship, M. Madigan & C. Bauer), pp. 503–526. Dordrecht: Kluwer Academic Publishers.

Larkum, T. & Howe, C. J. (1997). Molecular aspects of light-harvesting processes in algae. *Advan. botan. Res.* **27**, 257–330.

Leguijt, T., Visschers, R. W., Crielaard, W., van Grondelle, R. & Hellingwerf, K. J. (1992). Low-temperature fluorescence and absorption spectroscopy of reaction center/antenna complexes from *Ectothiorhodospira mobilis*, *Rhodopseudomonas palustris* and *Rhodobacter sphaeroides*. *Biochim. Biophys. Acta* **1102**, 177–185.

Leupold, D., Stiel, H., Teuchner, K., Nowak, F., Sandner, W., Ucker, B. & Scheer, H. (1996). Size enhancement of transition dipoles to one and two-exciton bands in a photosynthetic antenna. *Phys. Rev. Lett.* **77**, 4675–4678.

Leupold, D., Voigt, B., Beenken, W. & Stiel, H. (2000). Pigment–protein architecture in the light-harvesting antenna complexes of purple bacteria: does the crystal structure reflect the native pigment-protein arrangement? *FEBS Lett.* **480**, 73–78.

Ma, Y., Cogdell, R. & Gillbro, T. (1997). Energy transfer and exciton annihilation in the B800–850 antenna complex of the photosynthetic purple bacterium *Rhodopseudomonas acidophila* (strain 10050) – a femtosecond transient absorption study. *J. phys. Chem.* (*B*), **101**, 1087–1095.

Macpherson, A. M., Arellano, J. B., Fraser, N. J., Cogdell, R. J. & Gillbro, T. (2001). Efficient energy transfer from the carotenoid S_2 state in a photosynthetic light-harvesting complex. *Biophys. J.* **80**, 923–930.

Matsushita, M., Ketelars, M., Van Oijen, A., Köhler, J., Aartsma, T. & Schmidt, J. (2001). Spectroscopy of the B850 band of individual light-harvesting 2 complexes of *Rhodopseudomonas acidophila* II. Exciton states of an elliptically deformed aggregate. *Biophys. J.* **80**, 1604–1614.

Mauzerall, D. & Greenbaum, N. (1989). The absolute size of a photosynthetic unit. *Biochim. Biophys. Acta* **974**, 119–140.

McDermott, G., Prince, S., Freer, A., Hawthornthwaite-Lawless, A., Papiz, M., Cogdell, R. & Isaacs, N. (1995). Crystal structure of an integral membrane light-harvesting complex from photosynthetic bacteria. *Nature* **374**, 517–521.

McLuskey, K., Prince, S., Cogdell, R. J. & Isaacs, N. (2001). The crystallographic structure of the B800–820 LH3 light-harvesting complex from the purple bacterium *Rhodopseudomonas acidophila* strain 7050. *Biochemistry* **40**, 8783–8789.

Meckenstock, R., Krusche, K., Brunisholz, R. & Zuber, H. (1992). The light-harvesting core-complex and the B820-subunit from *Rhodopseudomonas marina*. Part II. electron microscopic characterisation. *FEBS Lett.* **311**, 135–138.

Michel-Beyerle, M. E. (Ed.) (1996).). *Reaction Centers of Photosynthetic Bacteria. Structure and Dynamics*. Berlin: Springer-Verlag.

Miller, K. (1982). Three-dimensional structure of a photosynthetic membrane. *Nature* **300**, 53–55.

Monger, T. & Parson, W. (1977). Singlet-triplet fusion in *Rhodopseudomonas sphaeroides* chromatophores. A probe of the organization of the photosynthetic apparatus. *Biochim. Biophys. Acta* **460**, 393–407.

Monshouwer, R., Abrahamsson, M., van Mourik, F. & van Grondelle, R. (1997). Superradiance and exciton delocalization in bacterial photosynthetic light-harvesting systems. *J. Phys. Chem.* (*B*), **101**, 7241–7248.

Nagae, H., Kakitani, T., Katohi, T. & Mimuro, M. (1993). Calculation of the excitation transfer matrix elements between the S_2 or S_1 state of carotenoid and the S_2 or S_1 state of bacteriochlorophyll. *J. chem. Phys.* **98**, 8012–8023.

Nagarajan, V. & Parson, W. (1997). Excitation energy transfer between the B850 and B875 antenna complexes of *Rhodobacter sphaeroides*. *Biochemistry* **36**, 2300–2306.

Naqvi, K. R. (1980). The mechanism of singlet-singlet excitation energy transfer from carotenoids to chlorophyll. *Photochem. Photobiol.* **31**, 523–524.

Nield, J., Kruse, O., Ruprecht, J., da Fonseca, P., Buchel, C. & Barber, J. (2000). Three-dimensional structure of *Chlamydomonas reinhardtii* and *Synechococcus elongatus* photosystem II complexes allows for comparison of their oxygen-evolving complex organization. *J. Biol. Chem.* **275**, 27940–27946.

Noguchi, T., Kolaczkowski, S., Gärtner, W. & Atkinson, G. H. (1990). Resonance Raman spectra of 13-demethylretinal bacteriorhodopsin and of a picosecond bathochromic photocycle intermediate. *J. Phys. Chem.* **94**, 4920–4926.

Novoderezhkin, V., Monshouwer, R. & van Grondelle, R. (1999). Disordered exciton model for the core light-harvesting antenna of *Rhodopseudomonas viridis*. *Biophys. J.* **77**, 666–681.

Novoderezhkin, V. I. & Razjivin, A. P. (1995). Exciton dynamics in circular aggregates: application to antenna of photosynthetic purple bacteria. *Biophys. J.* **68**, 1089–1100.

Nugent, J. H. A. (1996). Oxygenic photosynthesis – electron transfer in photosystem I and photosystem II. *Eur. J. Biochem.* **237**, 519–531.

Oppenheimer, J. R. (1941). Internal conversion in

photosynthesis. In *Proceedings of the American Physical Society*, vol. 60 of *Phys. Rev.*, p. 158.

Ort, D. & Yocum, C. (Eds.) (1996). *Oxygenic Photosynthesis: The Light Reactions*. Dordrecht: Kluwer Academic Publishers.

Papiz, M. Z., Prince, S. M., Hawthornthwaite-Lawless, A. M., McDermott, G., Freer, A. A., Isaacs, N. W. & Cogdell, R. J. (1996). A model for the photosynthetic apparatus of purple bacteria. *Trends Plant Sci.* **1**, 198–206.

Parson, W. W. & Warshel, A. (1995). Theoretical analysis of electron-transfer reaction. In *Anoxygenic Photosynthetic Bacteria* (eds. R. E. Blankenship, M. T. Madigan & C. E. Bauer), pp. 559–575. Dordrecht: Kluwer Academic Publishers.

Pearlstein, R. M. (1992). Theory of the optical spectra of the bacteriochlorophyll a antenna protein trimer from *Prosthecochloris aestuarii*. *Photosyn. Res.* **31**, 213–226.

Pearlstein, R. M. & Zuber, H. (1985). Exciton states and energy transfer in bacterial membranes: the role of pigment-protein cyclic unit structure. In *Antennas and Reaction Centers of Photosynthetic Bacteria* (ed. M. Michel-Beyerle), pp. 53–61. Berlin: Springer-Verlag.

Polivka, T., Herek, J., Zigmantas, D., Akerlund, H.-E. & Sundström, V. (1999). Direct observation of the (forbidden) S_1 state in carotenoids. *Proc. natn. Acad. Sci. USA* **96**, 4914–4917.

Priestley, J. (1772). Observations on different kinds of air. *Phil. Trans. Roy. Soc. Lond.* **62**, 147–264.

Pullerits, T., Chachisvillis, M. & Sundström, V. (1996). Exciton delocalization length in the B850 antenna of *Rhodobacter sphaeroides*. *J. phys. Chem.* **100**, 10787–10792.

Pullerits, T. & Sundström, V. (1996). Photosynthetic light-harvesting pigment–protein complexes: toward understanding how and why. *Acc. Chem. Res.* **29**, 381–389.

Ray, J. & Makri, N. (1999). Short-range coherence in the energy transfer of photosynthetic light-harvesting systems. *J. phys. Chem.* (*A*), **103**, 9417–9422.

Reddy, N., Picorel, R. & Small, G. (1992). B896 and B870 components of the *Rhodobacter sphaeroides* antenna – a hole burning study. *J. phys. Chem.* **96**, 6458–6464.

Reddy, N. R. S., Small, G. J., Seibert, M. & Picorel, R. (1991). Energy-transfer dynamics of the B800–B850 antenna complex of *Rhodobacter sphaeroides* – a hole burning study. *Chem. phys. Lett.* **181**, 391–399.

Rees, D. W. & Clayton, R. K. (1968). Isolation of a reaction center fraction from *Rhodopseudomonas sphaeroides*. *Biochem. Biophys. Res. Commun.* **12**, 471–475.

Rhee, K. H., Morriss, E. P., Barber, J. & Kuhlbrandt, W. (1998). Three-dimensional structure of the plant photosystem II reaction centre at 8 angstrom resolution. *Nature* **396**, 283–286.

Ritz, T. (2001). *The Quantum Physics of the Bacterial Photosynthetic System* (Ph.D. Thesis, University of Ulm), Osnabrück: Der Andere Verlag.

Ritz, T., Damjanović, A. & Schulten, K. (1998a). Light-harvesting and photoprotection by carotenoids: structure-based calculations for photosynthetic antenna systems. In *Photosynthesis: Mechanisms and Effects* (*Proceedings of the XIth International Congress on Photosynthesis*) (ed. G. Garab), vol. 1, pp. 487–490, Dordrecht: Kluwer Academic Publications.

Ritz, T., Damjanović, A., Schulten, K., Zhang, J. & Koyama, Y. (2000). Efficient light harvesting through carotenoids. *Photosyn. Res.* **66**, 125–144.

Ritz, T., Hu, X., Damjanović, A. & Schulten, K. (1998b). Excitons and excitation transfer in the photosynthetic unit of purple bacteria. *Luminescence* **76–77**, 310–321.

Ritz, T., Park, S. & Schulten, K. (2001). Kinetics of excitation migration and trapping in the photosynthetic unit of purple bacteria. *J. phys. Chem.* (*B*), **105**, 8259–8267.

Sashima, T., Koyama, Y., Yamada, T. & Hashimoto, H. (2000). The $1B_u^-$ and $2A_g^-$ energies of lycopene, β-carotene and mini-9-β-carotene as determined by resonance-Raman excitation profile: dependence of the $1B_u^-$-state energy on the conjugation length. *J. phys. Chem.* (*B*), **104**, 5011–5019.

Sashima, T., Nagae, H., Kuki, M. & Koyama, Y. (1999). A new singlet-excited state of all-*trans*-spheroidene as detected by resonance-Raman excitation profiles. *Chem. phys. Lett.* **299**, 187–194.

Sashima, T., Shiba, M., Hashimoto, H., Nagae, H. & Koyama, Y. (1998). The A_g^- energy of crystalline all-trans-spheroidene as determined by resonance-Raman excitation profiles. *Chem. phys. Lett.*. **290**, 36–42.

Sauer, K. (1975). Primary events and the trapping of energy. In *Bioenergetics of Photosynthesis* (ed. Govindjee), pp. 115–181. New York: Academic Press.

Sauer, K., Cogdell, R. J., Prince, S. M., Freer, A., Isaacs, N. W. & Scheer, H. (1996). Structure-based calculations of the optical spectra of the LH2 bacteriochlorophyll-protein complex from *Rhodopseudomonas acidophila*. *Photochem. Photobiol.* **64**, 564–576.

Sauer, K., Smith, J. R. L. & Schultz, A. J. (1966). The dimerization of chlorophyll a, chlorophyll b and bacteriochlorophyll in solution. *J. Am. chem. Soc.* **88**, 2681–2688.

Savage, H., Cyrklaff, M., Montoya, G., Kühlbrandt, W. & Sinning, I. (1996). Two-dimensional structure of light harvesting complex II (LHII) from the purple bacterium *Rhodovulum sulfidophilum* and comparison with LHII from *Rhodopseudomonas acidophila*. *Structure* **4**, 243–252.

Scheer, H. (Ed.) (1998). *Photosynthetic Light-Harvesting Systems*. Berlin, New York: Walter de Gruyter & Co.

Scheer, H. (Ed.) (1991). *Chlorophylls*. Boca Raton: CRC Press.

Schlick, T., Skeel, R., Brünger, A., Kalé, L., Board Jr., J. A., Hermans, J. & Schulten, K. (1999). Algorithmic challenges in computational molecular biophysics. *J. comp. Phys.* **151**, 9–48.

Scholes, G. & Fleming, G. (2000). On the mechanism of light harvesting in purple bacteria: B800 to B850 energy transfer. *J. phys. Chem.* (*B*), **104**, 1854–1868.

Scholes, G., Gould, I., Cogdell, R. & Fleming, G. (1999). *Ab initio* molecular orbital calculations of electronic couplings in the lh2 bacterial light-harvesting complex of *Rps. acidophila*. *J. phys. Chem.* (*B*), **103**, 2543–2553.

Scholes, G., Harcourt, R. & Ghiggino, K. (1995). Rate expressions for excitation transfer, an *ab initio* study of electronic factors in excitation transfer and exciton resonance interactions. *J. chem. Phys.* **102**, 9574–9581.

Scholes, G. D., Harcourt, R. D. & Fleming, G. R. (1997). Electronic interactions in photosynthetic light-harvesting complexes: the role of carotenoids. *J. phys. Chem.* (*B*), **101**, 7302–7312.

Schulten, K. & Karplus, M. (1972). On the origin of a low-lying forbidden transition in polyenes and related molecules. *Chem. Phys. Lett.* **14**, 305–309.

Sener, M. & Schulten, K. (In Press). Spectral properties and static disorder of the light harvesting complexes of purple bacteria. *Phys. Rev.* (*E*).

Shreve, A. P., Trautman, J. K., Frank, H. A., Owens, T. G. & Albrecht, A. C. (1991). Femtosecond energy-transfer processes in the B800–850 light-harvesting complex of *Rhodobacter sphaeroides*-2.4.1. *Biochim. Biophys. Acta* **1058**, 280–288.

Smith, E. L. (1938). Solutions of chlorophyll–protein compounds (phyllochlorins) extracted from spinach. *Science* **88**, 170–171.

Stahlberg, H., Dubochet, J., Vogel, H. & Ghosh, R. (1998). The reaction centre of the photounit of *Rhodospirillum rubrum* is anchored to the light-harvesting complex with four-fold rotational disorder. *Photosyn. Res.* **55**, 363–368.

Stanier, R. Y. (1961). Photosynthetic mechanisms in bacteria and plants; a unitary concept. *Bacteriolog. Rev.* **25**, 1–17.

Stark, W., Kühlbrandt, W., Wildhaber, I., Wehrli, E. & Mühlethaler, K. (1984). The structure of the photoreceptor unit of *Rhodopseudomonas viridis*. *EMBO J.* **3**, 777–783.

Stiel, H., Leupold, D., Teuchner, K., Nowak, F., Scheer, H. & Cogdell, R. (1997). One- and two-exciton bands in the LH2 antenna of *Rhodopseudomonas acidophila*. *Chem. phys. Lett.* **276**, 62–69.

Stoll, A. (1936). Zusammenhänge zwischen der Chemie des Chlorophylls und seiner Funktion in der Photosynthese. *Naturwissenschaften* **24**, 53–60.

Sundström, V., Pullerits, T. & van Grondelle, R. (1999). Photosynthetic light-harvesting: reconciling dynamics and structure of purple bacterial LH2 reveals function of photosynthetic unit. *J. phys. Chem.* (*B*), **103**, 2327–2346.

Sundström, V. & van Grondelle, R. (1991). Dynamics of excitation energy transfer in photosynthetic bacteria. In *Chlorophylls* (ed. H. Scheer), pp. 627–704. Boca Raton: CRC Press.

Sundström, V. & van Grondelle, R. (1995). Kinetics of excitation transfer and traping in purple bacteria. In *Anoxygenic Photosynthetic Bacteria* (eds. M. R. Blankenship, M. T. Madigan & C. E. Bauer), pp. 349–372. Dordrecht: Kluwer Academic Publishers.

Tavan, P. & Schulten, K. (1987). Electronic excitations in finite and infinite polyenes. *Phys. Rev.* (*B*), **36**, 4337–4358.

Thompson, M. & Zerner, M. (1991). A theoretical examination of the electronic structure and spectroscopy of the photosynthetic reaction center from *Rhodopseudomonas viridis*. *J. Am. chem. Soc.* **113**, 8210–8215.

Thornber, J. P., Cogdell, R. J., Pierson, B. K. & Sefter, R. E. B. (1983). Pigment–protein complexes of purple photosynthetic bacteria: an overview. *J. cell. Biochem.* **23**, 159–169.

Thrash, R., Fang, H.-B. & Leroi, G. (1979). On the role of forbidden low-lying excited states of light-harvesting carotenoids in photosynthesis. *Photochem. Photobiol.* **29**, 1049–1050.

Timpmann, K., Zhang, F., Freiberg, A. & Sundström, V. (1993). Detrapping of excitation-energy from the reaction center in the photosynthetic purple bacterium *Rhodospirillum rubrum*. *Biochim. Biophys. Acta* **1183**, 185–193.

Trautmann, J., Shreve, A., Violette, C., Frank, H. A., Owens, T. & Albrecht, A. (1990). Femtosecond dynamics of energy transfer in B800–850 light-harvesting complexes of *Rhodobacter sphaeroides*. *Proc. natn. Acad. Sci. USA* **87**, 215–219.

Tronrud, D., Schmid, M. & Matthews, B. (1986). Structure and X-ray amino acid sequence of a bacteriochlorophyll a protein from *Prosthecochloris aestuarii* refined at 1·9 Å resolution. *J. molec. Biol.* **188**, 443–454.

van Amerongen, H., Valkunas, L. & van Grondelle, R. (2000). *Photosynthetic Excitons* Singapore: World Scientific.

van Grondelle, R., Dekker, J., Gillbro, T. & Sundström, V. (1994). Energy transfer and trapping in photosynthesis. *Biochim. Biophys. Acta* **1187**, 1–65.

van Grondelle, R., Kramer, H. & Rijgersberg, C. (1982). Energy transfer in the B800–B850-carotenoid light-harvesting complex of various mutants of *Rhodopseudomonas sphaeroides* and of *Rhodopseudomonas capsulata*. *Biochim. Biophys. Acta* **682**, 208–215.

Van Niel, C. B. (1931). On the morphology and physiology of the purple and green bacteria. *Arch. Mikrobiol.* **3**, 1–12.

Van Niel, C. B. (1941). The bacterial photosynthesis and their importance for the general problem of photosynthesis. *Adv. Enzymol.* **1**, 263–328.

van Oijen, A., Ketelaars, M., Köhler, J., Aartsma, T. & Schmidt, J. (1999). Unraveling the electronic structure of individual photosynthetic pigment–protein complexes. *Science* **285**, 400–402.

Vermeglio, P. & Joliot, P. (1999). The photosynthetic apparatus of *Rhodobacter sphaeroides*. *Trends Microbiol.* **7**, 435–440.

Visscher, K., Bergstrom, H., Sundström, V., Hunter, C. & van Grondelle, R. (1989). Temperature dependence of energy transfer from the long wavelength antenna Bchl-896 to the reaction center in *Rhodospirillum rubrum*, *Rhodobacter sphaeroides* (w.t. and M21 mutant) from 77 to 177 K, studied by picosecond absorption spectroscopy. *Photosyn. Res.* **22**, 211–217.

Visscher, K. J., Chang, M. C., van Mourik, F., Parkes-Loach, P. S., Heller, B. A., Loach, P. A. & van Grondelle, R. (1991). Fluorescence polarization and low-temperature absorption spectroscopy of a subunit form of light-harvesting complex I from purple photosynthetic bacteria. *Biochemistry* **30**, 5734–5742.

Walz, T. & Ghosh, R. (1997). Two-dimensional crystallization of the light-harvesting I – reaction centre photounit from *Rhodospirillum rubrum*. *J. molec. Biol.* **265**, 107–111.

Walz, T. & Grigorieff, N. (1998). Electron crystallography of two-dimensional crystals of membrane proteins. *J. struct. Biol.* **121**, 142–161.

Walz, T., Jamieson, S. J., Bowers, C. M., Bullough, P. A. & Hunter, C. N. (1998). Projection structures of three photosynthetic complexes from *Rhodobacter sphaeroides*: LH2 at 6 angstrom LH1 and RC-LH1 at 25 angstrom. *J. molec. Biol.* **282**, 833–845.

Westerhuis, W. H. J., Vos, M., van Grondelle, R., Amesz, J. & Niederman, R. A. (1998). Altered organization of light-harvesting complexes in phospholipid-enriched *Rhodobacter sphaeroides* chromatophores as determined by fluorescence yield and singlet-singlet annihilation measurements. *Biochim. Biophys. Acta* **1366**, 317–329.

Wong, D.-H., Collins, W., Harmer, A., Lilburn, T. & Beatty, J. (1996). Directed mutagenesis of the *Rhodobacter capsulatus puhA* and Orf 214: pleiotropic effects on photosynthetic reaction center and light-harvesting 1 complexes. *J. Bacteriol.* **178**, 2334–2342.

Woodbury, N. W. & Allen, J. P. (1995). The pathway, kinetics and thermodynamics of electron transfer in wild type and mutant reaction centers of purple nonsulfur bacteria. In *Anoxygenic Photosynthetic Bacteria* (eds. R. Blankenship, M. Madigan & C. Bauer), pp. 527–557. Dordrecht: Kluwer Academic Publishers.

Wraight, C. (1982). Reaction centers, electron flow, and energy transduction. In *Photosynthesis* (ed. Govindjee), pp. 17–61. New York: Academic Press.

Wu, H. & Small, G. (1998). Symmetry-based analysis of the effects of random energy disorder on the excitonic level structure of cyclic arrays: application to photosynthetic antenna complexes. *J. phys. Chem.* (*B*), **102**, 888–898.

Wu, H. M., Reddy, N. R. S., Cogdell, R. J., Muenke, C., Michel, H. & Small, G. J. (1996). A comparison of the LH2 antenna complex of three purple bacteria by hole burning and absorption spectroscopies. *Molec. Cryst. Liq. Cryst.* **291**, 163–173.

Wu, H.-M., Reddy, N. R. S. & Small, G. J. (1997). Direct observation and hole burning of the lowest exciton level (B870) of the LH2 antenna complex of *Rhodopseudomonas acidophila* (strain 10050). *J. phys. Chem.* (*B*), **101**, 651–656.

Wurmser, R. (1925). Le rendement énergetique de la photosynthése chlorophylliene. *Ann. Physiol. Physicochim. Biol.* **1**, 47–63.

Young, C. & Beatty, J. (1998). Topological model of the *Rhodobacter capsulatus* light-harvesting complex I assembly protein LhaA (previously known as ORF1696). *J. Bacteriol.* **180**, 4742–4745.

Young, C., Reyes, R. & Beatty, J. (1998). Genetic complementation and kinetic analyses of *Rhodobacter capsulatus ORF1696* mutants indicate that the ORF1696 protein enhances assembly of the light-harvesting I complex. *J. Bacteriol.* **180**, 1759–1765.

Zhang, J.-P., Fujii, R., Qian, P., Inaba, T., Mizoguchi, T. & Koyama, Y. (2000). Mechanism of the carotenoid-to-bacteriochlorophyll energy transfer via the S_1 state in the LH2 complexes from purple bacteria. *J. phys. Chem.* (*B*), **104**, 3683–3691.

Zouni, A., Witt, H. T., Kern, J., Fromme, P., Krauss, N., Saenger, W. & Orth, P. (2001). Crystal structure of photosystem II from *Synechococcus elongatus* at 3·8 angstrom resolution. *Nature* **409**, 739–743.

Zuber, H. (1985). Structure and function of light-harvesting complexes and their polypeptides. *Photochem. Photobiol.* **42**, 821–825.

Zuber, H. (1986). Structure of light-harvesting antenna complexes of photosynthetic bacteria, cyanobacteria and red algae. *Trends Biochem. Sci.* **11**, 414–419.

Zuber, H. & Brunisholz, R. (1991). Structure and function of antenna polypeptides and chlorophyll–protein complexes: principles and variability. In *Chlorophylls* (ed. H. Scheer), pp. 627–692. Boca Raton: CRC Press.

Zuber, H. & Cogdell, R. (1995). Structure and organization of purple bacterial antenna complexes. In *Anoxygenic Photosynthetic Bacteria* (eds. R. Blankenship, M. Madigan & C. Bauer), pp. 315–348. Dordrecht: Kluwer Academic Publishers.